REPORT NO. 537

The Effects of Water Quality on REO Mineral Flotation

Results of research carried out as MRIWA Project M0537

at Curtin University

by

Bogale Tadesse, Laurence Dyer, Boris Albijanic

WA School of Mines: Minerals, Energy and Chemical Energy, Curtin University

October 2025

Distributed by: MRIWA
1 Adelaide Terrace
Perth WA 6000
to which all enquiries should be addressed

Executive Summary

Froth flotation, widely used for mineral beneficiation, is an important technique to concentrate rare earth (RE) minerals such as monazite, bastnaesite, and xenotime. Extensive research has been carried out to optimise the flotation process and the collection mechanism between the rare earth minerals and flotation reagents such as collectors and modifiers has been well documented. Moreover, various additional organic and inorganic reagents have been used to enhance the selectivity of collection for rare earth minerals and mitigate the negative effects caused by the sparingly soluble gangue minerals. Most of the literature on rare earth mineral flotation has focused on enhancing recovery and grade. However, research on the effects of water chemistry, such as ionic strength and the types of ionic species in solution, on rare earth mineral flotation has been rarely conducted.

The literature demonstrates that water chemistry affects flotation, and the presence of certain ions can lead to the compression of the electrical double layer on the particle, inhibition of bubble coalescence, destabilisation of the hydration layer around the particles, and precipitation/adsorption of hydroxide complexes on the surface of minerals. Hence it is imperative to understand the mechanisms affecting flotation when considering the use of alternative water sources. Literature on the effects of water quality on rare earth oxide minerals is rarely available. In this study, the effect of water quality on the flotation of rare earth oxide minerals was studied using single or multi-ionic system water to understand how and which ionic species affect flotation and their underlying mechanism.

This work also investigated the flotation performance of monazite in the presence of different ions such as Ca^{2+}, Mg^{2+}, Na^{+}, and K^{+}. The research integrates flotation experiments with colloid and surface characterisation techniques such as zeta potential measurement, X-ray photoelectron spectroscopy (XPS) and UV adsorption which were used to analyse the surface chemistry and particle interactions during flotation. The results showed that the presence of divalent metal ions (Mg^{2+}, Ca^{2+}) was highly detrimental to monazite flotation, while the presence of monovalent metal ions (K^{+} and Na^{+}) affected monazite flotation to a lesser extent. This is because the carrier anion oleate formed insoluble products with divalent metal ions while this did not occur with monovalent metal ions. Therefore, the amount of soluble oleate ions was significantly reduced in the presence of divalent ions, resulting in less adsorption of oleate ions on monazite particles and thus, reduced monazite recovery. The reduced adsorption of oleate on monazite was confirmed using XPS and UV adsorption experiments. Furthermore, the divalent cations acted as a bridge between the oxygen atoms of the adsorbed silicate and carboxylate ions, resulting in increased adsorption of fatty acid collector ions and higher recovery of FeO. Rheological measurements also revealed that the presence of $CaCl_2$ and $MgCl_2$ significantly increased the flotation pulp viscosity, which could be attributed to the reduced repulsive forces between particles due to the compression of the electrical double layer.

The impact of specific anions such as Cl^{-}, SO_4^{2-}, and HCO_3^{-} on the flotation performance of rare earth ore was also investigated. It was observed that an increase in the concentration of these anions led to a decrease in the recovery of RE minerals and an increase in the recovery of FeO minerals, negatively affecting flotation efficiency. This adverse effect was

most pronounced with Cl^- and least noticeable with HCO_3^-. Increased entrainment of gangue minerals was observed when the flotation pulp had higher viscosity. The reduction in the zeta potential of fine particles in the presence of these anions resulted in a higher pulp viscosity due to increased attractive forces between particles. These findings were verified by settling experiments and calculations based on the DLVO theory.

The performance of water treatment options such as nanofiltration, electrodialysis and precipitation to produce suitable water for rare earth oxide (REO) flotation was investigated. The nanofiltration membranes used in this study could reject more than 95% of divalent ions (such as Ca^{2+}, Mg^{2+}, SO_4^{2-}) and more than 74% of monovalent ions (e.g., Na^+ and Cl^-) at 12 bar of transmembrane pressure and 65% water recovery. These rejection rates were found to be sufficient to produce fit-for-purpose water for mineral processing. In addition, the effect of pressure on the mass transfer mechanism of each membrane was determined.

Precipitation studies conducted using an ultra-high aluminium method were shown to remove more than 97% of divalent ions such as calcium, magnesium, and sulphate and 68% of chloride ions under certain conditions. The process can be optimised to increase chloride removal by a further 22% by implementing a two-stage precipitation process. Operational variables such as pH and temperature were varied during the precipitation studies for process optimisation.

In the case of electrodialysis, the removals achieved were more than 90% and 98% for monovalent ions (Na^+ and Cl^-) and divalent ions (Ca^{2+}, Mg^{2+} and SO_4^{2-}), respectively, at 87% total dissolved solids (TDS). It was observed that increasing the flow velocity reduces the efficiency of the system by up to 8%. Additionally, higher flow rates increase the current density, decreasing the cell performance. The optimum operating conditions for electrodialysis were determined as an applied voltage of 1 V per membrane pair, a flow rate of 45 L/h and 40 minutes of treatment time.

The results showed that nanofiltration and electrodialysis are efficient methods to achieve the quality of water required for mineral processing without exceeding the ion concentration threshold for RE mineral froth flotation. From an economic point of view, electrodialysis was the best option due to its low energy consumption and the relatively low replacement cost associated with a long membrane lifetime.

Table of Contents

Executive Summary 3

Table of Contents 5

Terms, Abbreviations and Acronyms 8

Section 1: Background 9

1. Rare Earth Mineral and Application of Flotation 9

2. Effect of Water Quality on Mineral Flotation 12

3. Study Objectives 14

4. Significance 15

Section 2: Microflotation and Bench-scale Flotation Studies 17

5. Experimental Design: Microflotation and Bench-scale Flotation Studies 17

5.1 Feed for single mineral microflotation tests 17

5.2 Feed ore characteristics for bench scale tests 17

5.3 Chemicals 20

5.4 Microflotation experiments 20

5.5 Methods for bench-scale flotation experiments 21

5.6 Zeta potential experiments 23

5.7 Adsorption experiments 23

5.8 X-ray photoelectron spectroscopy (XPS) analysis 24

5.9 Rheological measurements 25

5.10 Entrainment experiments 25

5.11 Settling experiments 25

5.12 DLVO (Derja−guin−Landau−Verwey−Overbeek) theory calculation 25

6. Results and Discussion: Microflotation and Bench-scale Flotation Studies 27

6.1 Single mineral microflotation experiments of monazite 27

6.2 Effect of divalent cations on bench-scale flotation of Mt Weld ore 35

6.3 Flotation behaviour of Mt Weld ore in the presence of different anions 45

Section 3: Fit-for-purpose Water Treatment Methods for REO Flotation 61

7. Introduction to Fit-for-Purpose Water Treatment 61

7.1 Reagents 62

7.2 Water characterisation 63

7.3 Nanofiltration 64
7.4 Precipitation 66
7.5 Oxalic Acid 66
7.5.1 Effect of oxalic acid dose on ion removal 66
7.5.2 Kinetics of calcium precipitation 66
7.5.3 Effect of pH on calcium and magnesium precipitation 66
7.6 Ultra-High Lime with Aluminium (UHLA) 67
7.6.1 Effect of reagent dose on ion removal 67
7.6.2 Kinetics of ion removal 67
7.6.3 Effect of pH on chloride and sulphate removal 67
7.6.4 Effect of temperature on chloride and sulphate removal 68
7.7 Electrodialysis 68
7.8 Results and Discussion 71
7.8.1 Nanofiltration 71
7.8.2 Membrane properties 77
7.8.3 Mass transport through each membrane - hydrodynamic approach 79
7.8.4 The effect of a second nanofiltration stage on water recovery 81
7.8.5 Energy cost estimation for single stage and two-stage processes 81
7.8.6 Conclusions 84
8. Electrodialysis 84
8.1 Effect of flow velocity on limiting current density 84
8.2 Effect of ions concentration on Limiting Current Density 85
8.3 Effect of applied voltage on ion removal 86
8.4 Modelling of synthetic NaCl (4.5 g/L) solution by Nernst-Planck model 88
8.5 Effect of feed velocity on TDS removal 90
8.6 Specific treatment capacity (STC) 90
8.7 Effect of ion concentration 91
8.8 Energy cost estimation 91
8.9 Conclusions 94
9. Precipitation 95
9.1 Ultra-High Lime with Aluminium (UHLA) 95
9.2 Oxalic Acid 103
9.3 Conclusions 105
Section 4: Synthesis 107

10. Overall Study Conclusions 107
11. Recommendations for Future Study 108
12. References 109

Terms, Abbreviations and Acronyms

DLVO - Derja−guin−Landau−Verwey−Overbeek

ED - Electrodialysis

HREE - Heavy rare earth elements

ICP OES - Inductively coupled plasma optical emission spectroscopy

LCD - Limiting current density

LREE - Light rare earth elements

MIBC - Methyl isobutyl carbinol

MWCO - Molecular weight cut-off

NF - Nanofiltration

QEMSCAN - Quantitative Evaluation of Minerals by Scanning Electron Microscopy

REE - Rare earth elements

REO - Rare earth oxide

RO - Reverse osmosis

SEC - Specific energy consumption

SKK - Spiegler-Kedem-Katchalsky

STC - Specific treatment capacity

TDS - Total Dissolved Solids

UHLA - Ultra-High Lime with Aluminium

XRD - X-ray diffraction

XRF - X-ray fluorescence

XPS - X-ray photoelectron spectroscopy

Section 1: Background

1. Rare Earth Mineral and Application of Flotation

Rare earth elements (REE) comprise the lanthanide group elements from element number 57 (lanthanum) to 71 (lutetium), together with scandium (21) and yttrium (39). These elements can be divided into two groups: the heavy rare earth elements (HREE) from gadolinium (64) to lutetium (71), and light rare earth elements (LREE) from lanthanum (57) to europium (63), according to whether the electrons in the 4f sub-shell exist in the state of a pair or not. It was reported that the demand for LREE accounted for more than 80% of the total demand of all rare earth elements in 2007 (Alonso et al., 2012). REE have unique and irreplaceable properties that are important for applications such as permanent magnets, battery alloys, metal alloys, auto catalysis, petroleum refining and ceramics. (Long et al., 2010).

The crustal abundance of REEs (2.3×10^{-2} wt.%) is not very rare, compared to that of gold (5×10^{-7} wt.%) and silver (1×10^{-5} wt.%) reserves. However, the fact that REE are rarely found in a pure state, are widely distributed in low concentrations and are difficult to extract from their host minerals due to the nature of their mineralisation, makes these elements rare (Golev et al., 2014; Humphries, 2012; Gupta and Krishnamurthy, 2005).

To date, more than 250 types of rare earth bearing minerals including oxide, halide, carbonate, phosphate and silicate group minerals have been reported. However, only a few of these minerals, such as monazite, bastnaesite, xenotime, and ion-adsorbed clay, have been exploited commercially to produce rare earth oxide products (Jordens et al., 2013; Ito et al., 1991). These minerals have been concentrated using several beneficiation methods, such as magnetic, gravity, electrostatic separation and froth flotation, separately or in combination. Froth flotation is a physicochemical separation technique that takes advantage of the difference in wettability of the mineral surface. It is well known that froth flotation separation is most effective, compared to the other physical methods, when the ore particle size is less than 100 microns because the other physical separation methods cannot be used with such fine particles due to low efficiencies and difficulties in operation causing the loss of valuable minerals (Gupta and Krishnamurthy, 2005).

Flotation separation has been widely used at a number of major mines for rare earth minerals. Bayan Obo mine in China, which is one of the largest operating rare earth mines in the world, has been using low and high two-stage magnetic separation methods to produce a primary concentrate followed by froth flotation to produce a final concentrate of 55% grade (Li and Yang, 2006). Another one of the largest rare earth mines in the USA, Mountain Pass, has used a single beneficiation process by froth flotation and has been producing a 63% grade final concentrate from an initial feed ore grade of 7% (Pradip and Fuerstenau, 2013). In Western Australia, Mt. Weld mine, which has been reported to have the highest grade rare earth oxide deposit in the world, produces a concentrate by froth flotation. Along with the well-known mines above, many other mines, such as Thor Lake mine in Canada, Shangdon Weishan, and Dulacao, Maoniuping (MNP) mine in China have been using froth flotation for the beneficiation of rare earth minerals (Jordens et al., 2016; Xiong et al., 2018; Li and Yang, 2006).

Froth flotation operation can be varied by controlling several operating conditions, such as pulp density, particle size, agitation, and batch arrangement. In particular, the added reagent scheme is considered the most critical factor to enhance flotation performance, by selectively rendering hydrophobicity or hydrophilicity onto certain types of mineral surfaces depending on the reagents used. As the main purpose of flotation is the selective separation of valuable minerals from gangues, much research has been conducted to determine the optimum types of reagents (collectors) and the effects of their dosage on rare earth mineral flotation. Many efforts have been made to understand the mechanism of interactions between various collectors and rare earth mineral surfaces, shedding light on the complex interactions that influence flotation performance.

The collectors most widely used for rare earth minerals are from the hydroxamate, carboxylate, and phosphate groups. Fatty acids having carboxylate functional groups have conventionally been used as collectors for non-sulphide mineral flotation due to their high ability to render hydrophobicity on the mineral surfaces, and have been used as promising collectors for rare earth mineral flotation as well. Hydroxamic acid in the hydroxamate group is well known for its high selectivity for rare earth minerals, however, it is more expensive than other collectors. Research on the use of phosphoric acid has also been carried out and resulted in high recovery for rare earth minerals, but it was observed that oxide gangue minerals like quartz were also easily floated by this type of collector and the selectivity was slightly reduced when a higher dosage was applied (Liu et al., 2016; Jordens et al., 2014).

Along with the collectors, a vast variety of conditioners have been adopted to increase the flotation selectivity for rare earth minerals, and Table 1 shows a summary of the rare earth mineral flotation literature with organic and inorganic reagents.

Table 1. *Summary of the flotation research for rare earth minerals*

Author	Year	Mineral	Collector	Conditioner
J. Luo	1987	Bastnaesite, monazite (Baotou in China)	Hydroxamic acid	Sodium silicate Sodium fluorosilicate
J. Ren	1993	Bastnaesite, barite, fluorite, silicate, hematite	N-hydroxyl phthalicimide	Sodium silicate, NH_4Cl, ADTM
Ren et al.	2000	Bastnaesite, monazite	Benzoic acid	Potassium alum
Xia et al.	2015	Thor lake ore	Benzyl hydroxamic acid LF-P81 (hydroxamate)	Sodium silicate $Pb(NO_3)_2$
Jordens et al.	2016	Bastnaesite, monazite etc. (at Thor lake)	Benzo hydroxamic acid	Lead chloride
Cao et al.	2018	Bastnaesite (Zaozhuang in China)	Salicyl hydroxamic acid	Strontium chloride
Sorensen and Lundgaard	1966	Monazite, steenstrupine in the Ore (from Kavanefjeld in Greenland)	Oleic acid Sodium oleate	Sodium silicate $La(NO_3)_3$

A.M. Abeidu	1972	Monazite, zircon	Sodium dodecylsulphate Oleic acid Dodecylamine	Sodium sulphide
Zhang and Honaker	2018	Monazite (China), calcite (USA)	Octano hydroxamic acid	Sodium hexametaphosphate Sodium silicate Citric acid EDTA
Abaka-Wood et al.	2018	Monazite, hematite, quartz	Aero float 6494	Sodium silicate Starch
Pereira and Peres	1997	Xenotime (95%), zircon (5%) (from Pitinga mine in Brazil)	V3579 (hydroxamic acid)	Lignin sulfonate Quebracho Corn starch (RMR) Amylopectin Sodium metasilicate
Zhang and Anderson	2017	Xenotime	Sodium oleate Octanohydroxamic acid	Sodium silicate Ammonium lingo sulfonate

The adsorption of collectors on the rare earth mineral surface is believed to be chemisorption, where the adsorption occurs above the point of zero charge. This was shown by the results of surface analysis methods such as infrared spectroscopy (Pradip and Freustanau, 1983). Figure 1 shows the structure of adsorption of various collectors on a rare earth mineral surface. The mechanism of chemisorption was proposed to take place by the following steps: 1) dissolution of rare earth elements from the mineral surface, 2) formation of rare earth metal hydroxide in the form of $Ce(OH)_2^+$, $Ce(OH)^{2+}$, $La(OH)_2^+$, $La(OH)^{2+}$, 3) adsorption of the metal hydroxide on the mineral surface, 4) provision of newly activated site for the adsorption by the adsorbed hydroxide for adsorption of collectors (Pradip and Fuerstenau, 1983).

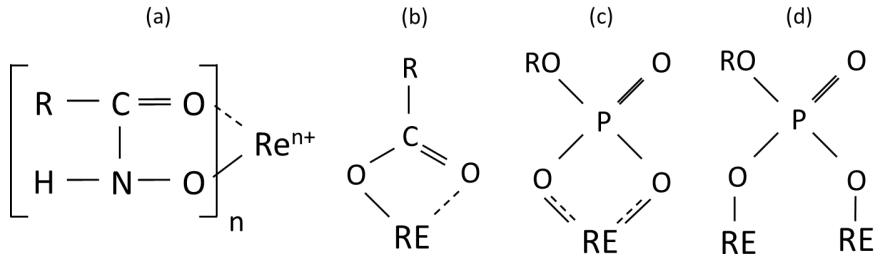

Figure 1. *Formation of the adsorption of (a) hydroxamic acid, (b) fatty acid, (c) phosphoric acid (bidentate complex), (d) phosphoric acid (binuclear complex) on the rare earth mineral surface*

As shown in Figure 2, there is a close match between the distribution of rare earth metal hydroxide species and the flotation recovery curve with pH, which provides evidence

regarding the critical role of hydroxide complexes for the enhancement of floatability of rare earth minerals (Pradip and Fuerstenau, 1983; Cheng et al., 1993).

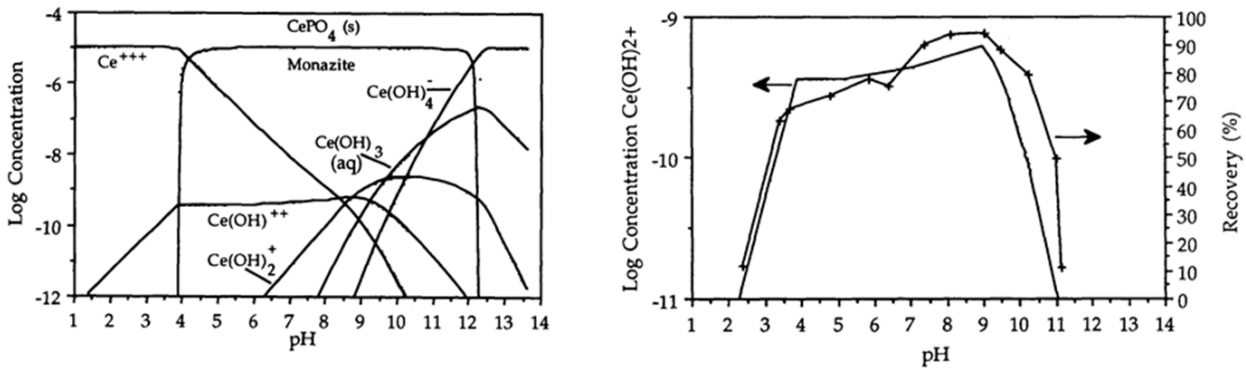

Figure 2. *Species diagram of monazite and correlation with flotation recovery*

2. Effect of Water Quality on Mineral Flotation

Limited freshwater availability, increasing competition for water among multiple users, cost of purification and corporate sustainability goals are the main factors driving the minerals industry to focus on water quality and usage (Rijsberman, 2006; Castro and Laskowski, 2011; Levay et al., 2001). Increasing water re-use and accessing alternatives to freshwater for mineral processing, particularly in flotation, are potential strategies being implemented to improve water efficiency. In flotation, a reasonable water quality is needed to develop an appropriate reagent scheme and optimise operating conditions to maximise performance. High concentrations of dissolved ions in groundwater, sea water or recycled water may alter the water structure, particle surface wettability and colloidal interactions between bubbles and particles, and therefore, may have a positive or negative effect on mineral flotation.

Several mine sites in Australia have introduced the use of saline water in their mineral processing practice. Base metal sulphide flotation plants at Mt Keith, Leinster and the Kambalda Nickel Concentrator in Western Australia use bore water with high ionic strength (Wang and Peng, 2014). Saline water is used at KCGM and Kanowna Belle for sulphide (gold ore) flotation. Saline or sea water is also used in many other flotation plants worldwide, including copper plants in Chile, gold-rich copper ore processing plants in Indonesia, and base metal sulphides flotation in South Africa (Castro 2012; Corin et al., 2011). In some cases (e.g., Kanowna Belle gold mine), the salinity of the water used in flotation can reach up to 200,000 ppm, which is several times higher than that of sea water.

The use of alternative water sources can bring positive or negative effects to the operation, but the effects can vary depending on the types of mineral target and gangue minerals. There is a general agreement that saline water enhances the flotation of gold and base metal-containing minerals (Moreno et al., 2011; Castro, 2012; Bicak et al., 2012; Corin et al., 2011; Miettunen et al., 2012; Shackleton et al., 2007; Wiese et al., 2007). The use of seawater has little or no effect on the flotation of pure chalcopyrite and pyrite, while it has a detrimental effect on the flotation of chalcocite and bornite. Bore water, on the other hand, results in significant recovery and grade improvement in the flotation of nickel sulphide ores such as pentlandite in Western Australia (Peng and Bradshaw, 2012). The flotation recovery

of coal generally increases with increasing concentration of inorganic electrolytes. Although the mechanisms by which saline water promotes flotation are not clear, the destabilisation of hydration layers surrounding the particles, inhibition of bubble coalescence, and the compression of the electrical double layer around particles have been proposed to explain the increased mineral flotation in saline water (Ricardo et al., 2016; Wang and Peng, 2014).

Adsorption of collectors is a prerequisite step to render or enhance the hydrophobicity of the target minerals in cases where the mineral is naturally hydrophilic or is less hydrophobic. Hencer et al. (2001) found that displacement of interfacial water molecules and penetration through the water structure around the particles should precede adsorption on the surface for collectors. The stability of the hydration layer around the particle can influence the probability of the approach of collectors. If the structure is strongly hydrogen bonded, it will be difficult to for the collector to reach the mineral surface and be absorbed. Some large inorganic ions such as K^+, I^-, Cs^+ and Br^- are known to disrupt the interfacial water structure around particles, while small ions such as Li^+, Na^+, Mg^{2+}, and Cl^- are considered as structure making ions. It was shown that the flotation of soluble salt minerals is reduced in the presence of structure making ions because these ions prevent the adsorption of collectors (Hencer et al., 2001). Thus, to understand the exact effect of various cations and anions, their individual and combined effects on water structure around the particle surface, zeta potential, surface hydrophobicity, and collector adsorption, particularly for REO and associated gangue minerals, need to be established.

The compression of the electrical double layer can give rise to changes in flotation results. In solution, particles have a surface charge according to their potential determining ions and layers, such as compact and diffusion layers around the particle, are formed for electrical equilibrium in solution. The potential at the phase boundary between the solution and the diffusion layer is called the zeta potential. The polarity and the charge around the particle are important factors to investigate the attractive or repulsive forces between particles, particle and bubble, and particles and reagents. Rao et al. (1988) found that the adsorption of a cationic collector was hindered by the reduced negative charge at the pyrochlore surface when cations such as Ca^{2+} and Mg^{2+} were in the pulp. An increase in malachite recovery was observed by higher aggregation due to a decrease in the absolute value of zeta potential caused by the addition of calcium chloride (Li et al., 2019).

Destabilisation of foams by the compression of the electrical double layer by electrolytes may reduce the repulsive force between the two opposing surfactant films (Bournival et al., 2014). It may also occur by compression of the surfactant tail group, which reduces their role of steric stabilisation of the foam lamellas (Schott, 1988). As above, it is evident that the electrical double layer should be taken into consideration to evaluate the effects of ions in the solution.

The inhibition of bubble coalescence by electrolytes results in a reduction in bubble size and the formation of stable froth. The probability of bubble-particle encounter increases with smaller bubble size. Marrucci and Nicodemo (1967) measured bubble size in the presence of different electrolytes, KCl, KOH, KNO, K_2SO_4, $CuSO_4$, K_3PO_4, $AlCl_3$ and $Co(NO_3)_2$, and showed that bubble coalescence was hindered by increasing the amount of salts. Froth stability is an important property, which can have a strong effect on flotation performance through phenomena involving carrying, entrainment, and drainage. Although low froth

stability reduces the recovery and grade of flotation significantly, excessive froth stability can also have detrimental effects through retarding drainage of entrained minerals, which may lead to higher gangue recovery (Subrahmanyam and Forssberg, 1988). The fact that inorganic ions result in stable froth is undesirable in rare earth flotation plants, where excessive froth stability is a major issue. It appears that high salt concentrations are not required to cause bubble coalescence inhibition and froth stability. Thus, it is necessary to determine the maximum tolerated salinity level without affecting froth stability and REO flotation recovery.

It is well known that the flotation behaviour of base metal and gold containing sulphides is completely different to that of rare earth minerals and other silicates. Thus, although observations such as the inhibition of bubble coalescence by some ions in water are transferable, the overall effects of water quality discussed above for other minerals do not necessarily apply to rare earth flotation. Some efforts have been made to understand the detrimental effects of ions induced by the dissolution of sparingly soluble gangue minerals such as dolomite, calcite, magnesite, and celestite. However, only limited studies have been carried out to investigate the effect of dissolved ions in saline water on flotation of rare earth bearing minerals.

For example, Wang et al., (2020a, 2020b) studied the flotation of bastnaesite using sodium oleate to investigate the effects of dissolved ions from gangue minerals such as barite and fluorite. It was suggested that Ca^{2+}, F^{-} and Ba^{2+} dissolved from the gangue minerals reduced the recovery of bastnaesite, probably due to the formation of insoluble oleate products with metallic ions. Flotation performance of monazite was investigated using a hydroxamic acid collector in the presence of different ions dissolved from calcite (Zhang et al., 2017; 2018). It was found that the Ca^{2+} ions in the solutions were detrimental to monazite recovery due to the preferential adsorption of calcium hydroxide on monazite surfaces, leading to a lower flotation recovery. Espiritu et al. (2019) also investigated the effects of dissolved ions from dolomite on monazite flotation using a density functional theory (DFT) simulation and found that Ca^{2+} and Mg^{2+} ions reduced the floatability of monazite due to the adsorption of calcium or magnesium carbonate/hydroxide on monazite and the precipitation of calcium or magnesium oleate.

However, there is no experimental research investigating the flotation performance of monazite with sodium oleate (a common collector for rare earth minerals) in the presence of different cations found in plant water. Therefore, the main focus of this study is to understand the flotation mechanisms of monazite with sodium oleate in the presence of different cations (Ca^{2+}, Mg^{2+}, Na^{+} and K^{+}) by integrating microflotation experiments with colloid and surface characterisations using zeta potential, XPS and UV adsorption.

3. Study Objectives

This research aimed to investigate the effects of various ionic species in water on the flotation performances of rare earth minerals. Although there is a consensus on the depressing effects of ionic species in bore water or recycled water on the flotation of rare earth minerals, the specific mechanism and the ions responsible for these detrimental effects have not been fully established. The specific objectives of this study are:

1) Quantify the effects of ions, such as Na^+, Ca^{2+}, Mg^{2+}, K^+, Cl^-, SO_4^{2-}, CO_3^{2-}, on the recovery and the final grade of rare earth minerals in a bench scale flotation cell
2) Evaluate the change of hydrophobicity on the mineral surfaces through wettability analysis with and without various ionic species, and its effect on flotation
3) Analyse the surface potential variation with and without ionic species and its correlation with flotation performance
4) Characterise the species distribution of collectors and ionic species expected to have detrimental effects
5) Investigate the change of pulp rheology with and without ionic species and the effects of froth stability on flotation performance
6) Study the adsorption mechanism of the collector on the mineral surface with and without ionic species
7) Suggest alternative water treatment processes which can mitigate the detrimental effects of ionic species on the flotation process.

4. Significance

The need to purify water for mineral processing unit operations could cost mining companies millions of dollars annually. Water treatment is particularly costly when the objective is to remove high concentrations of small ions such as Na^+, Ca^{2+} and Mg^{2+} by methods such as reverse osmosis. Given the large volume of processing water required in techniques such as flotation, it becomes financially unviable when considering the expansion of existing plants. Thus, the possibility of using process water that has undergone minimal treatment would have significant economic benefits in many mineral processing operations. In particular, Lynas Rare Earths Ltd and other REO processing companies will be direct beneficiaries of the outcomes of this project through reduced process water recycling costs, reduced chemical consumption, increased concentrate quality and higher process throughput. For example, if water treatment was avoided and recycled water was used for REO flotation, it is estimated that Lynas would save in excess of $6 million dollars annually at its Mt Weld operations.

Mining, manufacturing, and related industries use about 20% of all water consumed in Australia. Industrial water consumption by the mining industry in Australia has shown steady growth in the past and is likely to increase in the future. The industry discharges large quantities of wastewater into the environment, that requires proper management. Although many mining operations obtain water directly from groundwater, streams etc., water sources often need to be shared by multiple users. In remote areas where there is a scarcity of water, mining companies need to reduce their water usage to minimise impacts on the local community and the ecosystem.

The high dependence of the mining industry on water sources may lead to a range of environmental, social and economic risks. The perceptions of high water use at mines by local communities can cause tensions and conflict due to concerns about availability of water, security of their access to it and the potential for water contamination. Thus, there is an increasing pressure on mining companies to use water more efficiently by adopting new

technologies, more efficient processes, recycling and finding alternative sources of water. For example, Rio Tinto's Argyle Diamond Mine in the Kimberley region in Western Australia (WA) adopted water management strategies including recycling to reduce its freshwater consumption from Lake Argyle by 95%. Recycling of process water for further use would significantly reduce the impact of wastewater on the environment, in addition to the obvious economic benefits.

The ultimate goal of this project was to find ways of using recycled process water in mineral processing operations without compromising recovered value. This will be achieved by either counteracting the effect of impurities during processing and/or using cheaper treatment methods to make the recycled water suitable for processing. Although the project is focussed on one particular mine site, its findings could be applied to many operations in WA.

Section 2: Microflotation and Bench-scale Flotation Studies

5. Experimental Design: Microflotation and Bench-scale Flotation Studies

5.1 Feed for single mineral microflotation tests

Microflotation and bench-scale flotation experiments were conducted to investigate the impacts of water quality on rare earth mineral flotation. Monazite (67% purity) ore was received from Western Australia. The XRD spectrum of the monazite-bearing ore is given in Figure 3. Monazite was ground with a mortar and pestle and screened to collect the -75 +38 µm size fraction for the microflotation, adsorption test and XPS analysis. XRF analysis showed that the major rare earth elements in monazite were 25.86% CeO_2, 13.2% La_2O_3, 10.91% Nd_2O_3, 2.81% Pr_6O_{11}, 1.28% Sm_2O_3 and traces (i.e. less than 0.5%) of other rare earth elements such as samarium and yttrium.

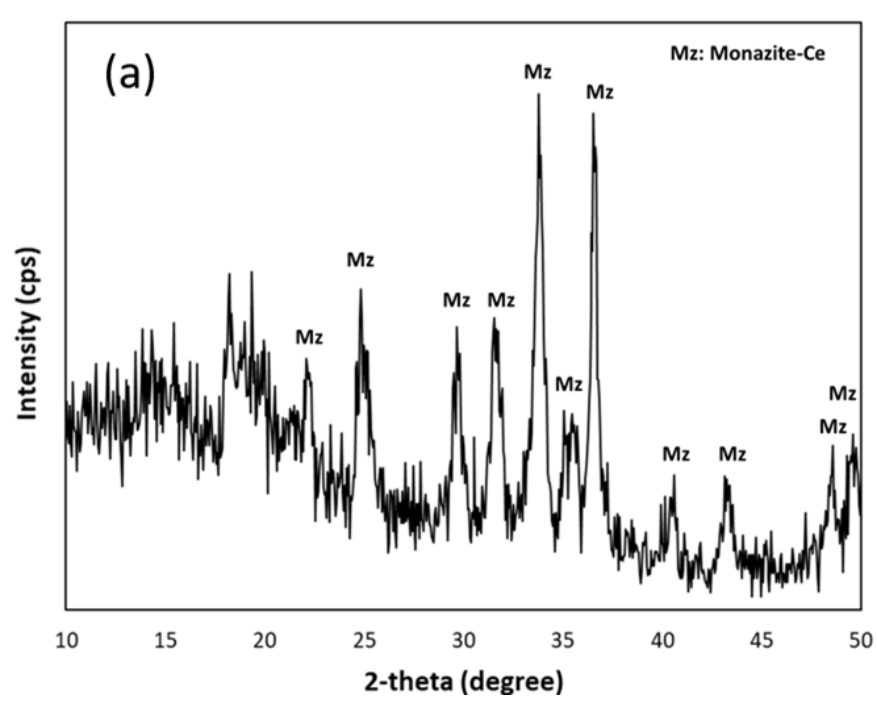

Figure 3. *XRD of monazite sample.*

5.2 Feed ore characteristics for bench scale tests

The rare earth ore was provided by Lynas Rare Earths Ltd (Lynas) in Western Australia. Table 2 shows the elemental composition of the ore characterised by XRF with a total REO grade of 9.8%. The mineralogical composition of the feed ore was determined using QEMSCAN as shown in Table 3. The most dominant RE minerals were monazite group minerals, and the most important gangue minerals were iron oxide minerals such as goethite and limonite. The distribution of mineral liberation classes of the monazite group minerals after grinding (D80 −38 µm) and their images are provided in Figure 4. As shown, more than

70% of the monazite group minerals were highly liberated (>60%) and 5.7% of those minerals were locked in gangue minerals.

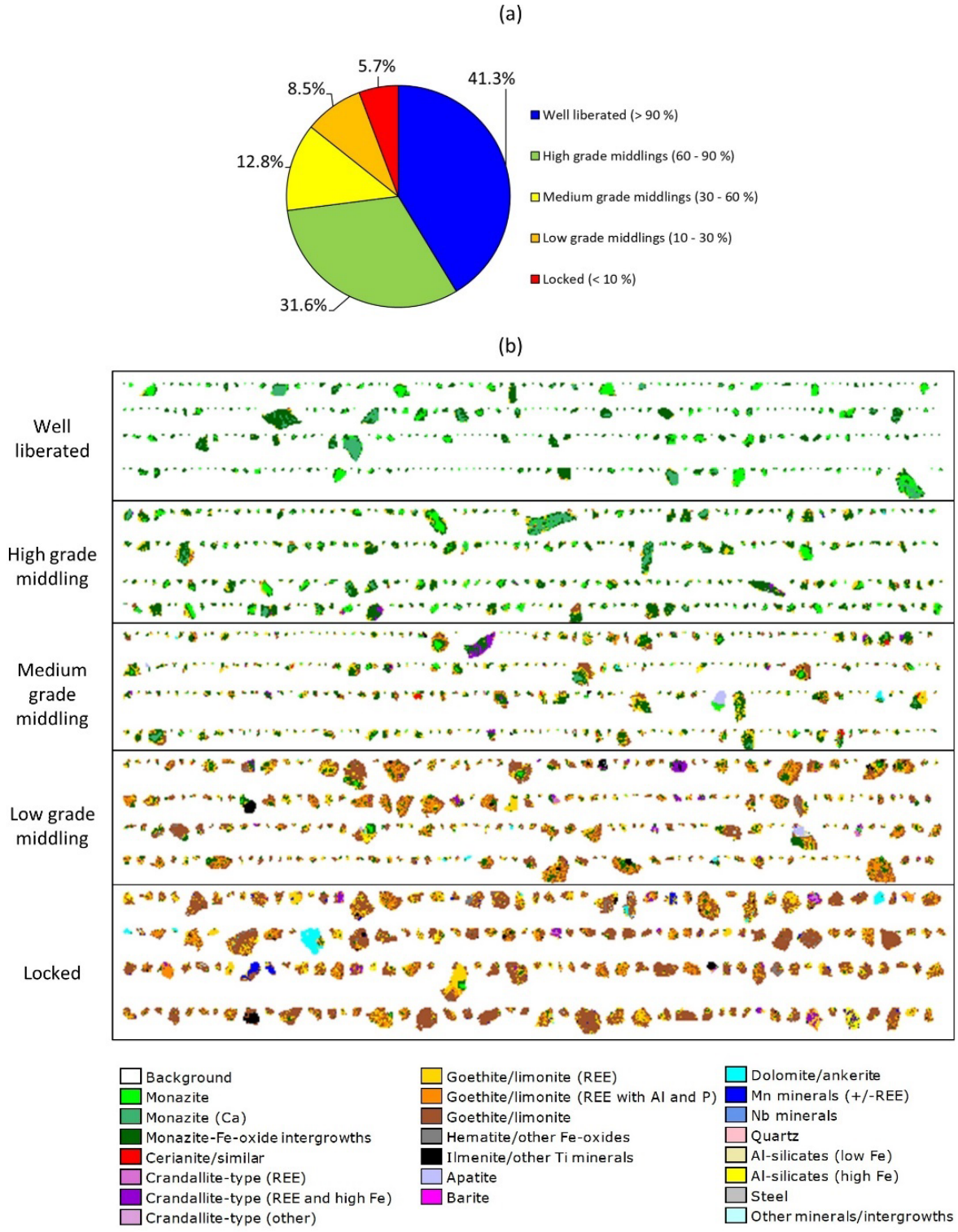

Figure 4. *Mineral liberation of monazite group minerals analysed by QEMSCAN; (a)the distribution of liberation classes and (b) image grid showing mineral liberation of monazite group minerals.*

Table 2. *Chemical composition of rare earth ore by XRF.*

Elements	**Fe_2O_3**	**SiO_2**	**Al_2O_3**	**P_2O_5**	**MnO**	**CaO**	**TiO_2**	**MgO**
Contents (%)	52.73	6.63	5.57	5.18	1.585	1.47	1.229	1.22
Elements	CeO_2	La_2O_3	Nd_2O_3	Pr_6O_{11}	Nb_2O_5	Sm_2O_3	Y_2O_3	Gd_2O_3
Contents (%)	4.38	2.35	2.062	0.494	0.317	0.264	0.125	0.103

Table 3. *The feed mineralogy analysed using QEMSCAN.*

Mineral	Mass %
Monazite	2.8
Monazite (Ca)	2.4
Monazite−Fe−oxide intergrowths	10.2
Cerianite/similar	0.5
Crandallite−type (REE)	0.5
Crandallite−type (REE and high Fe)	1.2
Crandallite−type (other)	0.1
Goethite/limonite (REE)	9.4
Goethite/limonite (REE with Al and P)	4.2
Goethite/limonite	51.6
Hematite/other Fe−oxides	3.7
Ilmenite/other Ti minerals	3.4
Apatite	0.9
Barite	0.1
Dolomite/ankerite	2.2
Mn minerals (+/−REE)	2.0
Nb minerals	0.2
Quartz	0.9
Al−silicates	2.9
Other minerals/intergrowths	0.6
TOTAL	100.0

5.3 Chemicals

Various chemicals were used during the grinding and flotation experiments. During grinding, Na_2SiO_3 depressant (44% in solution, Bisely Pty Ltd, Australia) and NaOH (99%, Chem−supply Pty Ltd., Australia) were used. The flotation chemicals used were Sylfat FA2 collector (Kraton Corporation, USA), diesel (>95%, Puma Energy, Australia), HCl (99% purity, Chem−Supply Pty Ltd, Australia), NaOH (99%, TCI America Inc., America), $CaCl_2$ (AR grade, Chem−supply Pty Ltd, Australia), and $MgCl_2.6H_2O$ (AR grade, Chem−supply Pty Ltd, Australia) and Na_2SiO_3 depressant (44% in solution, Bisely Pty Ltd). The chemical composition of Sylfat FA2 collector is given in Table 4. It should be noted that diesel was used in this study to enhance the solubility of fatty acid collectors.

The UV−vis adsorption experiments were carried out using the following reagents: copper nitrate (95% purity, Univar solutions), triethylenetetramine (60% purity, Sigma−Aldrich, America), ethanolamine (98% purity, Sigma Aldrich, America), isobutanol (99% purity, Sigma Aldrich, America), cyclohexane (95% purity, Univar solutions, America) and diethylammonium diethyldithiocarbamate (97% purity, Sigma Aldrich, America).

Table 4. *Chemical composition of the FA2 Syflat collector*

Species	Oleic acid	Linoleic acid	Palmitic acid	Stearic acid	Others	FA2 Sylfat
wt. %	54.31	30.64	5.28	7.65	2.12	100

5.4 Microflotation experiments

Flotation tests were conducted to investigate the influence of water quality on the flotation performance of monazite. Before the flotation experiments, the ground mineral sample (monazite) was mixed with water to obtain a 1% solid ratio. Synthetic water with various concentrations of $CaCl_2$, $MgCl_2$, NaCl and KCl was prepared in this study. The mineral samples were conditioned for 5 min using 2×10^{-4} mol/L of sodium oleate collector (99% purity, TCI America), different concentrations of sodium silicate depressant (98% purity, Redox Pty Ltd) and 30 ppm MIBC frother (98% purity, Orica Limited). It should be noted that sodium silicate was added considering that this reagent is typically used to depress gangue minerals during rare earth flotation. The pH of the solutions was modified using NaOH and HCl. The conditioned pulps were transferred to a 90 mL modified Partridge-Smith flotation column (25 mm in diameter and 180 mm in length) (Partridge and Smith, 1971) as seen in Figure 5. Magnetic stirring was used at the bottom of the flotation column to provide particle mixing in the cell; the speed of the magnetic bar was 400 rpm. Air was introduced at the bottom of the column through a fritted glass disk at a flow rate of 50 mL/min. All concentrates were collected after 3 min of flotation time. Each experiment was repeated three times, with a standard deviation of less than 5%. These experiments were conducted at 22±1^{o}C.

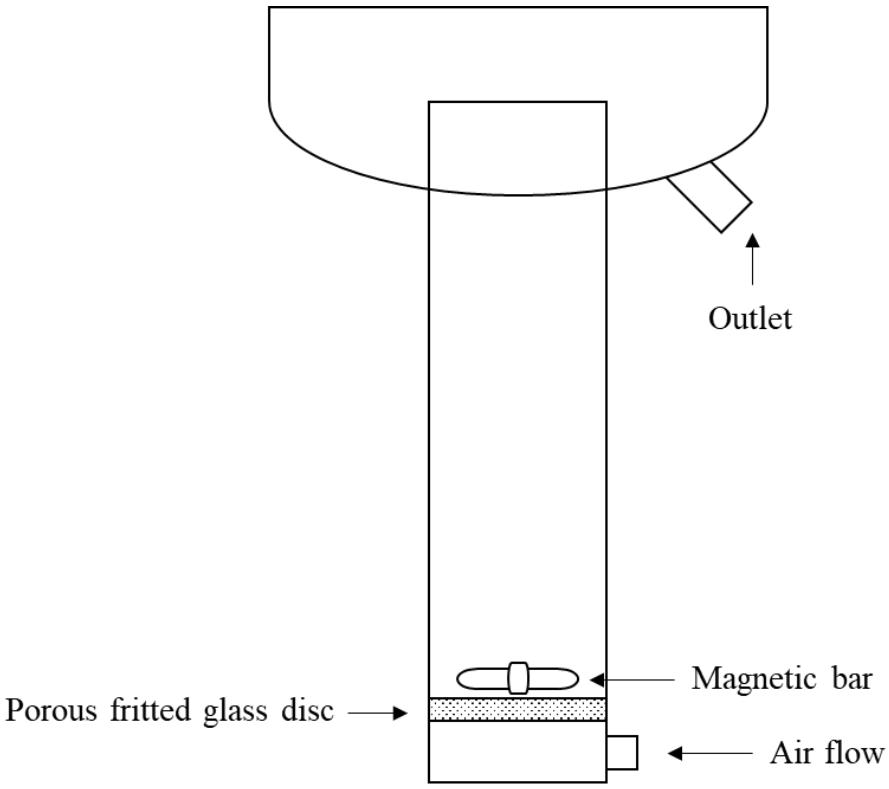

Figure 5. *Microflotation column cell schematic.*

5.5 Methods for bench-scale flotation experiments

One kilogram of the ore was wet ground in a rod mill (Labtech Essa Pty Ltd., Australia) to achieve 80% passing 38 µm (Figure 6). During grinding, 1000 mL of tap water (Kalgoorlie, Australia) was used with 3800 g/t of sodium silicate depressant and 1800 g/t of sodium hydroxide to achieve pH 10. It should be noted that the tap water, analysed by ICP−OES, contained 26.19 mg/L of Ca^{2+} and 11.33 mg/L of Mg^{2+}.

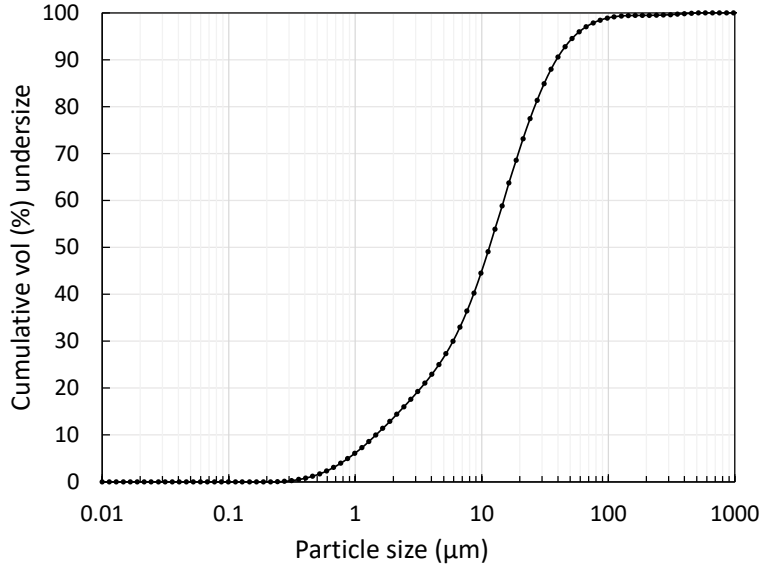

Figure 6. *Particle size distribution of ore sample after grinding.*

Figure 7 shows the experimental procedure for each flotation stage. As seen in Figure 7, after grinding, one roughing stage was conducted followed by three scavenging stages. The flotation concentrate was collected from the roughing and all the scavenging stages and then two cleaning stages were performed to collect the final flotation products.

The roughing and scavenging stages were conducted using a 5 L flotation cell (ESSA® FTM101, FLSmidth) while the cleaning stages were performed using a 3 L flotation cell (ESSA® FTM101, FLSmidth). Stirring speed was 900 rpm in the case of the 5 L flotation cell and 700 rpm in the case of the 3 L flotation cell. The air flow rate was 2.5 L/min during all the experiments. During the cleaning stage, the solids percentage was lower than during the roughing and scavenging stages if a 5 L cell was used; thus, the rare earth recovery was reduced in the cleaning stage, probably due to the reduced solids percentage and a lower probability of bubble−particle collisions. This means, in the cleaning stage, it is very important to maintain a higher solids percentage, which is possible to achieve in a smaller cell (i.e., 3 L cell), and thus increase flotation recovery of rare earths. The solids percentage in the first cleaning stage was around 20% while that in the second cleaning stage was around 10%.

Table 5 presents the chemicals used in the grinding stage and each flotation stage. All experiments were performed using synthetic water obtained by mixing tap water and different concentrations of $CaCl_2$ or $MgCl_2$, and the pulp pH was maintained at pH 10 in each flotation stage. Each flotation stage was conditioned for 4 min and then the flotation concentrates were collected for 2 min in the roughing stage and the first scavenging stage, 3 min for the second and third scavenging stage, and 3.5 min for the cleaning stages (see Figure 7). All concentrates and tailings were filtered, weighed and assayed using XRF.

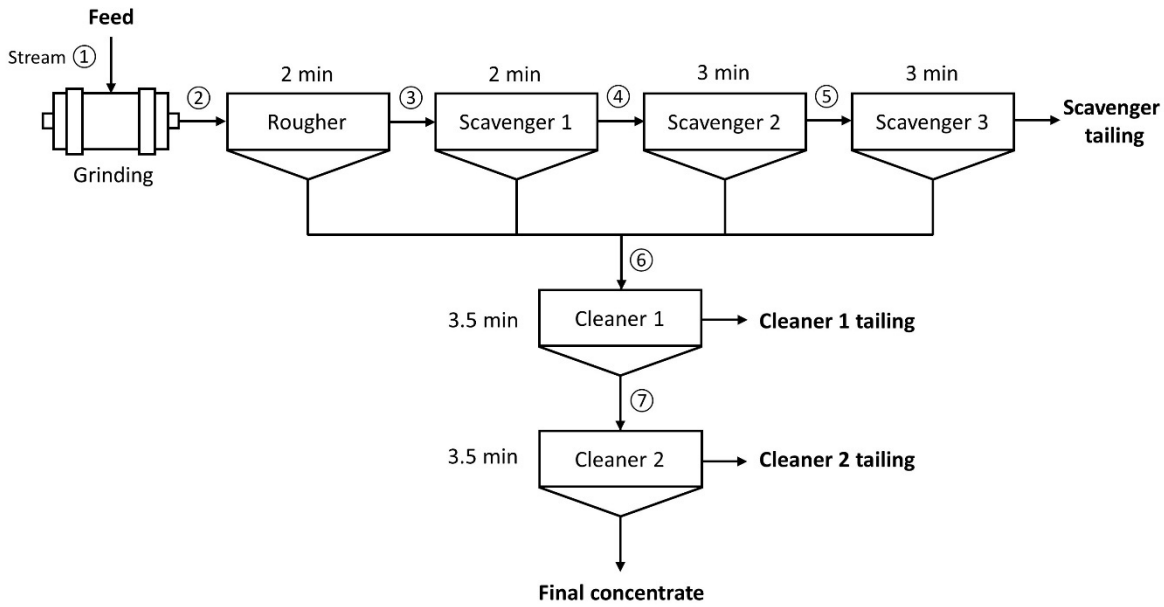

Figure 7. *The procedure for bench flotation experiments.*

Table 5. *Reagent scheme for bench flotation experiments.*

Stream	Na_2SiO_3 (g/t)	NaOH (g/t)	Diesel (g/t)	Sylfat FA2 (g/t)
1	3,800	1,800	–	–
2	–	–	1,100	2,200
3	–	–	350	700
4	300	400	200	400
5	–	–	–	–
6	600	200	350	700
7	300	100	–	–

5.6 Zeta potential experiments

Zeta potential experiments were carried out using a Malvern NanoZ zeta sizer (Malvern, UK). Mineral samples were ground using a mortar and pestle and screened through 10 µm sieves to collect the undersize fraction. Before zeta potential experiments, the samples were conditioned for 15 min at 0.1% solids ratio in the presence of 1×10^{-4} mol/L NaCl as a background electrolyte. The conditioning procedure was similar to the flotation experiments. The pH of the solution was adjusted with HCl and NaOH solution. After conditioning, large particles were allowed to settle down from the suspension. Then, the supernatant was collected and transferred to a zeta potential measurement cell. All the tests were conducted in triplicate, and the mean value of measurement was used for further analysis.

5.7 Adsorption experiments

The adsorption experiments were carried out by the solution depletion method (Gregory, 1966). The solution was centrifuged at 4000 rpm to separate solution from solid particles and the clear supernatants were used for experiments. This method is based on mixing oleate solutions, copper – triethylenetretramine mixture (copper nitrate, 95% purity, Univar solutions; triethylenetetramine, 60% purity, Sigma Aldrich; ethanolamine, 98% purity, Sigma Aldrich), and 20% isobutanol (99% purity, Sigma Aldrich) and 80% cyclohexane solvent (95% purity, Univar solutions) (Gregory, 1966). The solution mixture was allowed to stand for 10 minutes to allow the two separate liquid phases to separate. Finally, the organic phase was transferred to a test tube and 2 drops of diethylammonium diethyldithiocarbamate dye (97% purity, Sigma Aldrich) were added to colour the organic phase. The maximum absorbance of the organic phase was determined at 435 nm wavelength with a UV-visible spectrophotometer (Lambda35, PerkinElmer, USA) which agrees well with the literature (G.R.E.C., Gregory, 1966). Based on the maximum absorbance values, the calibration curve was determined as seen in Figure 8. The adsorption kinetics using the monazite-oleate

system showed that adsorption equilibrium was achieved after 2 min as seen in Figure 9. Thus, the duration of all the adsorption experiments using monazite was 2 min. The specific surface area for monazite was 0.1028 m^2/g.

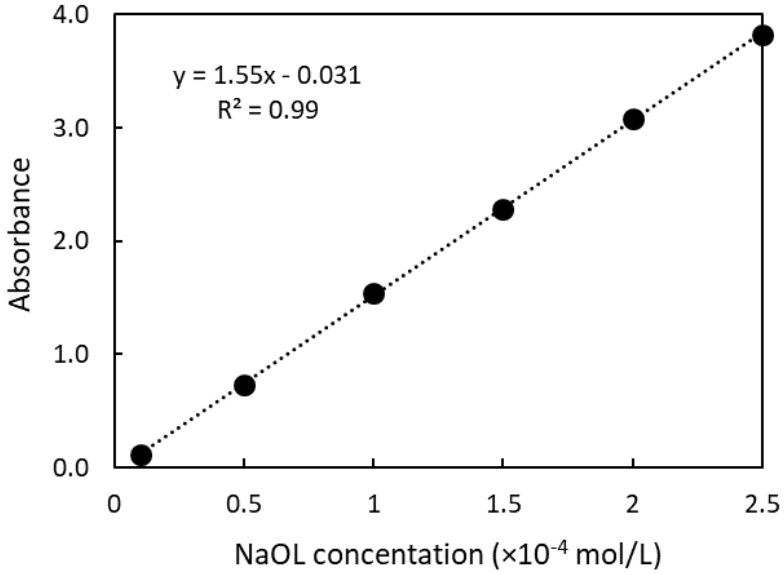

Figure 8. *Standard curve fitting using the absorbance at 435 nm wavelength of different concentration of oleate solutions.*

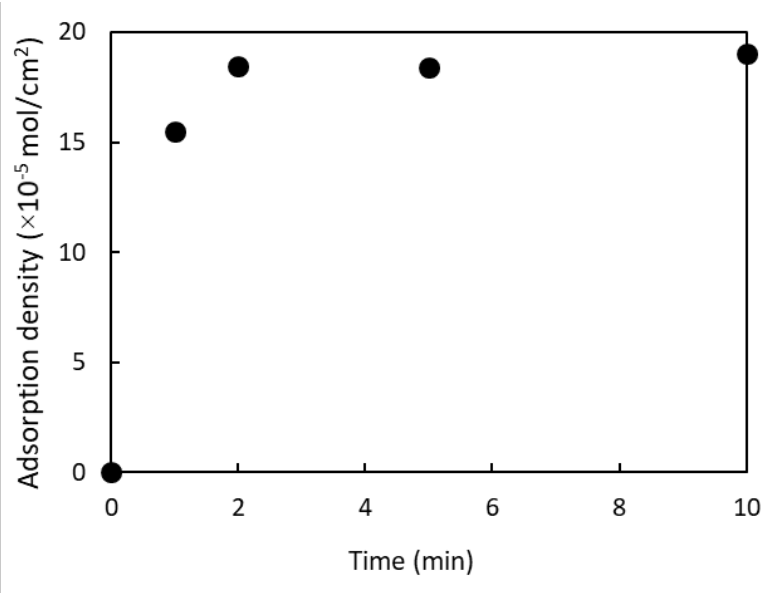

Figure 9. *Adsorption kinetics tests of monazite using 2 × 10^{-4} mol/L sodium oleate.*

5.8 X-ray photoelectron spectroscopy (XPS) analysis

XPS analysis was carried out to investigate the effects of $CaCl_2$ and $MgCl_2$ on surface changes of monazite. The mineral sample was conditioned in a similar manner to the procedure used for the flotation tests. After conditioning, samples were filtered and washed using deionised water followed by drying in a desiccator under vacuum at room temperature

for 24 hours. The XPS analysis was carried out with a Kratos Axis Supra instrument (Kratos Analytical, UK) using monochromatic Al K_α radiation (1486.7eV) at 225 W. The spectral data were processed using CasaXPS software and the C 1s binding energy of 284.8eV was used to calibrate the spectrum.

5.9 Rheological measurements

The rheological properties of the flotation pulp were measured using a DV1 MLV digital viscometer (Brookfield, USA). The flotation pulp, collected in the roughing stage, was used for the rheological measurements. For each measurement, 16 mL of the conditioned pulp was introduced into the UL adapter, which is ideal for low viscosity materials, using the LV4 spindle. A rheogram was produced using a shear rate ranging between 0.612 s^{-1} and 122.3 s^{-1}. All rheological measurements were performed at room temperature (25 ± 2 °C).

5.10 Entrainment experiments

The flotation experiments were conducted without using a collector to determine the non−selective recovery of particles. The same method was used to prepare the flotation pulp as in the bench scale flotation experiment. The ground slurry was placed into a 2 L mechanical flotation cell and tap water was added to create a solids concentration of 22%. The pulp was agitated at 600 rpm for 5 min with different anions using the same reagents as those used in the flotation experiments. Then, 30 mg/L of MIBC was added to create the froth phase. The air flow rate was 10 L/min and synthetic water was added during the experiments to maintain the slurry level. The froth phase was collected at intervals of 1, 2, 5, 10 and 15 min by scraping every 10 s, and the mass of the slurry and dried samples were measured to calculate the water recovery and mass recovery.

5.11 Settling experiments

The settling behaviour of a flotation feed slurry was investigated in the presence and absence of anions used in the flotation experiments. The feed slurry was prepared after wet grinding (50% solids); 500 mL of the slurry was collected and conditioned with different types of anions for a period of 10 min. The conditioned feed slurry was then introduced into 500 mL graduated cylinders. The slurry was left undisturbed for 144 h to allow settling of particles, and photographs were taken for analysis.

5.12 DLVO (Derja−guin−Landau−Verwey−Overbeek) theory calculation

The interaction energy between fine particles was calculated based on DLVO theory, which is a widely used model that explains the stability and interaction between colloidal particles in various electrolytes. The total interaction energy (E_{tot}) was given as the sum of the van der Waals forces (E_{vdw}) and the electrostatic forces (E_{edl}) between two particles as presented in Eq (1).

$$E_{tot} = E_{vdw} + E_{edl} \quad (1)$$

The van der Waals interaction energy E_{vdw} between two particles is determined by Eq (2).

$$E_{vdw} = -\frac{A}{6H}\left(\frac{R_1 R_2}{R_1+R_2}\right) \quad (2)$$

where, R_1 and R_2 are the particle size and H (m) is the distance between two particles. A is the effective Hamaker constant of interaction between particles in aqueous medium, which can be calculated using Eq (3).

$$A = (\sqrt{A_m} - \sqrt{A_w})^2 \quad (3)$$

where A_m is the Hamaker constant of goethite (1.9×10^{-19} J) or monazite (3.8×10^{-20} J) in water and A_w is the Hamaker constant of H_2O (3.7×10^{-20} J) in vacuum.

The electrostatic interaction force was determined by using Eq (4).

$$E_{edl} = \pi\varepsilon_0\varepsilon_r\left(\frac{R_1 R_2}{R_1+R_2}\right)(\psi_1^2+\psi_2^2)\left\{\frac{2\psi_1\psi_2}{\psi_1^2+\psi_2^2}\ln\left[\frac{1+\exp(-\kappa H)}{1-\exp(-\kappa H)}\right] + \ln[1-\exp(-2\kappa H)]\right\} \quad (4)$$

where ε_0 is the dielectric constant in vacuum (8.854×10^{-12} C^2/Jm), ε_r is the dielectric constant of medium (78.5 C^2/Jm), ψ_i is the zeta potential of the mineral for i (i=1, 2), and κ is the thickness of the electric double layer, which was calculated using Eq (5).

$$\kappa^{-1} = \sqrt{\frac{\varepsilon_0\varepsilon_r k_B T}{e^2\sum_i n_i z_i^2}} \quad (5)$$

where k_B is the Boltzman constant (1.38×10^{-23} J/K), T is the absolute temperature (298 K), e is the elementary electric charge (1.602×10^{-19} C), Z_i is the valence of the ion i, and n_i is the number of ions of type i per unit volume in the bulk solution, which was calculated by using Eq (6).

$$n_i = C_i \times N_A \times 1000 \quad (6)$$

where C is the molar concentration of ion i (mol/L), N_A is the Avogadro constant (6.023×10^{23} /mol).

6. Results and Discussion: Microflotation and Bench-scale Flotation Studies

6.1 Single mineral microflotation experiments of monazite

6.1.1 Effect of pH and sodium silicate

Flotation experiments were conducted using pure water systems to benchmark performance (i.e., recoveries) in the absence of ionic species. Figure 10 shows the influence of pH on monazite recovery in distilled water using oleate. As seen in Figure 10a, the maximum monazite recovery was achieved at pH 8, probably due to the highest concentration of oleate ions at this pH; thus, all the experiments were conducted at pH 8. This agrees well with the results obtained by some authors (A.M. Abeidu, 1972; Pavez and Peres, 1993; Cheng et al., 1993; Espiritu and Waters, 2018). There was a slight decrease in recovery of monazite in the presence of sodium silicate (Figure 10(b)); sodium silicate is typically added during rare earth flotation to depress oxide minerals and thus this chemical was also used in this work to simulate the chemical conditions during flotation of monazite from its ore (Pavez and Peres, 1993).

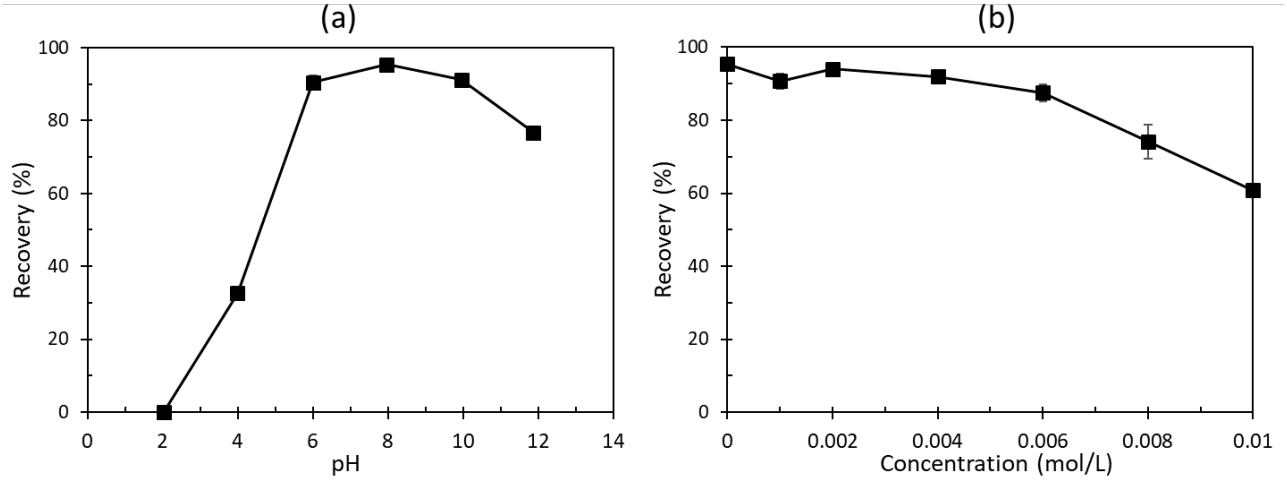

Figure 10. *Effect of (a) pH and (b) sodium silicate at pH 8 on the recovery of monazite in the presence of 2×10^{-4} M sodium oleate*

6.1.2 Effect of Ca^{2+}, Mg^{2+}, K^{+} and Na^{+} on flotation

Figure 11(a) shows that an increase in Ca^{2+} ions resulted in a low flotation recovery of monazite, probably due to the formation of calcium oleate precipitate, reducing the concentration of oleate ions in solution. As a result, less oleate ions were adsorbed on monazite surfaces, reducing the flotation recovery of monazite. Similar observations were also found in the presence of Mg^{2+} ions as shown in Figure 11(b). However, Mg^{2+} ions were less detrimental for monazite flotation than Ca^{2+} ions.

The presence of Na^{+} and K^{+} ions slightly reduced monazite flotation recovery as seen in Figures 11(c) and 11(d). The reason for this is that the oleate concentration in solution did not change significantly with increasing in Na^{+} and K^{+} concentration (see Figure 12).

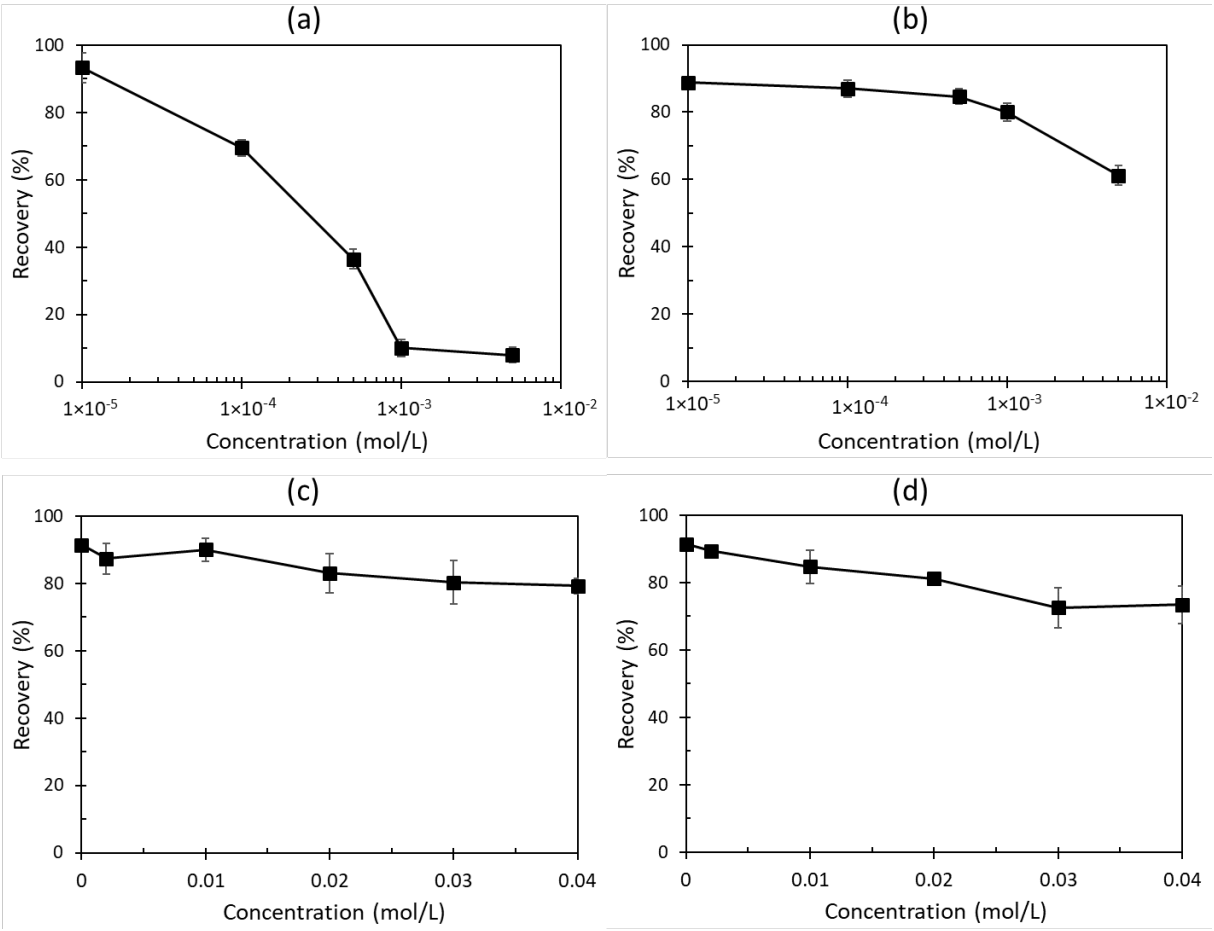

Figure 11. *Effect of (a) Ca^{2+}, (b) Mg^{2+}, (c) Na^{+} and (d) K^{+} ions on the recovery of monazite in the presence of 6×10^{-3} mol/L sodium silicate and 2×10^{-4} mol/L sodium oleate at pH 8.*

6.1.3 Flotation solution chemistry of oleate in presence of Ca^{2+}, Mg^{2+}, Na^{+} and K^{+}

Flotation performance of monazite in the presence of different ions is affected by solution chemistry. For this reason, it is important to determine the concentration of oleate ions in the presence of Ca^{2+}, Mg^{2+}, Na^{+}, and K^{+} (see Figure 12). As seen in Figure 12, the concentration of oleate was significantly reduced from the initial concentration of 2.0×10^{-4} mol/L in the presence of Ca^{2+} due to the formation of insoluble calcium oleate; the solubility product of calcium oleate is very low ($K_{sp} = 10^{-15.4}$). A similar effect was also observed in the presence of Mg^{2+}, however, the concentration of oleate in the presence of Mg^{2+} was higher than that in the presence of Ca^{2+}. The reason for this is that the solubility product of magnesium oleate ($K_{sp} = 10^{-13.8}$) is 40 times higher than that of calcium oleate. The presence of Na^{+} and K^{+} ions did not reduce the concentration of oleate ions in solution, considering that sodium oleate and potassium oleate have a very high solubility product ($K_{sp} = 10^{-5.92}$).

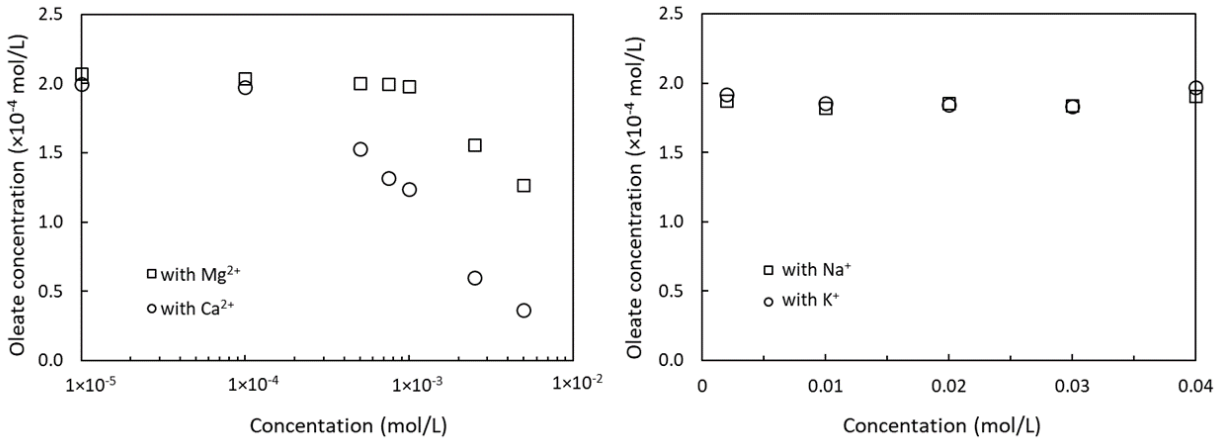

Figure 12. *Oleate concentration in the presence of Ca^{2+}, Mg^{2+}, Na^{+} or K^{+} and 6×10^{-3} mol/L sodium silicate.*

Figure 13 shows the changes in the free energy of formation of calcium oleate, magnesium oleate, potassium oleate and sodium oleate as a function of pH. Figure 13 also shows the free energies of formation of calcium oleate and magnesium oleate were much lower than the free energies of formation of potassium oleate and sodium oleate, demonstrating that the formation of calcium oleate and magnesium oleate was much more favourable than the formation of sodium and magnesium oleate.

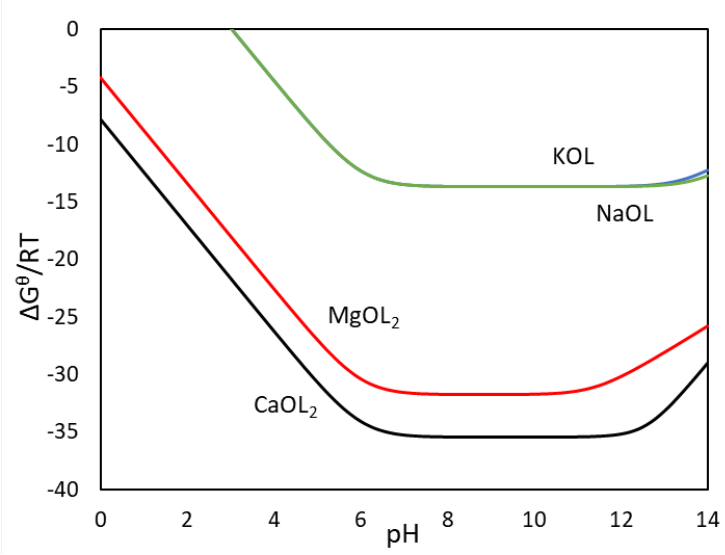

Figure 13. *The free energy of the reaction between ions and oleate ions as a function of pH*

The standard Gibbs free energy of formation (ΔG^{θ}) between different ions and oleate ions was calculated as follows:

$$\Delta G^{\theta}_{M^{n+}} = RTln(K_{sp}\alpha_{(M^{n+})}\alpha^{n}_{(OL^{-})}) \quad (1)$$

$$M^{n+} + OL^{-} = M(OL)_{n}, \quad K_{sp} = [M^{n+}][OL^{-}]^{n} \quad (2)$$

where R is the universal gas constant (8.306 J/(molK)), T is the temperature in K and Ksp is the solubility product of metallic oleate.

The reaction coefficients ($\alpha_{(\mathrm{OL^-})}$, $\alpha_{(\mathrm{M^{n+}})}$) were calculated as follows:

$$H^+ + OL^- = HOL, \qquad K^H = \frac{[HOL]}{[H^+][OL^-]} \tag{3}$$

$$\alpha_{(OL^-)} = 1 + K^H[H^+] \tag{4}$$

$$\alpha_{(M^{n+})} = 1 + \beta_1[OH^-] + \beta_2[OH^-]^2 + \cdots + \beta_n[OH^-]^n \tag{5}$$

where $\mathrm{K^H}$is the dissociation constant of oleic acid, $\alpha_{(\mathrm{OL^-})}$ is the protonation constant, $\alpha_{(\mathrm{M^{n+}})}$ is the hydrolysis coefficient of metallic ions, and β_n is the cumulative stability constant (ß$_1$ for Ca^{2+}, Mg^{2+}, Na^+ and K^+ are 1.4, 2.58, 0.2, 0.5, respectively; ß$_2$ for Ca^{2+}, Mg^{2+} are 2.77 and 1, respectively).

6.1.4 Zeta potential of monazite in distilled water

Figure 14 shows that the zeta potential of monazite in distilled water was higher than that in the presence of oleate due to the adsorption of oleate ions on monazite surfaces. There was no significant difference in the zeta potential of monazite in the presence of oleate and silicate ions compared to that in the presence of oleate ions only. This means that the adsorption of oleate ions on monazite was more significant than the adsorption of silicate ions on the same mineral, and that silicate ions do not appear to interfere with oleate adsorption on monazite.

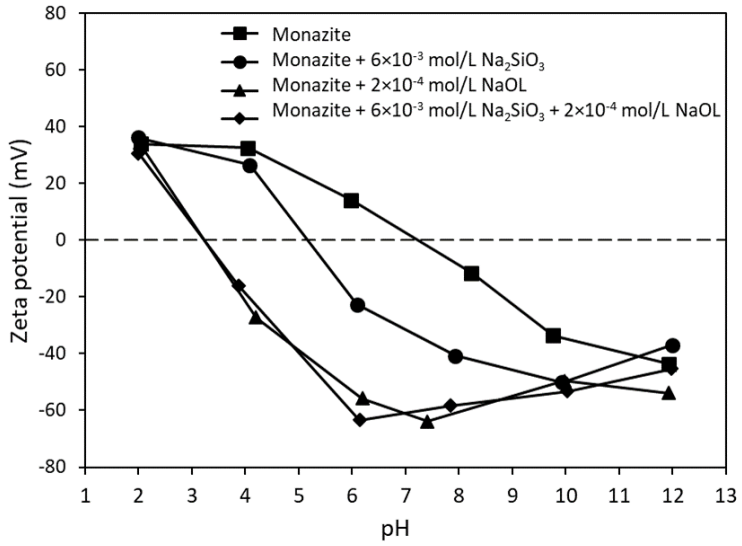

Figure 14. *Zeta potential of monazite as a function of pH before and after conditioning in 2× 10^{-4} mol/L NaOL and 6×10^{-3} mol/L Na_2SiO_3, respectively.*

6.1.5 Effect of Ca^{2+}, Mg^{2+}, Na^{+} and K^{+}

Figure 15 shows the influence of different cations on the zeta potential of monazite. As seen in Figure 15, the increase in concentrations of all cations made the zeta potential of monazite less negative due to the adsorption of monovalent or divalent cations on monazite surfaces. In the case of divalent cations, different metal ion species are formed in solution (Ca^{2+} and $CaOH^{+}$ ions; Mg^{2+} and $MgOH^{+}$ (see Figure 16)) while in the case of monovalent cations, one type of metal ion is formed in solution (Na^{+} and K^{+}). This means that the ionic strength of solutions in the presence of divalent ions is higher than that of monovalent ions (e.g., when the solution concentration of monovalent or divalent ions is 0.005 mol/L, the ionic strength of solutions containing divalent ions is 0.015 mol/L and that of solutions containing monovalent ions is 0.005 mol/L); the ionic strength is calculated using the well-known equation:

$$Ionic\ strength = \frac{1}{2}\sum_{i=1}^{n} c_i z_i^2 \quad (6)$$

Where c_i is the concentration of ion (mol/L), and z_i is the ion charge.

Considering that solutions with divalent metal ions have higher ionic strength than solutions with monovalent metal ions, the same shift in zeta potential was achieved with a larger shift of monovalent metal ion concentrations and a lower shift of divalent ion concentrations. For example, a change of zeta potential from -60 mV to -40 mV of monazite was achieved when the concentration of NaCl or KCl changed from 0 to 0.02 mol/L; the same change in zeta potential was accomplished when the concentration of $CaCl_2$ or $MgCl_2$ changed from 0 to 0.0005 mol/L.

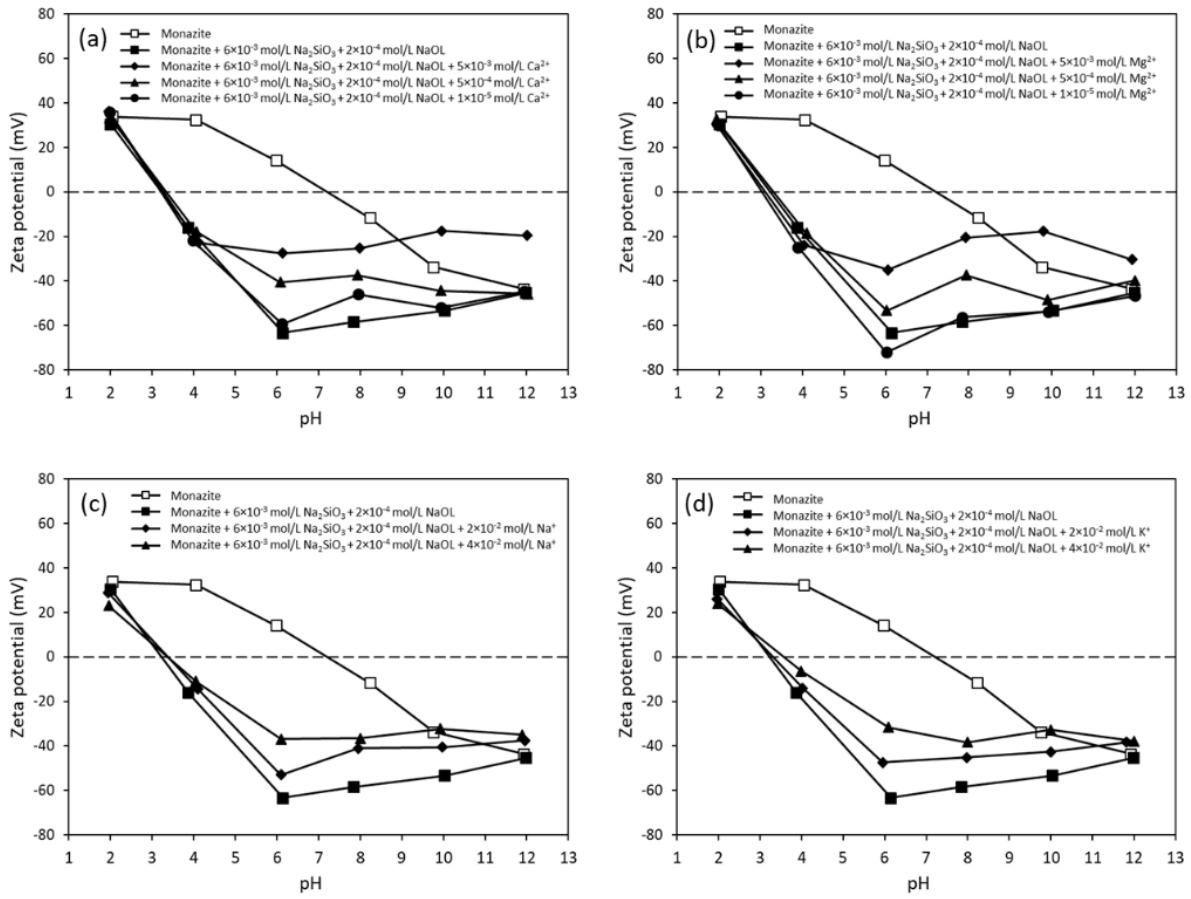

Figure 15. *Effects of different concentration of (a) Ca^{2+}, (b) Mg^{2+}, (c) Na^{+}, and (d) K^{+} on the surface potential of monazite*

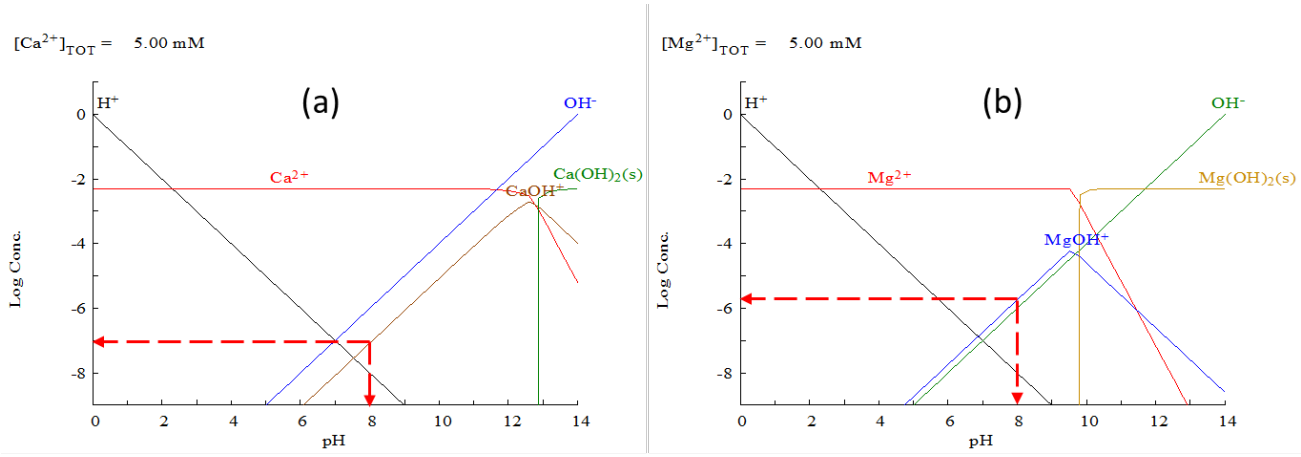

Figure 16. *LogC-pH diagram of (a) calcium and (b) magnesium species; the calculations were performed using Medusa open-source software.*

6.1.6 Adsorption of oleate on monazite

Figure 17 shows the influence of both monovalent and divalent ions on the adsorption of oleate on monazite surfaces. As seen in Figure 17, the increase in Ca^{2+} concentration resulted in reduced adsorption of oleate due to the formation of insoluble calcium oleate (Figure 17(a)). The same trend was also observed in the presence of Mg^{2+} (Figure 17(b));

however, the adsorption of oleate in the presence of Ca^{2+} was significantly lower than that in the presence of Mg^{2+}. The increase in Na^{+} or K^{+} concentration did not affect oleate adsorption, considering that these monovalent ions do not react with oleate ions (Figure 17(c) and Figure 17(d)).

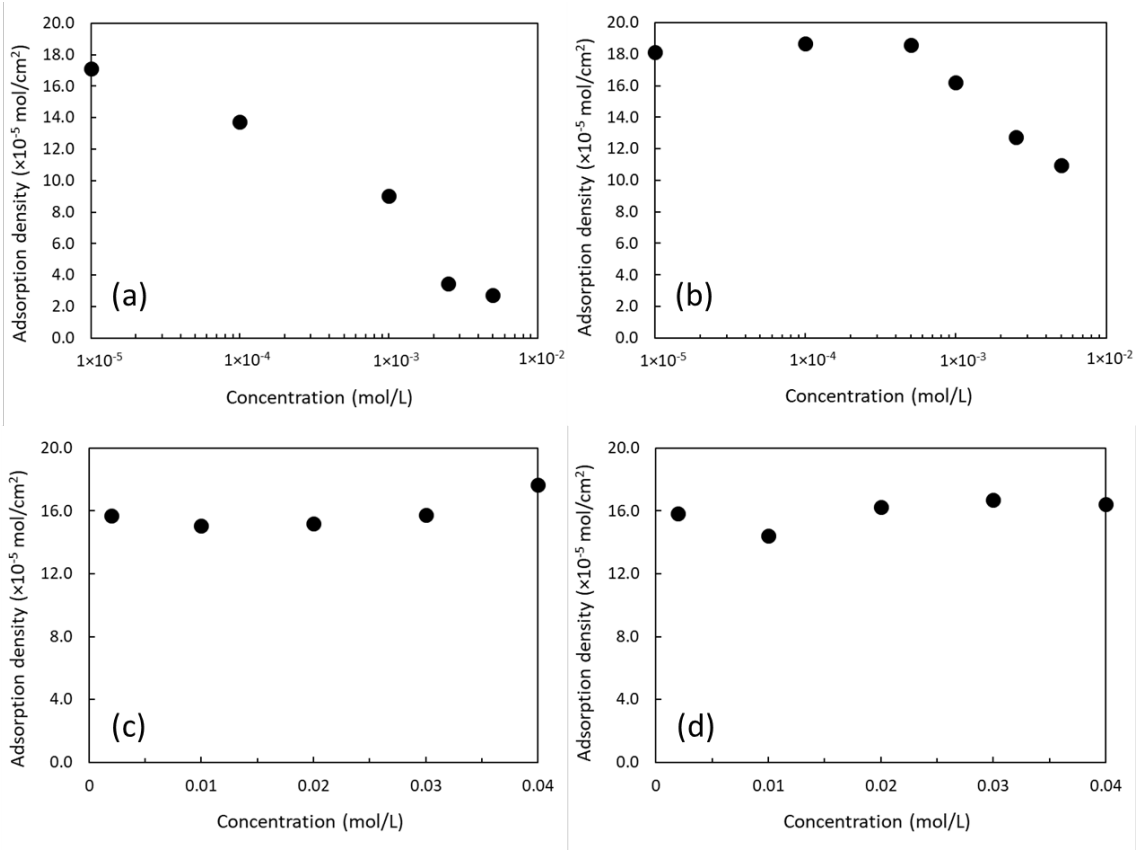

Figure 17. *Effects of (a) $CaCl_2$, (b) $MgCl_2$, (c) NaCl, and (d) KCl on the adsorption density of oleate on monazite in the presence of 2×10^{-4} mol/L sodium oleate and 6×10^{-3} mol/L sodium silicate.*

6.1.7 XPS analysis of monazite surface

Table 6 and Figure 18 show that when monazite particles were conditioned in the presence of sodium oleate in distilled water, the percentage of carbon (C 1s) on monazite surfaces was the highest, probably due to high adsorption of oleate, which agrees well with the adsorption results obtained in this work. The percentage of carbon on monazite surfaces was lower in the oleate solutions in the presence of Ca^{2+} or Mg^{2+}, probably due to the lower adsorption of oleate. This observation agrees well with our adsorption data (see Figure 17). Table 6 also shows that the presence of Ca^{2+} led to slight adsorption of Ca^{2+} or calcium oleate. A similar trend was also observed in the presence of Mg^{2+} due to the adsorption of Mg^{2+} or magnesium oleate.

Table 6. *Elemental composition on the surface of monazite before and after conditioning*

	Monazite + NaOL	Monazite + Na_2SiO_3 + NaOL + $CaCl_2$	Monazite + Na_2SiO_3 + NaOL + $MgCl_2$
C 1s	16.99%	10.84%	9.94%
O 1s	58.13%	66.57%	65.27%
Ca 2p	1.92%	2.24%	1.87%
Mg 1s	1.45%	1.46%	1.96%
Al 2p	2.84%	2.22%	2.48%
Ce 3d	5.66%	4.99%	5.65%
La 3d	3.15%	2.72%	3.12%
P 2p	9.06%	8.41%	8.99%

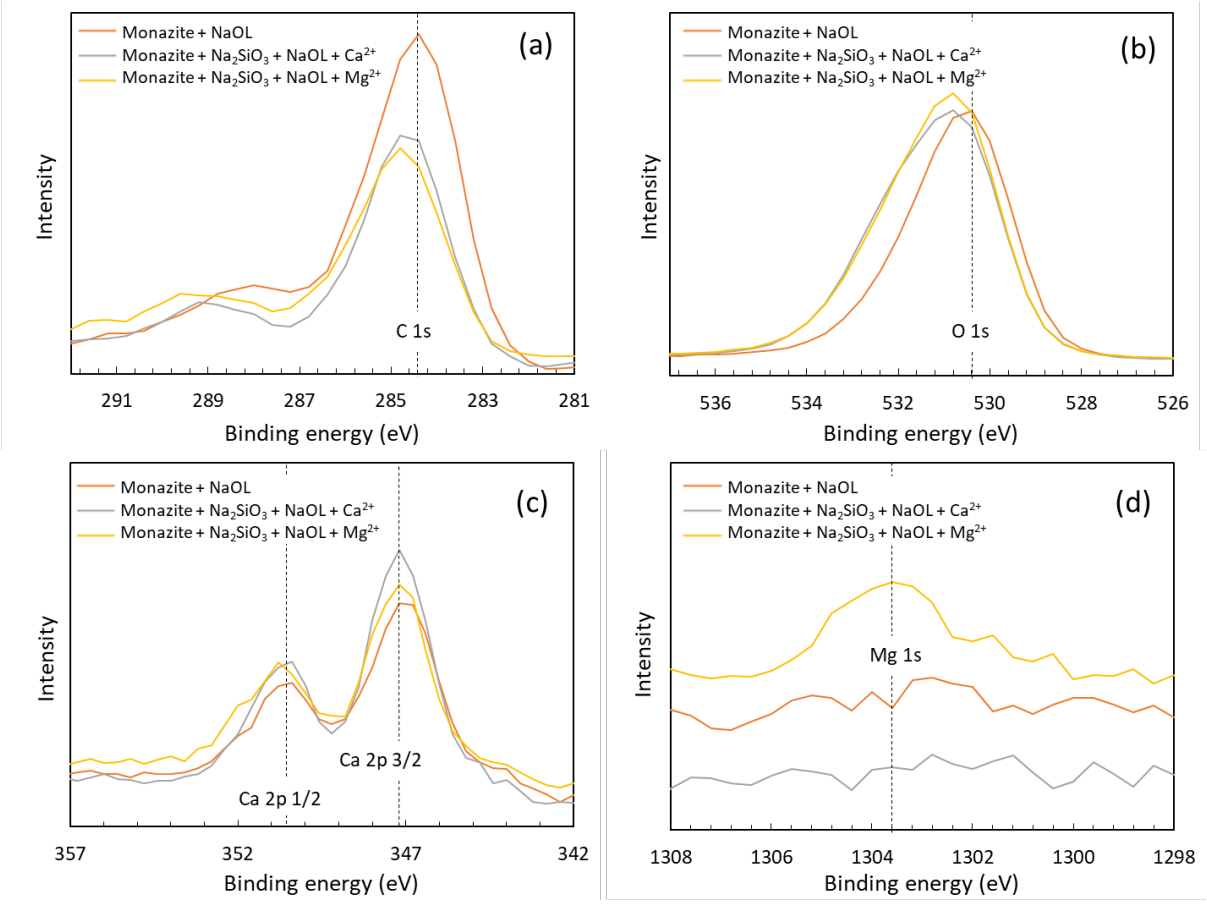

Figure 18. *XPS spectra of monazite conditioned in 2×10^{-4} mol/L sodium oleate, 6×10^{-3} mol/L sodium silicate, 5×10^{-3} mol/L calcium chloride, or 5×10^{-3} mol/L magnesium chloride; (a) C 1s, (b) O 1s, (c) Ca 2p, (d) Mg 1s.*

6.1.8 Conclusions

This study investigated the monazite flotation mechanism with an oleate collector in the presence of different ions (Ca^{2+}, Mg^{2+}, Na^{+}, and K^{+}) by integrated microflotation and surface characterisation analysis using zeta potential, XPS and UV adsorption. It was found that the presence of Mg^{2+} or Ca^{2+} were highly unfavourable to monazite flotation due to the formation of insoluble oleate products with divalent metal ions, leading to less adsorption of oleate ions on monazite surfaces and hence reduced flotation recovery of monazite. The presence of Na^{+} or K^{+} influenced the flotation recovery of monazite slightly, considering that these ions do not react with oleate ions. All these results were confirmed using adsorption experiments, XPS analysis and zeta potential measurements.

6.2 Effect of divalent cations on bench-scale flotation of Mt Weld ore

Figure 19 shows the effect of divalent cations (Ca^{2+} or Mg^{2+}) on the recovery of RE minerals (Figure 19a) and FeO minerals (Figure 19c) and the grade of these minerals (Figure 19b and Figure 19d) in the presence of fatty acids and sodium silicate at pH 10. As seen in Figure 19a, the recovery of RE minerals was greatly reduced in the presence of divalent cations, when the concentrations of $CaCl_2$ or $MgCl_2$ were higher than 100 mg/L, particularly during the cleaning stage of flotation considering that in this stage, the grade of RE minerals is the highest (see Figure 19b). Figure 19 also shows that the increase in concentration of

divalent cations resulted in a higher FeO recovery, especially in the roughing and scavenging stage because in this stage, the grade of FeO minerals is the highest (see Figure 19d). The results also indicate that the flotation performance deteriorated more in the presence of $MgCl_2$ than $CaCl_2$.

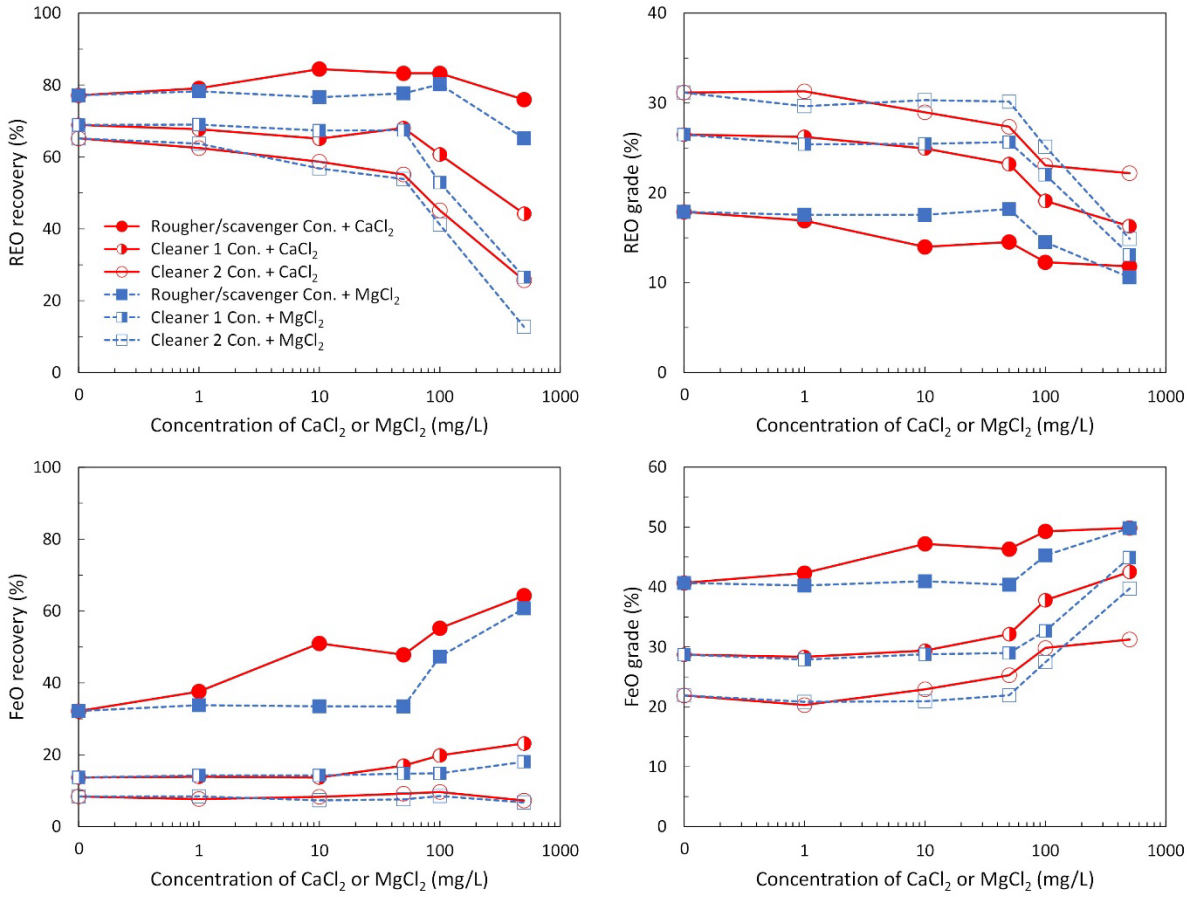

Figure 19. *The effect of $CaCl_2$ and $MgCl_2$ on (a) REO recovery (b) REO grade, (c) FeO recovery, and (d) FeO grade.*

6.2.1 Proposed flotation mechanism

Figure 20 shows the proposed adsorption mechanism on RE minerals after grinding and before flotation in the presence and absence of divalent cations. As seen in Figure 20a and Figure 20c, after grinding, silicates are rarely adsorbed on monazite surfaces while the opposite is true in the case of fatty acids, based on the results obtained in our previous work using pure monazite in distilled water (Jung et al., 2022). Figure 20b shows that silicate ions are adsorbed on FeO surfaces during grinding, which agrees well with the literature (Dietzel, 2002; Jorden et al., 2007; Hansen et al., 1994; Swedlund et al., 1999; Davis et al., 2002; Yang et al., 2008) and thus oleate ions cannot be adsorbed on FeO surfaces as shown in Figure 20d. A similar finding was reported by Qi et al. (1993), where the presence of adsorbed silicate on hematite surfaces hindered the adsorption of oleate.

When divalent cations are added to the flotation pulp during conditioning (Figure 20e), in the case of monazite, divalent cations react with the fatty acid collector, leading to the formation of insoluble products (e.g., $Ca(RCOO)_2$ or $Mg(RCOO)_2$) thus reducing the amount of available fatty acid collector ions in the pulp (Araujo and Lima, 2017). This is also supported

in our previous work using pure monazite (Jung et al., 2022). Therefore, the increase in divalent cations reduced the REO recovery (see Figure 19a).

In the case of FeO minerals, added divalent cations react with the adsorbed silicate ions and act like a bridge between oxygen atoms of adsorbed silicate and carboxylate ions, increasing adsorption of fatty acid collector ions and thus recovery of FeO mineral. This mechanism was observed in the case of magnetite (Potapova et al., 2010; Dixon, 1985) and it is hypothesised that a similar mechanism occurs on FeO minerals. It means that the higher the concentration of divalent cations, the higher the recovery of FeO (see Figure 19c).

Figure 19 also shows that the recovery of RE minerals and FeO minerals are higher in the presence of Ca^{2+} than that in the presence of Mg^{2+}. It means that both RE minerals and iron minerals are more hydrophobic in the presence of Ca^{2+} than in the presence of Mg^{2+}. The reason is that Ca^{2+} binds more strongly to oxygen atoms in fatty acid collector ions than Mg^{2+} (see Figure 21), considering that the solubility product of calcium oleate is 40 times lower than that of magnesium oleate (Jung et al., 2022). By contrast, magnesium atoms prefer binding to oxygen atoms in silicate depressant ions than calcium atoms (see Figure 21) because the solubility product of magnesium silicate precipitate is significantly lower than that of calcium silicate (Yuehua et al., 2003; Nied et al., 2016).

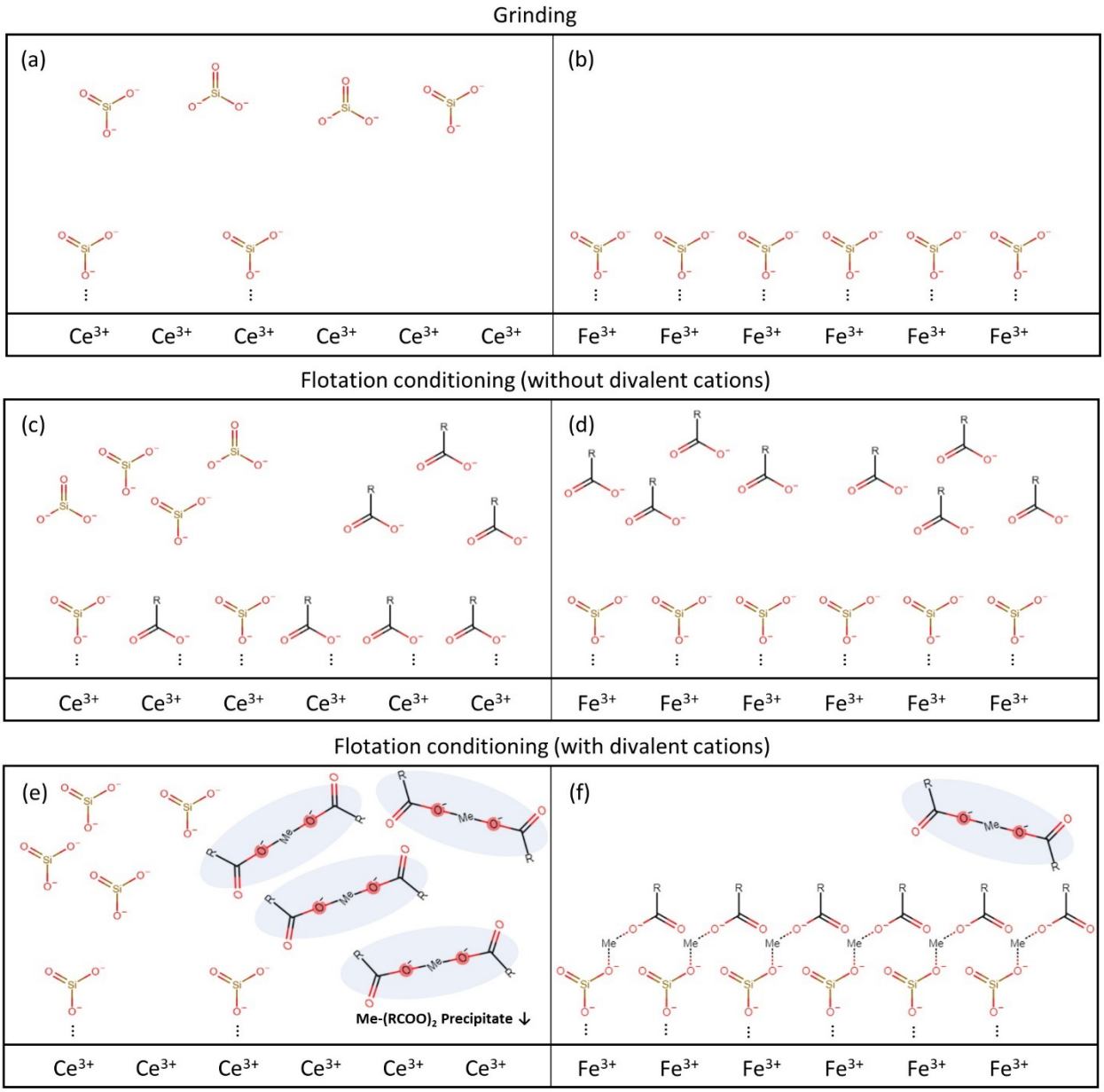

Figure 20. *The adsorption mechanism of silicate, divalent cations and carboxylate ion (Me denotes divalent cations such as Ca^{2+} and Mg^{2+}).*

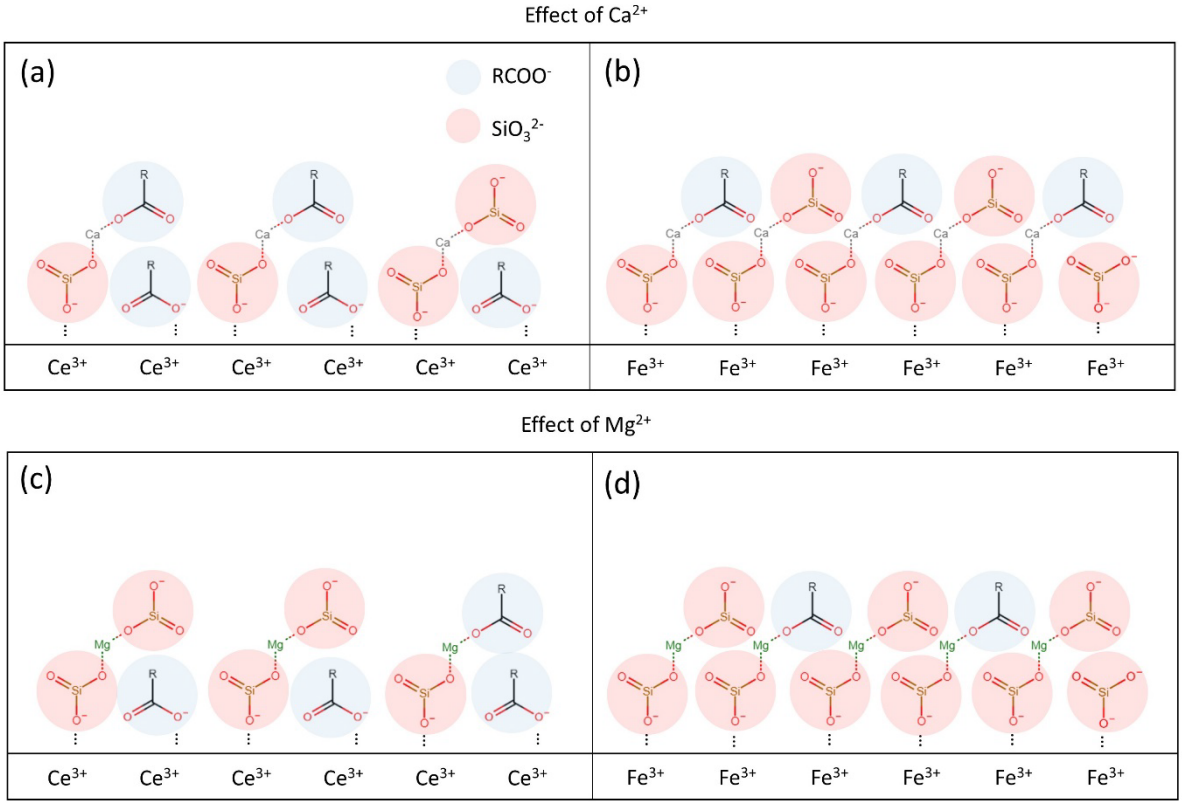

Figure 21. *The effect of Ca^{2+} or Mg^{2+} on the synergistic adsorption of silicate ions and fatty acid ions on RE minerals and iron oxide mineral surfaces; the effect of Ca^{2+} on the (a) RE mineral and (b) iron oxide mineral surface, and the effect of Mg^{2+} on the (c) RE mineral and (d) iron oxide mineral surface.*

6.2.2 Effect of divalent cations on fatty acid concentrations

Figure 22 presents the influence of different concentrations of divalent cations, Ca^{2+} and Mg^{2+}, on the concentration of fatty acids in the flotation pulp at pH 10. The results show that when the concentration of $CaCl_2$ or $MgCl_2$ is less than 100 mg/L, the concentration of dissolved fatty acid collector remains unchanged. However, when the concentration of $CaCl_2$ or $MgCl_2$ increased beyond 100 mg/L, the concentration of dissolved fatty acid collector decreased significantly, leading to a lower flotation recovery of RE minerals (see Figure 19). This is probably because at lower concentrations of Ca^{2+} and Mg^{2+} ions, the added divalent ions are adsorbed onto the mineral surfaces. At higher concentrations of these cations, the amount of added divalent ions can exceed the maximum adsorption capacity of the mineral surfaces. As a result, some of the Ca^{2+} or Mg^{2+} cations may remain in solution, as shown in Figure 24. Therefore, the reduction in fatty acids concentration in the flotation pulp was a result of the creation of insoluble compounds, such as $Ca(RCOO)_2$ or $Mg(RCOO)_2$, with extremely low solubility products, leading to the low Gibbs free energies (see Figure 23). It should be noted that the following calculation assumed a reaction between oleate ions and cations; detailed calculations are provided in the supplementary materials.

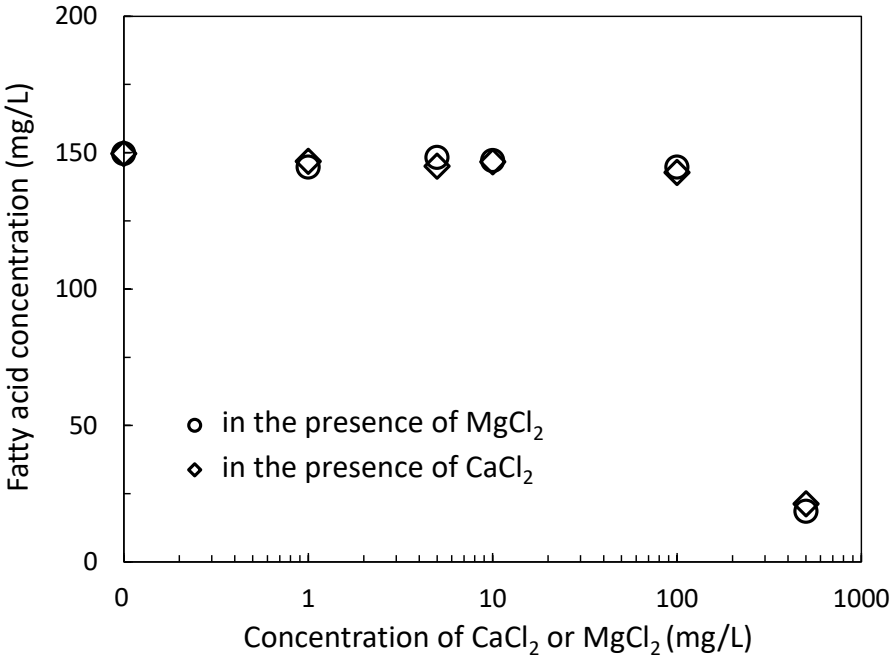

Figure 22. *Effects of $CaCl_2$ and $MgCl_2$ concentrations on the fatty acids concentration.*

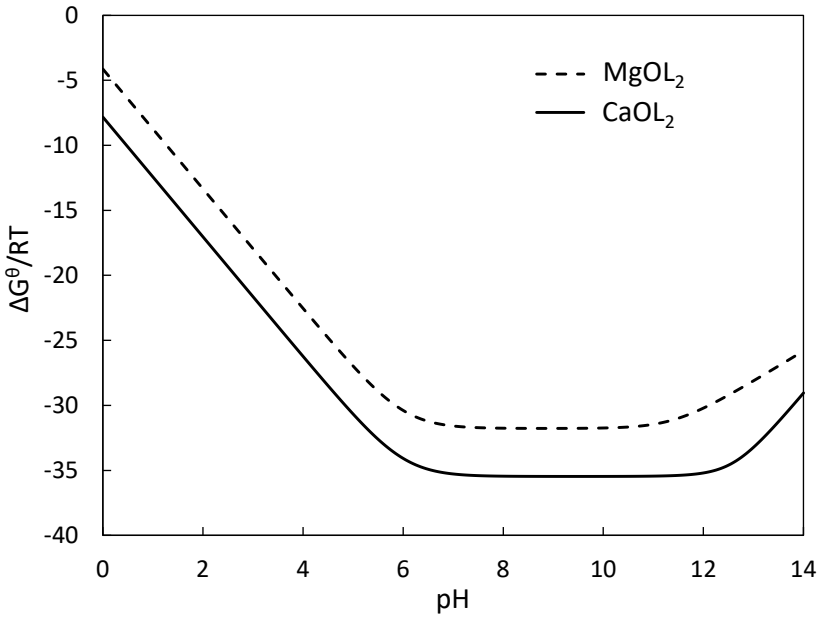

Figure 23. *The free energy of the reaction between oleate ions and cations such as Ca^{2+} and Mg^{2+} by pH (Jung et al., 2022).*

6.2.3 Effect of divalent cations on sodium silicate concentrations

Figure 24 shows the impact of adding $CaCl_2$ and $MgCl_2$ on the concentrations of divalent cations in the rougher feed for concentrations ranging from 1 mg/L to 500 mg/L. The results demonstrate that when the concentration of $CaCl_2$ or $MgCl_2$ is less than 100 mg/L, an increase in divalent cations in the flotation pulp does not lead to a corresponding increase in the flotation pulp. This suggests that divalent cations are being adsorbed on the mineral surfaces, which may be due to silicate ions already being adsorbed during grinding. The

added divalent cations can then react with the adsorbed silicate to form silicate salts ($CaSiO_3$ or $MgSiO_3$) on the mineral surfaces. However, at $CaCl_2$ or $MgCl_2$ concentrations above 100 mg/L, a significant number of divalent cations can be found in the flotation pulp, and fatty acid ions may react with these cations.

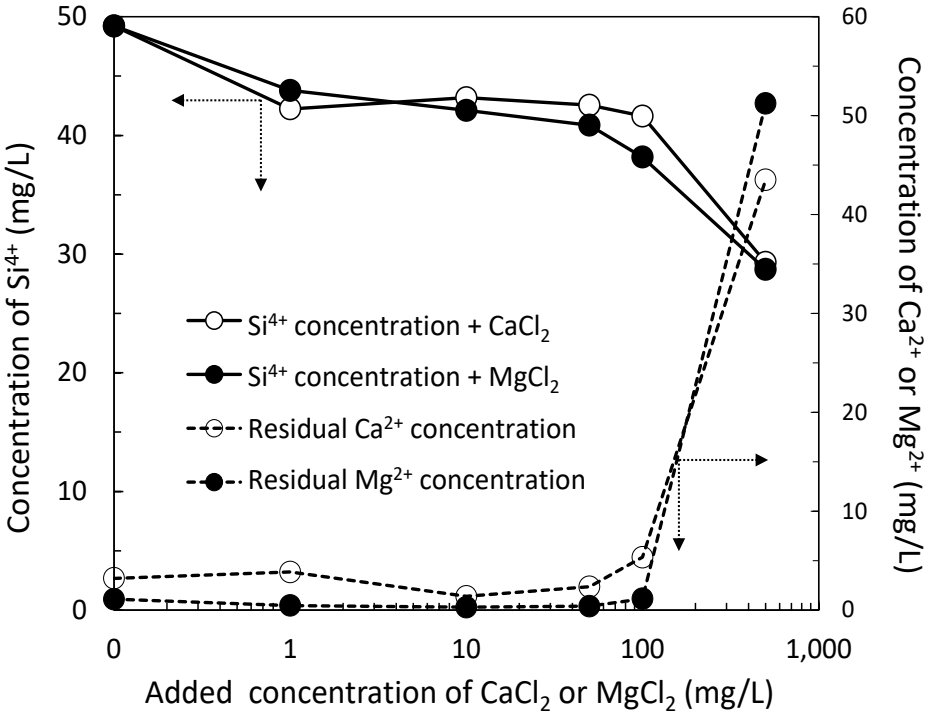

Figure 24. *The residual concentration of Si^{4+} (primary axis) and divalent cations (secondary axis) in the presence of different concentrations of $CaCl_2$ and $MgCl_2$ in the flotation pulp.*

Figure 25 shows the Si^{4+} concentration measurements obtained in the presence of Ca^{2+} and Mg^{2+} ions in deionised water at pH 10. As illustrated in Figure 25, the concentration of Si^{4+} gradually decreased with increasing Ca^{2+} and Mg^{2+} concentration. The experimental results confirm that the concentration of Si^{4+} decreases more significantly in the presence of Mg^{2+} ions than Ca^{2+} ions. Moreover, almost all Si^{4+} ions were depleted from the solution when 500 mg/L Mg^{2+} ions were present, whereas some Si^{4+} ions remained in the presence of 500 mg/L Ca^{2+} ions. This observation is consistent with the species distribution diagrams (i.e., calcium−silicate, and magnesium−silicate systems) shown in Figure 26, which indicate that $Mg_3Si_4O_{10}(OH)_2$ was more prevalent than $CaSiO_3$. Thus, the results suggest that the binding of silicate ions is more favourable to Mg^{2+} ions than to Ca^{2+} ions.

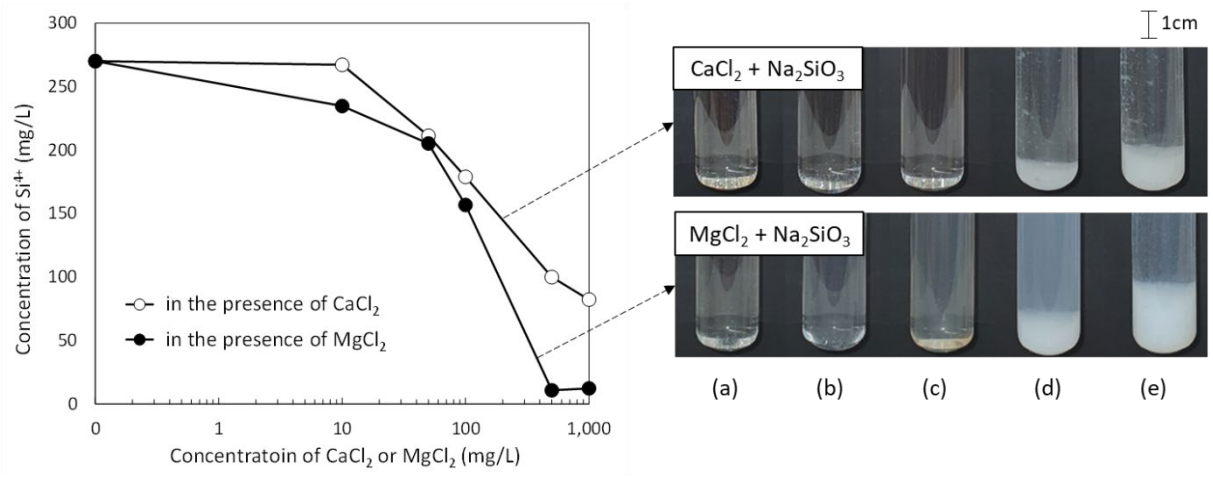

Figure 25. *Sodium silicate solution behaviour with the initial concentration of 1000 mg/L when the concentration of $MgCl_2$ or $CaCl_2$ is (a) 10 mg/L, (b) 50 mg/L, (C) 100 mg/L, (d) 500 mg/L, (e) 1000 mg/L.*

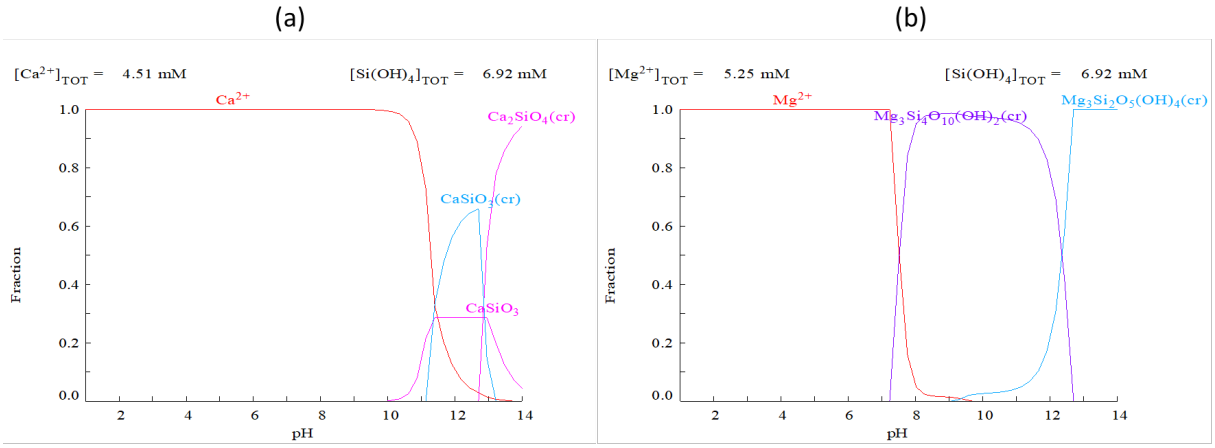

Figure 26. *The species distribution diagram for calcium−silicate and magnesium−silicate system.*

Figure 27 illustrates the changes in the free energy of formation (ΔG^{θ}) between divalent ions and SiO_3^{2-} ions as a function of pH. As shown in Figure 27, the free energy of formation for $Mg_3Si_4O_{10}(OH)_2$ was significantly lower than that for $CaSiO_3$, indicating that the formation of $Mg_3Si_4O_{10}(OH)_2$ was much more favourable than the formation of $CaSiO_3$ at pH 10. These findings are supported by measurements shown in Figure 25, which demonstrate that Mg^{2+} ions tend to consume more Si^{4+} ions than Ca^{2+} ions. Detailed calculations are provided in the supplementary materials.

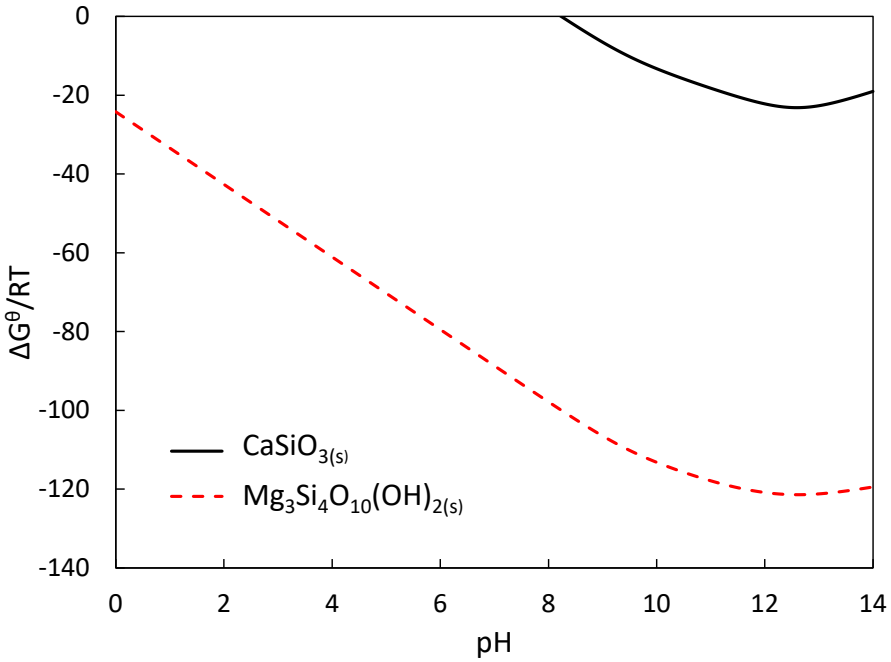

Figure 27. *The free energy of the reaction between divalent ions and silicate ions as a function of pH.*

6.2.4 Effects of $CaCl_2$ and $MgCl_2$ on the viscosity of flotation pulp

The rheological properties of flotation pulp are crucial for determining flotation performance. High pulp viscosity can reduce flotation efficiency by decreasing the motion of particles and bubbles and increasing bubble coalescence and thus reducing the probability of particle and bubble collision (Sajjad and Otsuki, 2022; Becker et al., 2013). Therefore, in this study, rheological measurements were carried out to investigate the effect of Ca^{2+} and Mg^{2+} on rheological properties of flotation pulps.

Figure 28 presents the impact of $CaCl_2$ and $MgCl_2$ on flotation pulp rheology measurements at pH 10. As seen in Fig 28a, the presence of less than 100 mg/L $CaCl_2$ and $MgCl_2$ does not affect pulp viscosity because there was no change in interactions between particles in this experimental range. However, the viscosity of the pulp increases significantly in the presence of 500 mg/L $CaCl_2$ or $MgCl_2$, transforming the pulp from a Newtonian fluid to a Bingham plastic fluid (see Figure 28b and 28c). This increase in pulp viscosity is likely caused by the reduced repulsion forces between particles resulting from the presence of divalent cations in the solution above 500 mg/L of $CaCl_2$ and $MgCl_2$ as seen in Figure 24. The increase in pulp viscosity resulted in a reduced flotation recovery (see Figure 19).

Sodium silicate is known for its ability to act as both a depressant and a dispersant. The dispersion of particles is mainly due to the adsorption of negatively charged silicate species on mineral surfaces at alkaline pH conditions, where monosilicate ($SiO(OH)^-$) becomes dominant (Hao et al., 2021). This results in an increase in electronegativity of the particles, leading to an increase in the repulsive forces between particles. In contrast, the decreased magnitude of zeta potential of mineral particles can reduce the repulsive forces between particles, ultimately leading to higher aggregation near the PZC (point of zero charge) where zeta potential becomes zero (Baldassarre et al., 2015). Farrokhpay et al. (2012) explained that the neutralisation of negative zeta potential resulted in an increase in the pulp viscosity

due to particle aggregation. Therefore, the observed increase in pulp viscosity was probably due to the compression of the electric double layer by the presence of Ca^{2+} and Mg^{2+} ions in the flotation pulp as seen in Figure 24.

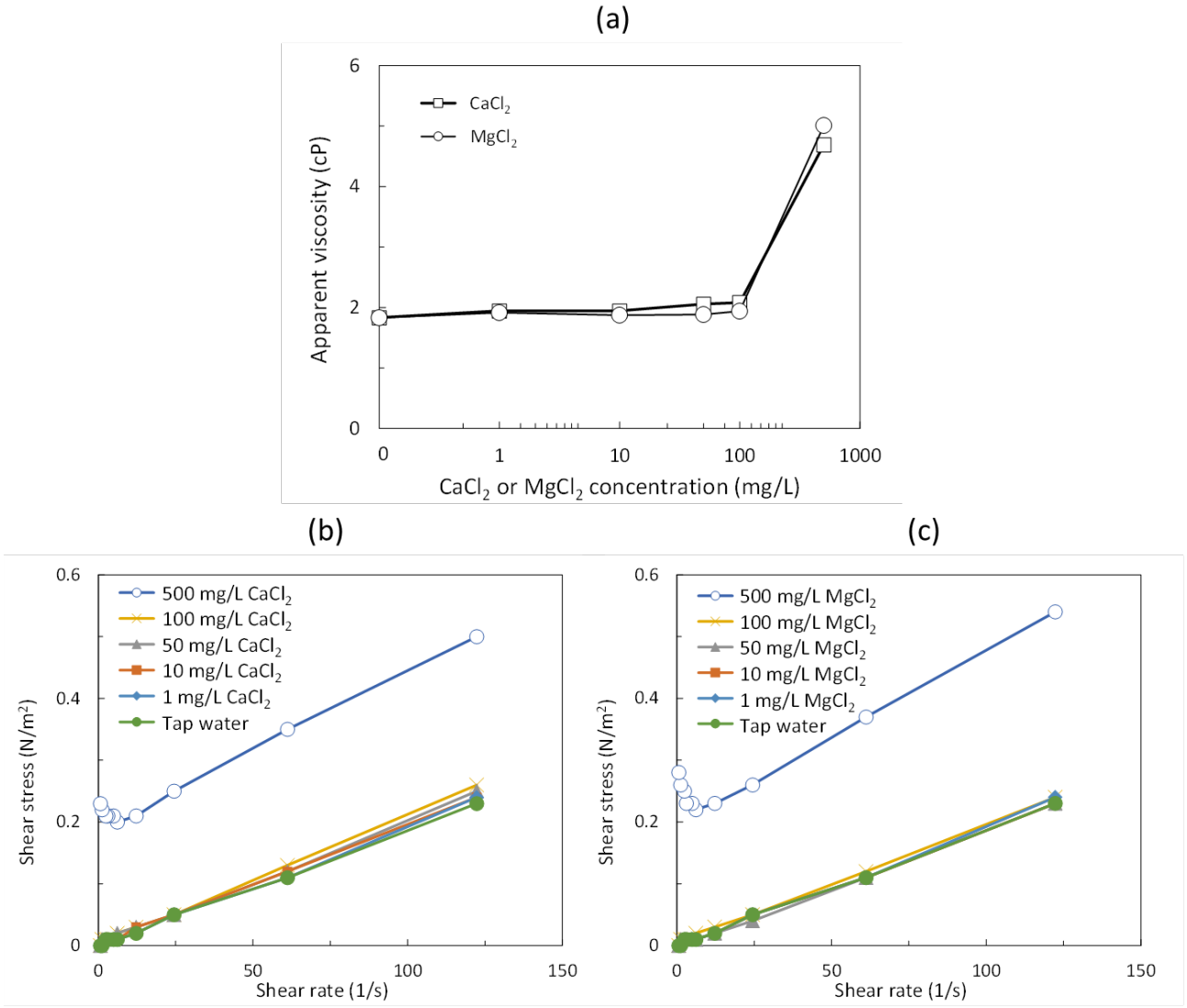

Figure 28. *The effect of the different concentrations of divalent ions (a) on the apparent viscosity and on the shear stress in the presence of (b) $CaCl_2$ and (c) $MgCl_2$; the apparent viscosities were obtained at 100 s^{-1}, at which the average shear rate in the flotation cell is (Ralston et al., 2007).*

6.2.5 Conclusions

In this study, the effects of $CaCl_2$ and $MgCl_2$ on the flotation of rare earth oxide minerals were investigated through multi−stage batch flotation experiments, UV−vis spectroscopy, rheological measurements, and solution chemistry. The results indicated that both $CaCl_2$ and $MgCl_2$ had a negative impact on the selectivity and recovery of RE minerals due to the chemical reaction between the divalent cations and the collector and depressant. The formation of insoluble calcium and magnesium carboxylate compounds resulted in the depletion of residual collector concentration and a lower RE recovery. Moreover, the divalent cations acted as a bridge between the oxygen atoms of the adsorbed silicate and carboxylate ions. This resulted in an increased adsorption of fatty acid collector ions, ultimately leading to a higher recovery of FeO. The negative impacts of $MgCl_2$ were more pronounced compared to those of $CaCl_2$, perhaps because magnesium has a greater attraction for silicate ions whereas calcium has a stronger preference for oleate. The presence of $CaCl_2$ or $MgCl_2$ increased the flotation pulp viscosity, which may be attributed to the reduced repulsion forces between particles due to the compression of the electrical double layer by the presence of divalent ions. This study highlights the significance of water quality in enhancing RE flotation.

6.3 Flotation behaviour of Mt Weld ore in the presence of different anions

Bench scale flotation experiments were performed to evaluate the effect of different anions on the flotation of RE ore using a fatty acid collector and sodium silicate depressant at pH 10. Figure 29 shows the effect of NaCl, Na_2SO_4, and $NaHCO_3$ on the recovery of RE minerals (Figure 29a) and FeO minerals (Figure 29b) as well as the grade of these minerals (Figure 29c and 29d). The results revealed that higher levels of anion concentrations caused a decrease in the recovery of RE minerals, while simultaneously increasing the recovery of FeO minerals. It is important to note that the decrease in the recovery of RE minerals was more significant in the cleaner 2 stage, which had the highest grade of RE minerals. In contrast, the increase in the recovery of FeO minerals was more prominent in the rougher/scavenger stages, which had the highest grade of FeO minerals.

As shown in Figure 29a, the largest decrease in the recovery of RE minerals in the cleaner 2 stage was observed when NaCl was added to the pulp, followed by Na_2SO_4 and $NaHCO_3$. Conversely, the recovery of FeO minerals in the rougher/scavenger stage increased the most in the presence of NaCl, followed by Na_2SO_4 and $NaHCO_3$ as seen in Figure 29c. This result clearly shows that the flotation efficiency was adversely affected in the presence of dissolved anions such as NaCl, Na_2SO_4 and $NaHCO_3$. Thus, the separation efficiency was reduced in the order of NaCl > Na_2SO_4> $NaHCO_3$; the separation efficiency was defined as the difference between the recovery of RE minerals (R_m) and FeO minerals (R_g) as seen in Eq (7), which was proposed by Schulz (1970).

$$\text{Separation efficiency (S. E.)} = R_m - R_g \tag{7}$$

In addition to examining the influence of NaCl, Na_2SO_4, and $NaHCO_3$ on the flotation experiments, the effects of KCl, K_2SO_4, and $KHCO_3$ were also investigated, and the findings are illustrated in Figure 30. The results consistently demonstrated that the presence of KCl, K_2SO_4, and $KHCO_3$ had a detrimental effect on the flotation experiments. Moreover, the negative impact followed the order of KCl > K_2SO_4 > $KHCO_3$; that is, the decrease of RE mineral recovery and the increase of FeO mineral recovery were most significant in this order. Moreover, the separation efficiency decreased the most in the presence of KCl and the least in the presence of $KCHO_3$ as seen in Figure 31(b). This aligns with the results obtained from the flotation experiments conducted with NaCl, Na_2SO_4, and $NaHCO_3$.

It was hypothesised that the reduced flotation efficiency resulted from changes in the rheology of the flotation pulp. Therefore, additional investigations were conducted in order to comprehensively examine the impact of these ions on the viscosity of the flotation pulp.

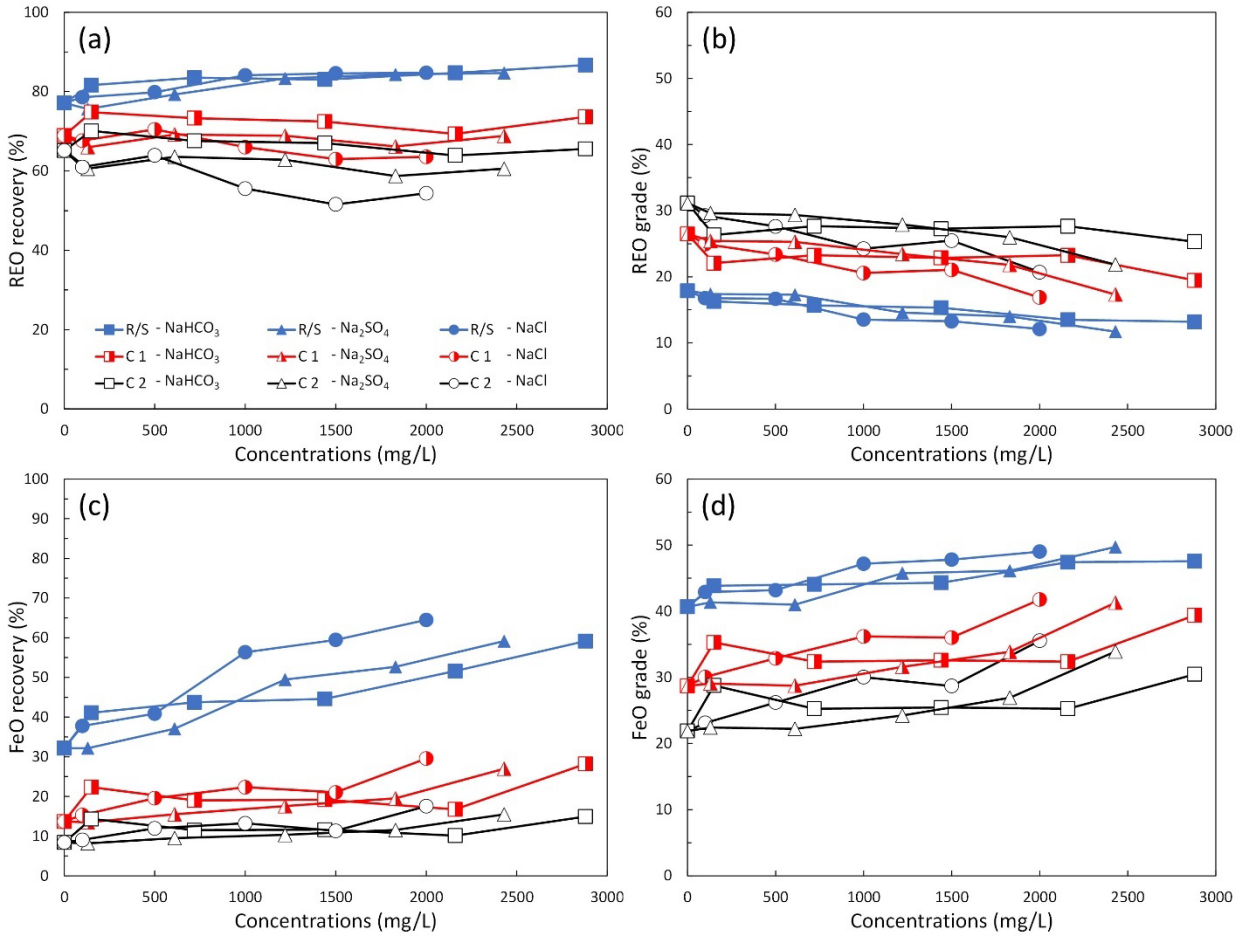

Figure 29. *Effects of NaCl, Na_2SO_4 and $NaHCO_3$ on (a) REO recovery, (b) REO grade, (c) FeO recovery and (d) FeO grade; R/S, C1 and C 2 denote the rougher/scavenger concentrate, cleaner 1 concentrate and cleaner 2 concentrate, respectively.*

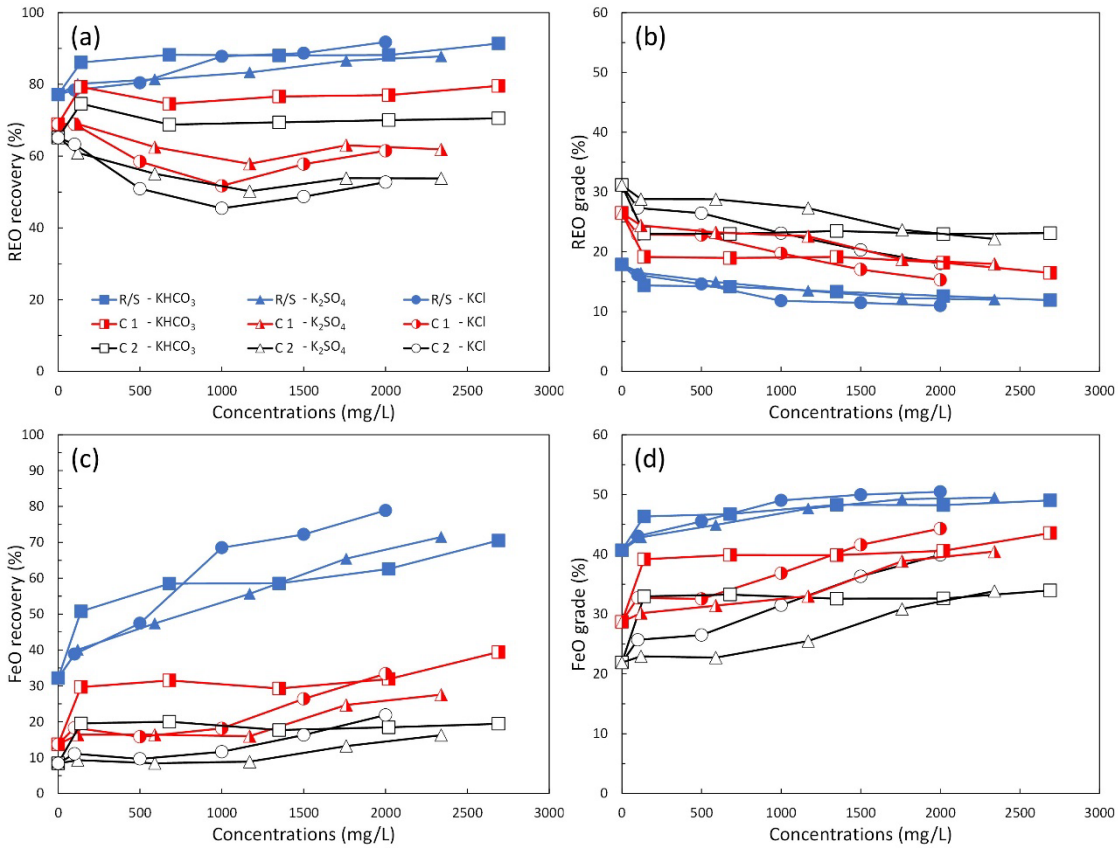

Figure 30. *Effects of KCl, K_2SO_4 and $KHCO_3$ on (a) REO recovery, (b) REO grade, (c) FeO recovery and (d) FeO grade; R/S, C1 and C 2 denote the rougher/scavenger concentrate, cleaner 1 concentrate and cleaner 2 concentrate, respectively.*

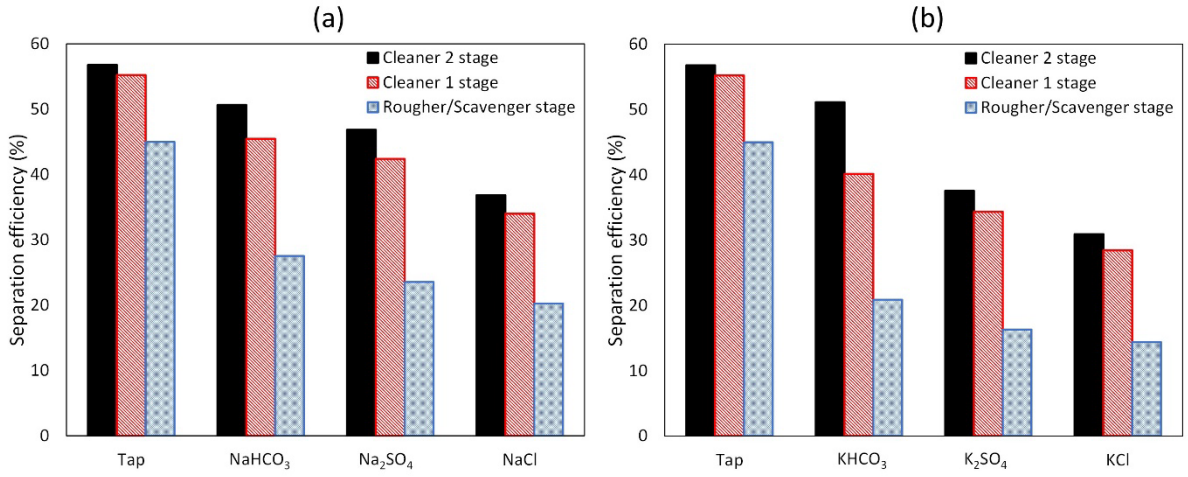

Figure 31. *The separation efficiency in the presence of (a) NaCl, Na_2SO_4 and $NaHCO_3$ and (b) KCl, K_2SO_4 and $KHCO_3$.*

6.3.1 Effects of anions on the viscosity of flotation pulp

Figure 32 illustrates the relationship between shear rate and apparent pulp viscosity in the presence of different concentrations of anions in the flotation pulp. As seen in Figure 32(a), a substantial increase in apparent viscosity was observed as the concentration of NaCl increased, with a slightly smaller increase in apparent viscosity observed with Na_2SO_4. However, the effect of $NaHCO_3$ concentration on the apparent viscosity was insignificant, which agrees well with the literature (Ozdemir et al., 2007). Similarly, Figure 32(b) shows that the increase in pulp viscosity was the highest when KCl was introduced and the lowest when $KHCO_3$ was present in the flotation pulp. These findings align with the flotation results, demonstrating that elevated pulp viscosity leads to a decrease in the flotation separation efficiency between RE minerals and FeO minerals.

It is postulated that the increase in pulp viscosity in the presence of anions can be attributed to the alteration of the electrical double layer surrounding mineral particles, thereby affecting the electrostatic interaction forces between particles. For example, a reduced zeta potential of mineral particles results in a reduction of repulsion forces between particles (Laskowski and Iskra, 1970; Laskowski et al., 1991; Li et al., 2017). As a consequence, the decrease in repulsion forces can lead to an increase in particle aggregation via the operation of van der Waals attraction forces, and ultimately an elevation in pulp viscosity (Ancey and Jorrot, 2001; Chen et al., 2019; Li et al., 2017). Ong et al., (2008) showed that the maximum yield stress of aluminium oxide dispersion was achieved at near PZC (point of zero charge) where the van der Waals attraction forces are present only while electrostatic repulsion is absent. Given the significant influence of mineral particle zeta potential on pulp viscosity, a detailed investigation and discussion of zeta potential was conducted.

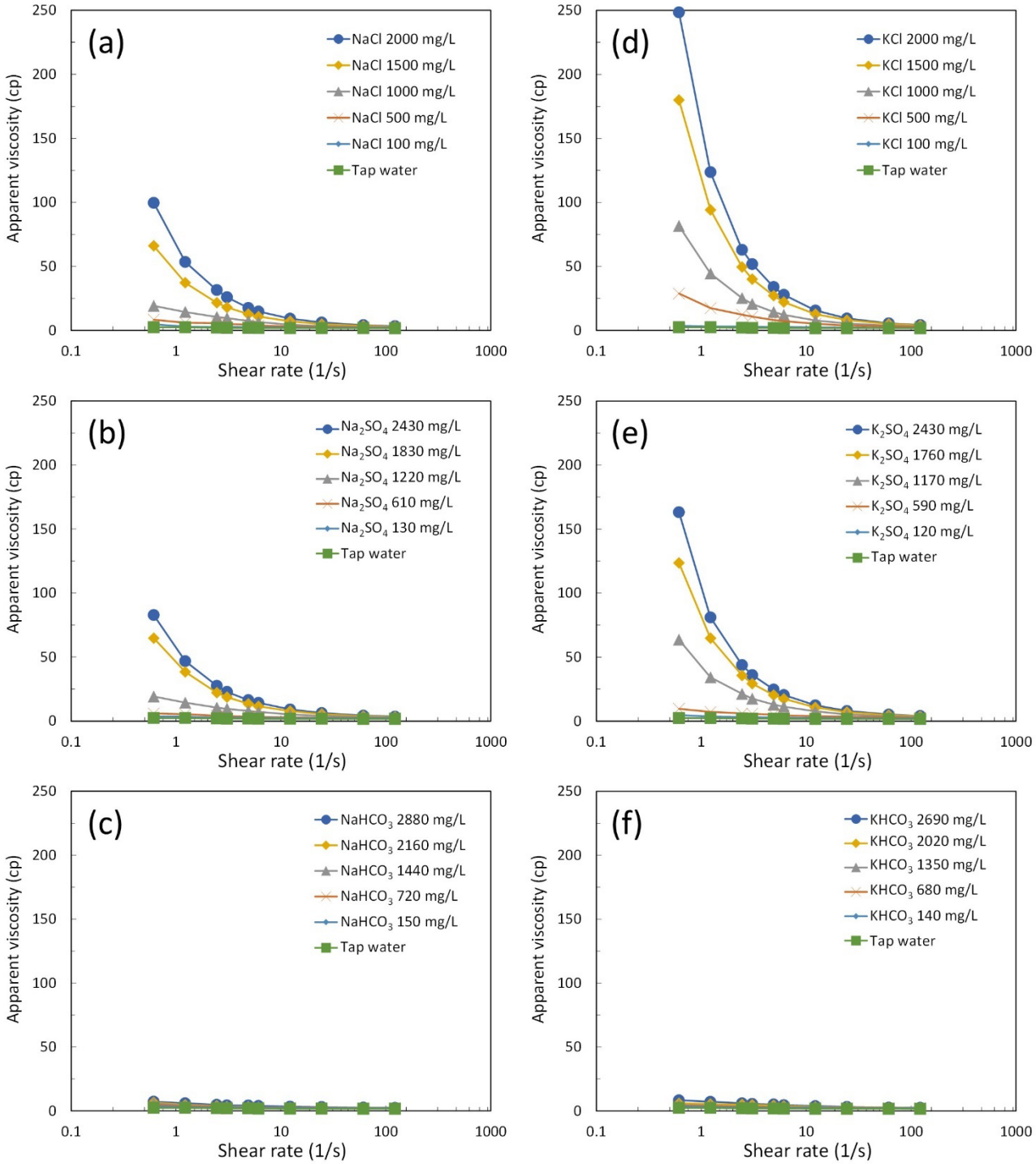

Figure 32. *The effect of different concentrations of anions on pulp viscosity.*

The rheogram of the flotation pulp, both in the absence and presence of various anions, is shown in Figure 33. In the absence of anions and in the presence of HCO_3^- ions, the pulp exhibited Newtonian fluid characteristics, displaying a linear relationship between shear stress and shear rate without any yield stress. However, the introduction of Cl^- and SO_4^{2-} ions resulted in a transition from Newtonian behaviour to Bingham plastic fluid properties, with the presence of yield stress observed. Notably, the yield stress was found to be higher in the presence of Cl^- ions compared to SO_4^{2-} ions. This change in fluid type from Newtonian to Bingham plastic has important implications for flotation efficiency, as it has been reported

that such a transition can lead to an increase in non-selective gangue entrainment (Kirjavainen et al., 1992; Fu et al., 2018; Chen et al., 2017). Non-selective gangue entrainment can adversely affect the selectivity of the flotation process, reducing the efficiency of separating valuable minerals from unwanted gangue minerals.

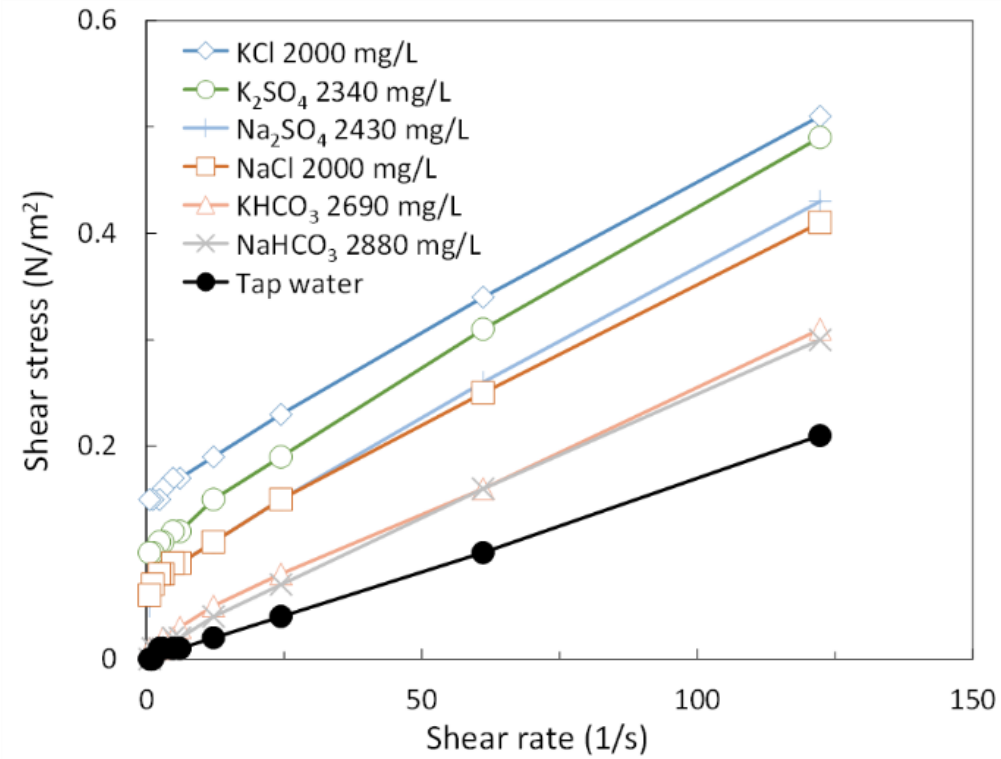

Figure 33. *Rheogram of flotation pulp in the absence and presence of different types of anions*

6.3.2 Effect of anions on the entrainment

Figure 34 illustrates the impact of various anions on the degree of entrainment of mineral particles. The results indicate that the increase in entrainment was most pronounced when KCl was present, followed by K_2SO_4, NaCl, and Na_2SO_4. These findings align with the observed increase in pulp viscosity caused by these ions, where the magnitude of the viscosity increase followed the order KCl > K_2SO_4 > NaCl > Na_2SO_4. This correlation suggests that the rise in pulp viscosity hindered the transportation of fine particles through the froth phase, resulting in a higher retention of particles within the froth and subsequent recovery. However, the presence of high concentrations of HCO_3^- ions did not lead to a significant increase in the degree of entrainment. This observation can be attributed to the fact that the pulp viscosity did not substantially increase when these ions were introduced into the flotation pulp.

Fu et al. (2018) introduced an equation that combines the effects of gravity, capillary force, and viscous force to calculate the average velocity of fluidic cells present in the plateau border in froth, as shown in Equation (8).

$$u = \frac{1}{f\mu}\left(\rho g A + \left(\sqrt{3} - \frac{\pi}{2}\right)^{0.5} \frac{\gamma}{\sqrt{A}} \frac{\partial A}{\partial x}\right) \quad (8)$$

where f is a parameter related to the shape of the plateau border, μ is the pulp viscosity, ρ is the pulp density, g is the gravitational acceleration, A is the cross−sectional area of the plateau border, γ is the tension of the liquid surface, and x is the unit length of the fluid cells.

In accordance with Eq (8), higher pulp viscosity (μ) causes a slower average velocity of the fluidic cells (u), thus the entrainment may be enhanced due to the slower rate of froth drainage.

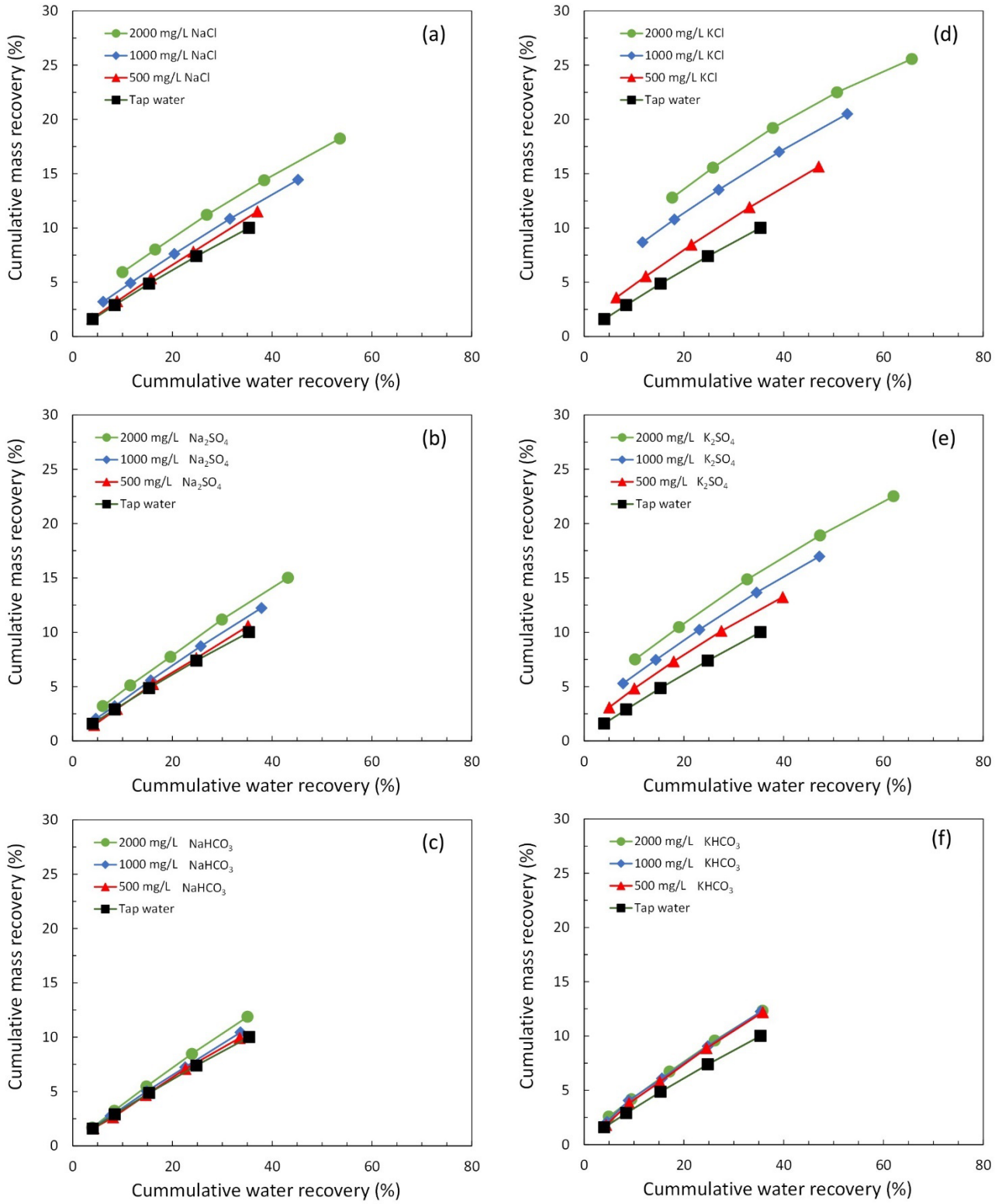

Figure 34. *The degree of particle entrainment in the presence of (a) NaCl, (b) Na_2SO_4, (c) $NaHCO_3$, (d) KCl, (e) K_2SO_4 and (f) $KHCO_3$.*

6.3.3 Effect of anions on zeta potential of mineral particles

Direct measurement of the zeta potential of ore samples was found to be challenging due to the complex mineral composition of the feed ore as seen in Table 7. To overcome this challenge, zeta potential measurements were conducted using pure minerals such as monazite and goethite. These minerals were selected as representatives of valuable and gangue minerals in the ore.

Figure 35 illustrates the results of zeta potential measurements conducted on pure monazite and goethite under various conditions, including in both the absence and presence of different anions at pH 10. In distilled water at pH 10, the pure monazite and goethite minerals exhibited negative zeta potentials of −18.0 mV and −37.37 mV, respectively. The addition of sodium oleate and sodium silicate led to a more negative zeta potential for both minerals. This shift is attributed to the adsorption of anions such as OL^- and SiO_4^{2-} onto the surfaces of these minerals. When Cl^-, SO_4^{2-} and HCO_3^- were introduced into the solution, a shift of zeta potentials for both monazite and goethite minerals was also observed. The zeta potential became less negative in the following order: $Cl^- > SO_4^{2-} > HCO_3^-$.

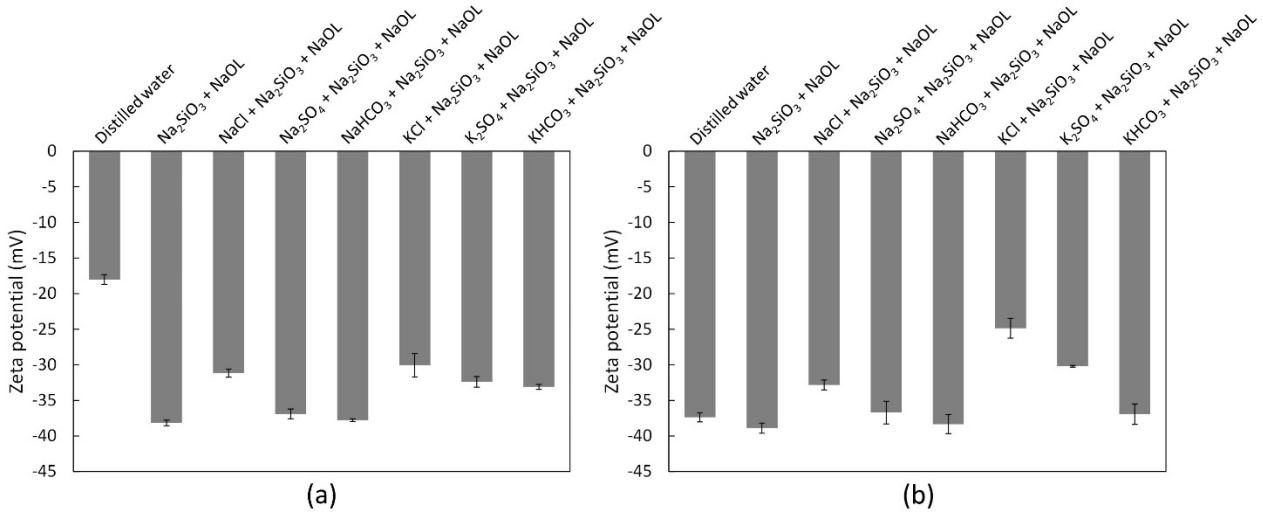

Figure 35. *The zeta potential of (a) monazite and (b) goethite under various conditions at pH 10 ([Na_2SiO_3] = 3800 g/t and [NaOL] = 2200 g/t).*

The introduction of Cl^- and SO_4^{2-} in the solution resulted in a significant shift of the zeta potential for both monazite and goethite to a less negative value. This observation may be attributed to the compression of the electrical double layer caused by the increased ionic strength of the solution, as reported in previous studies (Burns et al., 2000; Zhao et al., 2005). Interestingly, it was noted that the shift in zeta potential was more pronounced in the presence of Cl^- ions compared to SO_4^{2-} ions. This finding contradicts the expected relationship between zeta potential and ionic strength, where higher ionic strength typically leads to a greater shift of zeta potential. In this study, the ionic strength was higher in the presence of SO_4^{2-} ions than Cl^- ions, yet the shift in the zeta potential was greater for Cl^- ions (see Table 7). Similar observations were reported by Niriella et al. (2006), who found that the zeta potential of bentonite was more negative in the presence of 0.01 M Na_2SO_4 compared to 0.01 M NaCl, despite the higher ionic strength of Na_2SO_4. Additionally, Salgin

et al. (2013) discovered that the zeta potential of polyethersulfone ultrafiltration membranes was more negative in the presence of 0.001 M K_2SO_4 compared to 0.001 M KCl within a pH range between 4 and 8. These results suggest that the zeta potential of mineral surfaces can be influenced not only by the ionic strength of a solution but also by the type of anions present. Tang and Wen (2019) proposed that SO_4^{2-} ions can adsorb through hydrogen bonding with hydroxyl ions on iron oxide mineral surfaces, whereas Cl^- ions tend to form outer-sphere complexes and remain highly hydrated within the diffusion ion swarm as seen in Fig. 36. Therefore, the zeta potential in the presence of SO_4^{2-} was lower compared to that in the presence of Cl^-, which may be attributed to the adsorption of SO_4^{2-} ions.

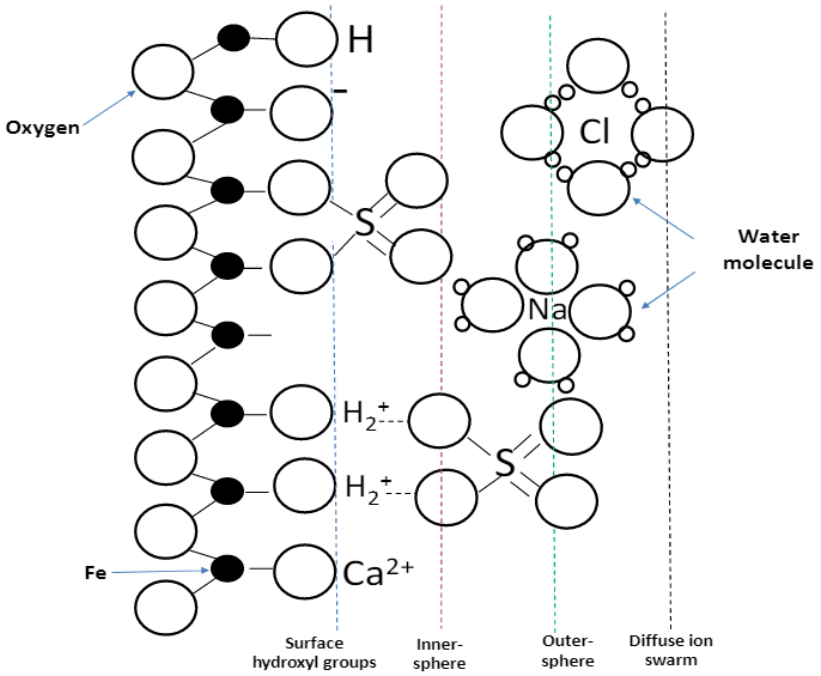

Figure 36. *Schematic diagram of surface complex structure in hydrous iron oxide: surface hydroxyl groups, inner−sphere complexes, outer−sphere complexes, and diffuse Ion Swarm (Tang and Wen, 2019).*

Table 7. *Ionic strength of solution in the presence of different salts.*

	NaCl	KCl	Na_2SO_4	K_2SO_4	$NaHCO_3$	$KHCO_3$
Ionic strength	0.0342	0.0268	0.0513	0.0403	0.0288	0.0269

Adding HCO_3^- to the solution had a lesser effect on the zeta potential of the minerals compared to Cl^- and SO_4^{2-}. This is likely due to the limited solubility of metallic carbonate compounds, as indicated in Table 8. Previous studies (Espiritu and Waters, 2018; Li et al., 2017b) have reported that chemisorption occurs between CO_3^{2-} ions and lattice cations (such as Ce^{3+} and Fe^{2+}) on the mineral surfaces. The reactions in Eq (9) and Eq (10) demonstrate that at pH 10, HCO_3^- ions exist in the form of HCO_3^- and CO_3^{2-}, as shown in Fig 37 (Castro, 2012). It was noted that CO_3^{2-} ions adsorb onto iron oxide surfaces (i.e.,

magnetite) through hydrogen bonding and form complexes with Fe ions (Roonasi and Holmgren, 2010a).

$$H_2CO_3 \rightarrow H^+ + HCO_3^-,\ pK_{a1} = 6.352 \quad (9)$$

$$HCO_3^- \rightarrow H^+ + CO_3^{2-},\ pK_{a2} = 10.329 \quad (10)$$

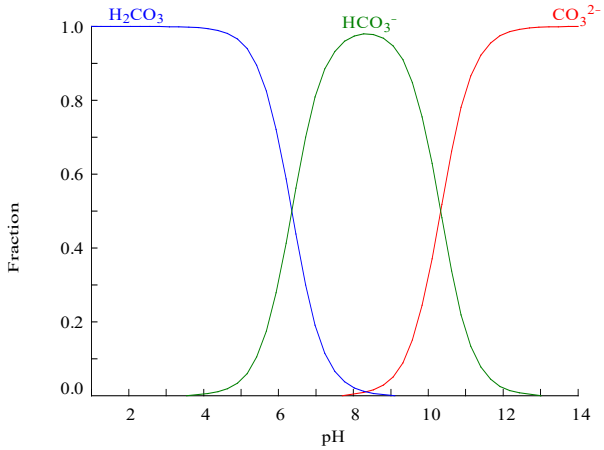

Figure 37. *Species distribution diagram of carbonate species by pH.*

Table 8. *Chemical reactions and thermodynamic constants.*

Chemical reaction	Equilibrium constant	References
$FeCO_{3(s)} \rightarrow Fe^{2+} + CO_3^{2-}$	$K_{sp} = 10^{-10.68}$	Li et al. (2017)
$La_2(CO_3)_{3(s)} \rightarrow 2La^{3+} + 3CO_3^{2-}$	$K_{sp} = 10^{-29.91\pm0.05}$	Firsching et al. (1986)
$Ce_2(CO_3)_{3(s)} \rightarrow 2Ce^{3+} + 3CO_3^{2-}$	$K_{sp} = 10^{-21.80\pm0.05}$	Ferri et al. (1983)

6.3.4 Effect of anions on settling behaviour of flotation pulp

Figure 38 presents the results of settling experiments conducted over 144 h in the presence and in the absence of anions (HCO_3^-, Cl^- and SO_4^{2-}). In tap water, a large number of particles remained suspended, resulting in a significantly turbid flotation pulp, as illustrated in Figure 39a. However, when anions were present, the settling rate of particles was noticeably enhanced. The settling rates decreased in the following order: KCl > K_2SO_4 ≈ NaCl > Na_2SO_4 > $KHCO_3$ > $NaHCO_3$. This can be attributed to a decrease in the repulsive forces between particles due to the reduction in the zeta potential of mineral particles when these ions were present. Figure 39 provides a visual demonstration of this effect, displaying photographs of flotation pulp taken over a period of 144 h. These photos provide clear evidence of the impact of anions on particle settling, with a faster settling rate observed in the flotation pulp containing Cl^- and SO_4^{2-}, compared to those containing HCO_3^-.

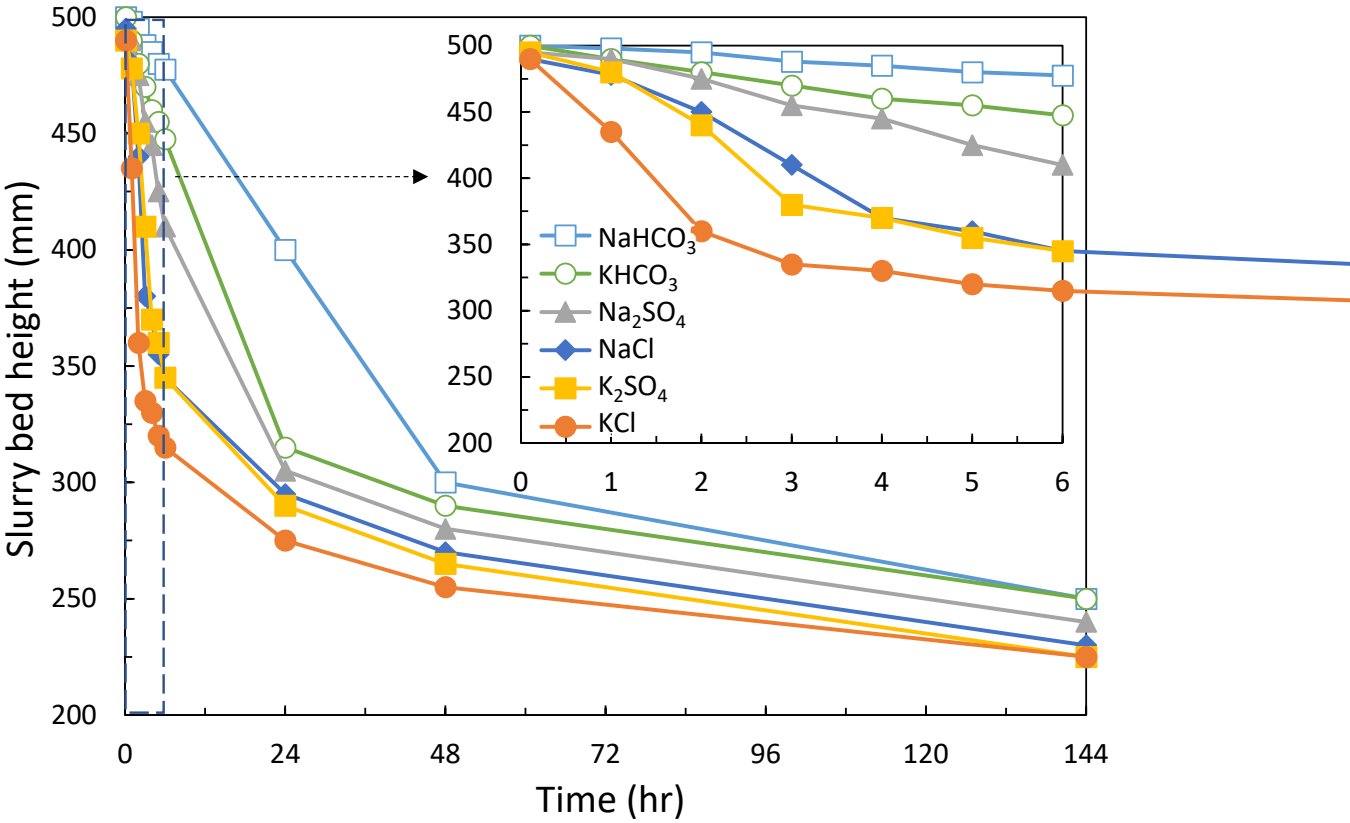

Figure 38. *Settling behaviour of flotation feed slurry in the presence of different anions.*

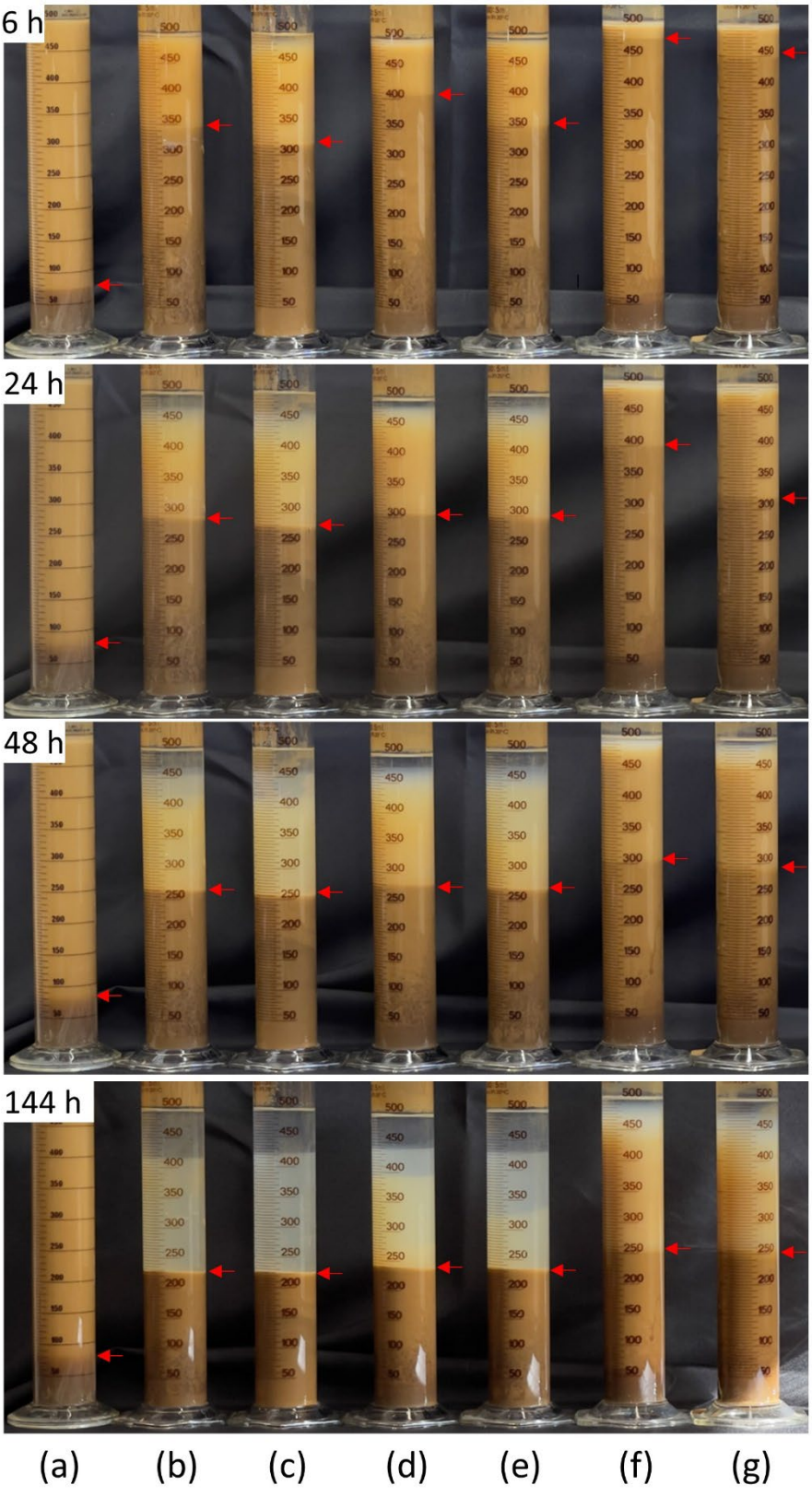

Figure 39. *Photographs of flotation pulp after 6, 24, 48, and 144 h settling (a) in the absence of anions and in the presence of (b) NaCl, (c) KCl (d) Na_2SO_4, (e) K_2SO_4, (f) $NaHCO_3$ and (g) $KHCO_3$.*

6.3.5 DLVO theory calculation

The total interaction energy between the same mineral particles (i.e., monazite−monazite particles or goethite/goethite particles), based on the DLVO theory, is presented in Figures 40a and 40b, respectively. Figure 40 shows that the total interaction energy remains positive in the presence of SiO_3^{2-} and OL^- ions. This indicates that strong repulsive forces are the dominant force between the particles. Consequently, the settling of fine particles is slow, making the flotation pulp turbid even after 144 h, as illustrated in Figure 39a.

When anions are added to the flotation pulp, there is a clear shift in interaction energy between particles. The total interaction energy between monazite particles decreases and becomes negative, indicating that attractive forces are dominant between these particles as shown in Figure 40(a). In the case of goethite particles, the total interaction energy decreases when Cl^- and SO_4^{2-} ions are present in the pulp; however, the addition of HCO_3^- ions resulted in repulsive interactions between these particles, making them suspended in the flotation pulp. In contrast, the presence of Cl^- and SO_4^{2-} ions increases the rate of particle settling, as seen in Figure 39.

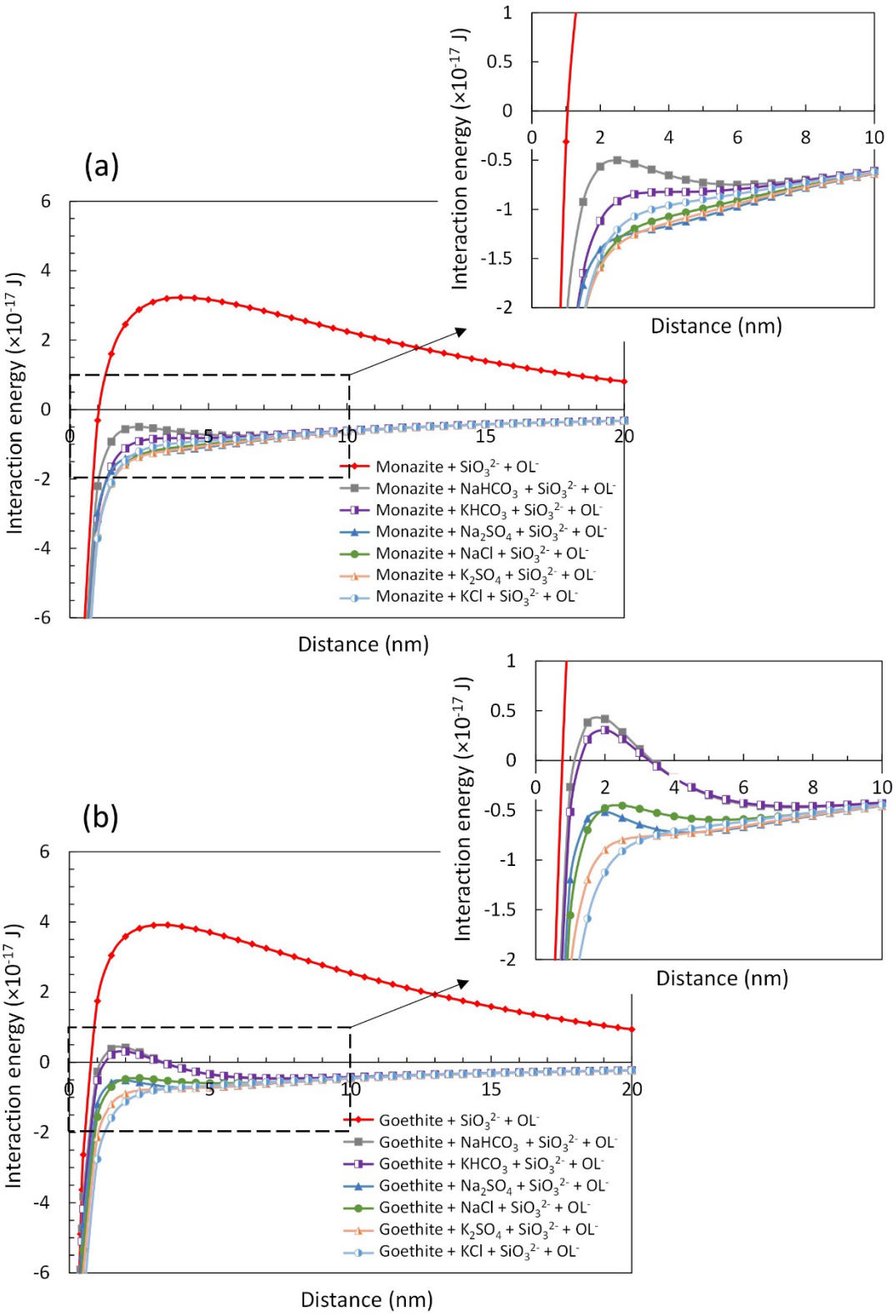

Figure 40. *DLVO interaction energy between (a) monazite-monazite particles and (b) goethite-goethite particles*

6.3.6 Conclusions

In this study, the influence of anions, specifically Cl^-, SO_4^{2-}, and HCO_3^-, on the flotation performance of RE ore was investigated by integrating various techniques such as flotation experiments, rheology measurements, entrainment experiments, zeta potential measurements, settling experiments, and DLVO theory. The results revealed that an increased concentration of Cl^-, SO_4^{2-}, and HCO_3^- had an adverse effect on flotation efficiency, leading to a decrease in the recovery of RE minerals while increasing the recovery of FeO minerals. The presence of Cl^- had a particularly detrimental effect on the flotation of rare earth minerals, likely attributed to the significant increase in pulp viscosity. The reduction in zeta potential of fine particles in the presence of high concentrations of these ions appears to be a critical factor contributing to the increase in pulp viscosity. The stronger the attractive forces between particles, the higher the pulp viscosity, leading to increased mechanical entrainment. These results were validated through settling experiments and calculations using the DLVO theory. This study emphasises the importance of water quality in maximising RE flotation efficiency.

Section 3: Fit-for-purpose Water Treatment Methods for REO Flotation

7. Introduction to Fit-for-Purpose Water Treatment

The mineral processing sector consumes a considerable amount of water; for example, processes that do not reuse water use between 1.9 to 3 m^3 per ton of ore processed. Water is used in a wide range of mining activities, and water scarcity and community sensitivity to water use by industry is increasing. The mining industry is constantly evaluating the best way to use water. The search for improvements in water conservation and reuse increases recycling and the use of lower-quality water in different sections of industrial operations, such as groundwater or seawater, which usually contain high concentrations of ions and salts. At the same time, mining operations tend to be in areas where there is competition among other industrial sectors for the use of domestic water, or are in areas where access to high-quality water is scarce and expensive due to extraction and transportation costs.

Currently, treatment options to improve water quality involve physical, electro, and chemical processes that remove salts through a membrane or an ion exchange resin induced by a specific current, or precipitation of the ions as an insoluble salt. Membrane separation methods such as reverse osmosis (RO) have been implemented in several processes because this method provides rates of removal of dissolved species as high as 98%. However, many mineral processing operations do not require ultra-high-quality water; thus, reverse osmosis becomes an unnecessary and expensive option.

In RO treatment, water with a sulphate concentration of >700 mg/L and calcium >100 mg/L is not recommended because of the high scaling potential of precipitated $CaSO_4$, and the expense associated with frequent membrane replacement. RO is an energy-intensive process, accounting for around 44% of the total treatment cost. In countries such as Australia, where the cost of energy is relatively high, it becomes an appreciable portion of minerals processing expenses.

Nanofiltration (NF) is an option that can provide suitable water quality for mineral processing operations by removing divalent ions and a portion of the monovalent ions through proper membrane selection and under specific conditions. It has lower cost implications because nanofiltration uses lower transmembrane pressures compared with RO. Nanofiltration membranes have a microporous structure and can retain particles with a size of 0.1 nm-0.001 µm, which allows most impurities to be separated from the water, although those of lower molecular weight are partially retained in the membrane. In this process, the separation of substances is carried out both by the size of the pores and by the solution-diffusion mechanisms that are characteristic of processes such as ultrafiltration and RO respectively. Therefore, nanofiltration allows the separation of organic substances (proteins, sugars), microorganisms and some multivalent salts. Different studies with brackish water have demonstrated that nanofiltration can remove up to 98% of calcium and magnesium salts and up to 66% of sodium chloride.

Despite the promising performance of nanofiltration demonstrated in lab-scale studies, a recent review indicated that there is still a lack of detailed pilot scale trials that are crucial to realise its application for a larger scale mineral processing operation. Therefore, in this study, a pilot scale nanofiltration rig was employed to investigate the possibility of producing

high quality water from groundwater obtained from a mining operation in Western Australia. Multiple operation parameters such as pressure and recovery were investigated to evaluate the performance of two different membranes in removing dissolved ions that would otherwise be problematic for different mineral processing operations. Furthermore, a two-stage nanofiltration system was evaluated to improve water recovery. The results obtained in this study present nanofiltration as a technology that can be implemented in the mining industry to supply water of suitable quality.

Charged membranes are used to remove ionic species from one solution to another during the electrochemical separation process known as electrodialysis (ED). This method is frequently used for producing salt, treating industrial effluents, producing organic acids, recovering usable components from effluents, and producing drinking and process water from brackish water and seawater. In the ED process, cation and anion exchange membranes alternately sit between the cathode and the anode, and anions travel towards the anode and cations towards the cathode when a voltage difference is applied between the two electrodes. The anion-exchange membranes retain the cations after they have passed through the cation-exchange membranes, which contain sulphone groups on their surface. Conversely, the cation-exchange membranes retain the anions, which move via the anion-exchange membranes, which have quaternary ammonium as ion-exchange fixed groups. As a result of this flow of ions, concentration rises in the concentrate compartment of the cell while falling in the diluate compartment.

This study evaluates alternative technologies to RO that are capable of producing water with low ion concentrations suitable for mineral processing operations such as non-sulphide flotation. More specifically, NF and ED are promising technologies that use lower pressure and low electrical potential to separate ions across membranes. Hence, this study aims to compare the performance and energy consumption of NF and ED applied to bore water from one mine site in the Goldfields area of Western Australia.

7.1 Reagents

The raw water for this study was from the Mt Weld operation in the Goldfields, and the characterisation of the water is shown in Table 9. Bore water salinity in the Goldfields region ranges from 1 g/L - 250 g/L. The bore water used in this study contained relatively low Total Dissolved Solids (TDS) with the main ions of interest being Mg^{2+}, Ca^{2+}, Na^{+}, Cl^{-} and SO_4^{2-}. Additionally, synthetic waters were prepared for some of the precipitation and electrodialysis experiments and their compositions are listed in Table 9.

Table 9. *Characterisation of water samples used in this study.*

Parameter	Unit	Bore water	Synthetic water	Synthetic sea water
pH	-	7.5	7.8	8.0
Conductivity	µS/cm	8280	24000	49400
TDS	mg/L	4150	11970	24700

TSS	mg/L	<10	<10	<10
Alkalinity (total)	mg/L	265	70	180
Alkalinity (OH)*	mg/L	0	0	0
Alkalinity (CO_3)*	mg/L	0	0	0
Alkalinity (HCO_3)*	mg/L	265	70	180
Calcium	mg/L	140	150	310
Magnesium	mg/L	167	290	600
Sodium	mg/L	1547	4700	10600
Chloride	mg/L	2340	5170	11420
Sulphate	mg/L	735	1300	2560

* Calculated as $CaCO_3$

The synthetic saline water and the corresponding solutions were prepared with ultrapure water and the main reagents used in this section of the research were: calcium chloride (99.9% Chem supply), magnesium chloride (99% Thermo Fisher Scientific), sodium chloride (99.9% Chem supply), sodium sulphate (99%) and sodium bicarbonate (99% Thermo Fisher Scientific).

The reagents used in the precipitation test were oxalic acid (99.9% Chem supply), calcium hydroxide (>99%, Sigma Aldrich), sodium aluminate (99%), and nitric acid and sodium hydroxide at analytical grade to adjust pH. Chemical cleaning of the membranes was conducted using NaOH and HNO_3, which along with the Na_2SO_4 used as the electrolyte in the electrode compartments of the electrodialysis stack and the NaCl used for synthetic solutions, were analytical grade and were supplied by Chem-Supply, Australia.

7.2 Water characterisation

7.2.1 Cations

These analyses were performed using the inductively coupled plasma optical emission spectroscopy (ICP OES) technique following the USEPA 6010 standard procedure. This analysis is based on the vaporisation, dissociation, ionisation and excitation of the different chemical elements of a sample inside a plasma. During the deexcitation process of the neutral atoms and ions inside the plasma, electromagnetic radiation emissions are produced in the UV-visible zone. These emissions, characteristic of each element, are separated according to their wavelength and finally, their intensity is measured. This technique, therefore, provides the concentrations of the chemical elements present in each sample. It was used for the determination of Ca, Na and Mg in the samples obtained experimentally.

7.2.2 Anions

The sulphate concentration was measured following the standardised procedure APHA 4500 SO_4^{2-} E in which the sulphate is precipitated in an acetic acid medium with barium chloride producing crystals of barium sulphate which are measured by a photometer and compared with a standard curve. For the analysis of chloride, the standard method APHA 4500 Cl G was used in which N, N-diethyl-p-phenylenediamine reacts with free chlorine producing a red colour indicator which then was compared with a standard curve by spectrophotometer.

7.3 Nanofiltration

The filtration experiments were conducted in a pilot unit supplied by Ecotechnol Australia (Figure 41). This pilot unit was designed to test different ultrafiltration and nanofiltration membranes under various conditions such as pressure and permeate recovery. The Ecotechnol rig is composed of one feed tank with a volume of 0.1 m^3, a high-pressure booster pump which was used for the filtration and for cleaning the membrane, and one pressure vessel housing a standard 40” x 4” membrane module with retractile end and feed caps allowing the change of membrane, with a manual regulation valve on the concentrate line to adjust the pressure of operation and on both the permeate and concentrate lines which can be fitted as a recirculation loop with the feed tank. An external scale was used to measure the weight of the desirable recovery of permeate.

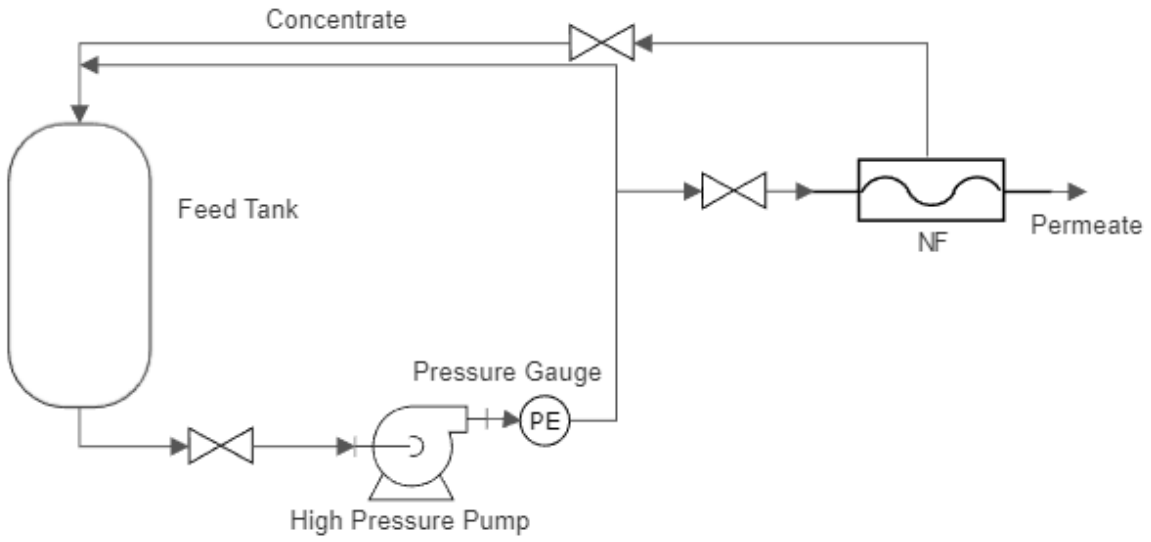

Figure 41. *Ultrafiltration / Nanofiltration rig used in this study (Ecotechnol).*

Two organic nanofiltration (NF) membranes fabricated by different companies (Dow Filmtec and Ecotechnol) were studied. The nanofiltration membranes used were thin-film composite membranes. NF90-4040 and 4040 A are characterised as tight nanofiltration membranes with relatively high sodium chloride rejection (>85%). In addition, one ultrafiltration (UF) membrane was used as a pre-treatment to remove suspended solids, to avoid undesirable fouling of the NF membranes studied. Table 10 shows the commercial names of the membranes and their corresponding suppliers as well as the primary polymer used for their fabrication.

Table 10. *Commercial name and manufacturer of the NF and UF membranes*

Commercial name	**Application**	**Manufacturer**	**Polymer**
UF Ecotechnol	Ultrafiltration	MDS- Ecotechnol	Polyamide
NF90-4040	Nanofiltration	DOW Filmtec	Polyamide
4040 A Ecotechnol	Nanofiltration	MDS- Ecotechnol	Polyamide

Before each experiment, the membranes were washed with caustic solution (0.2% w/w) to restore the membrane's permeability. Each membrane was pressurised using deionised

water at 4 bars for 30 minutes until the conductivity of the permeate was steady and similar to the initial deionised water. As the raw water used in the experiments was obtained from one of the bores at Mt Weld mine, an ultrafiltration stage was required as pre-treatment to avoid nanofiltration membrane fouling. The nanofiltration experiments were carried out with three different nanofiltration membranes and an initial mass of 22 kg of ultra-filtrated bore water from the Mt Weld mine site. The concentrate was recirculated to the feed tank, and the permeate was collected and sampled at three different recoveries (15, 45 and 65%). The feed pressure was adjusted for each test and was varied in the range of 8 to 20 bar. Additionally, the permeate flux and ion rejection were determined by measuring the permeate flow and the concentration of ions in the permeate.

7.4 Precipitation

The precipitation experiments were executed by adding the respective precipitant (oxalic acid, lime, sodium aluminate) to the synthetic water and the bore water.

7.5 Oxalic Acid

7.5.1 Effect of oxalic acid dose on ion removal

For the precipitation with oxalic acid, a volume of 0.6 L of both of water bore water (BW) and synthetic water (SW) was used in each experiment. This set of experiments was conducted with synthetic and bore water as the concentration of magnesium in the bore water was low, to evidence the selective precipitation of magnesium. A jar tester apparatus with a variable stirring rate was used as a batch mixed reactor, equipped with 1 L beakers. The precipitation experiments were carried out at ambient temperature (20-24 ºC) and a mixing rate of 200 rpm. To evaluate the effect of oxalic acid a set of experiments was conducted at different oxalic acid molar ratios (1, 1.2, 1.5 and 2 for each mole of Ca and Mg) with a fixed mixing time of 120 min.

7.5.2 Kinetics of calcium precipitation

Kinetics and equilibrium experiments were developed to establish the minimum time required to achieve equilibrium ion removal. This set of experiments was conducted at a stoichiometric ratio of 2 (Oxalic acid: Magnesium + Calcium), ensuring that there was an excess of reagent to complete the reaction of all the ions in solution. During the kinetics and equilibrium experiments samples were taken at different times (30, 60, 120, and 240 min) which were filtered by vacuum filtration through a Whatman 0.8 µm membrane filter of polyvinylidene fluoride for further ion analysis.

7.5.3 Effect of pH on calcium and magnesium precipitation

The experiments performed to evaluate the effect of pH on ion precipitation were conducted under similar conditions as established in the kinetics and equilibrium experiments. However, these experiments were carried out in two different stages in which 0.5 L of

solution was mixed with oxalic acid at a molar ratio of 2:1 for 120 min, followed by 30 min of settling. After the settling time the supernatant was filtered through a Whatman 0.8 µm membrane. 0.3 L of the filtrate was collected, and its pH was adjusted to the desired pH (1, 3, 5, 7, 11) with 1 M sodium hydroxide. The pH-adjusted solutions were stirred for 120 min, followed by 30 minutes of settling before finally being filtered by vacuum filtration through a Whatman 0.8 µm membrane filter of polyvinylidene fluoride for ion analysis.

7.6 Ultra-High Lime with Aluminium (UHLA)

7.6.1 Effect of reagent dose on ion removal

In the case of the UHLA precipitation test, 0.3 L of bore water was used and the experiments were conducted in 0.5 L sealed plastic bottles to avoid CO_2 contamination and alteration of the precipitation process. The bottles were shaken at 200 rpm in a temperature-controlled room (25 ºC) in a Labwit ZWY-211B shaking incubator for 24 hours with different ratios of calcium/anions (1:1, 1, 5:1 and 2:1) and aluminium/anions (1, 2 and 3). Also, a series of experiments were conducted in two stages (Figure 42), structured as a first stage with half of the lime dosage and a second stage with half of the lime dosage. In addition, different doses of aluminium at different Al/anions ratios were added to optimise the chloride and sulphate removal and avoid competition between ions with high affinity for forming calcium and aluminium complexes.

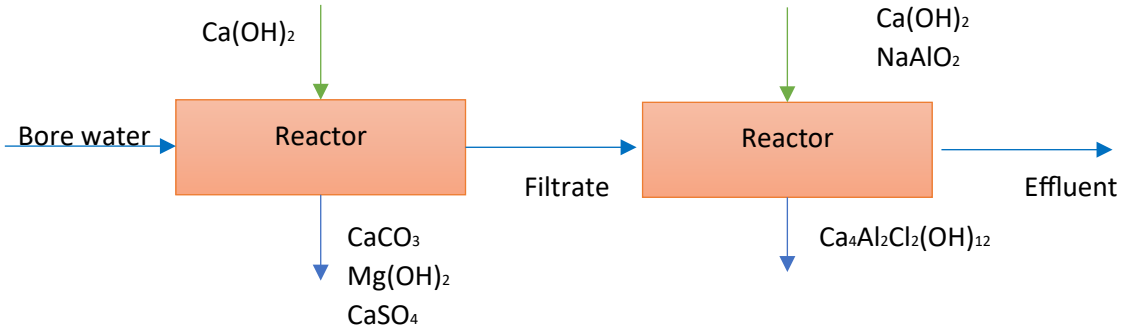

Figure 42. *Two-stage UHLA precipitation*

7.6.2 Kinetics of ion removal

A series of kinetic experiments were performed to determine the reaction equilibrium. In this set of experiments, 0.9 L of bore water was reacted with calcium hydroxide and sodium aluminate at molar ratios of Ca/anions of 2:1 and Al/anions of 1.5:1. The solution was kept under constant agitation at 200 rpm and 25 ºC ± 1 ºC in a shaking incubator and 200 mL aliquots of the solution were taken at different times (2, 4, 8, and 24 hours) to determine the equilibrium time.

7.6.3 Effect of pH on chloride and sulphate removal

A set of experiments were performed to evaluate the effect of pH on chloride and sulphate precipitation. The experiments were carried out at 200 rpm and 25 ºC in a shaking incubator for 24 hours at different pH (4, 7, 9, 11 and 13), adjusted with 1 M nitric acid. The Ca/anions

ratio and Al/anions ratio used in these experiments were 1.5:1 and 1:1 respectively. After 24 hours of mixing the reactors were left to settle for 30 minutes and filtered through 0.8 µm membranes for further analysis.

7.6.4 Effect of temperature on chloride and sulphate removal

In order to evaluate the effect of temperature on chloride and sulphate removal a series of experiments were conducted by mixing 0.3 L of solution and Ca/anions ratio of 1.5:1 and Al/anions ratio of 1:1 at 200 rpm and different temperatures (25, 35, 45, and 55 ºC) for 24 hours. After 24 hours of mixing the reactors were left to settle for 30 minutes and filtered through 0.8 µm membranes for further analysis.

Samples from the precipitation experiments were taken and filtered by vacuum filtration through a Whatman 0.8 µm membrane filter of polyvinylidene fluoride. The solids were washed with deionised water and dried at ambient temperature for further analysis by x-ray diffraction (XRD). The filtrates were collected and analysed by ICP OES following the USEPA 6010 standard procedure to determine cation concentration and by photometric methods APHA 4500 SO_4^{2-} E and APHA 4500 Cl G for sulphate and chloride determination respectively.

7.7 Electrodialysis

An electrodialysis module EDR-Z/2X10-0.8_19 (Membrain) was used in this section (Figure 43 and Table 11). This module was fitted with ten pairs of Ralex® membranes with 1344 cm^2 total effective surface, arranged by pairs of cation and anion exchange membranes. 1 L of bore water was fed to the module through the concentrate and diluate compartments by two peristaltic pumps (Master flex L/S) at different flow rates and recirculated in the stack until the desired concentration of ions was achieved. The effect of different applied voltages was investigated by adjusting the applied voltage through a rectifier. Na_2SO_4 solution was recirculated at a flow rate of 25 L/h through the electrode compartment to avoid electrode reaction during experiments. Samples were taken at different times to analyse the concentration of ions, conductivity, and total dissolved solids.

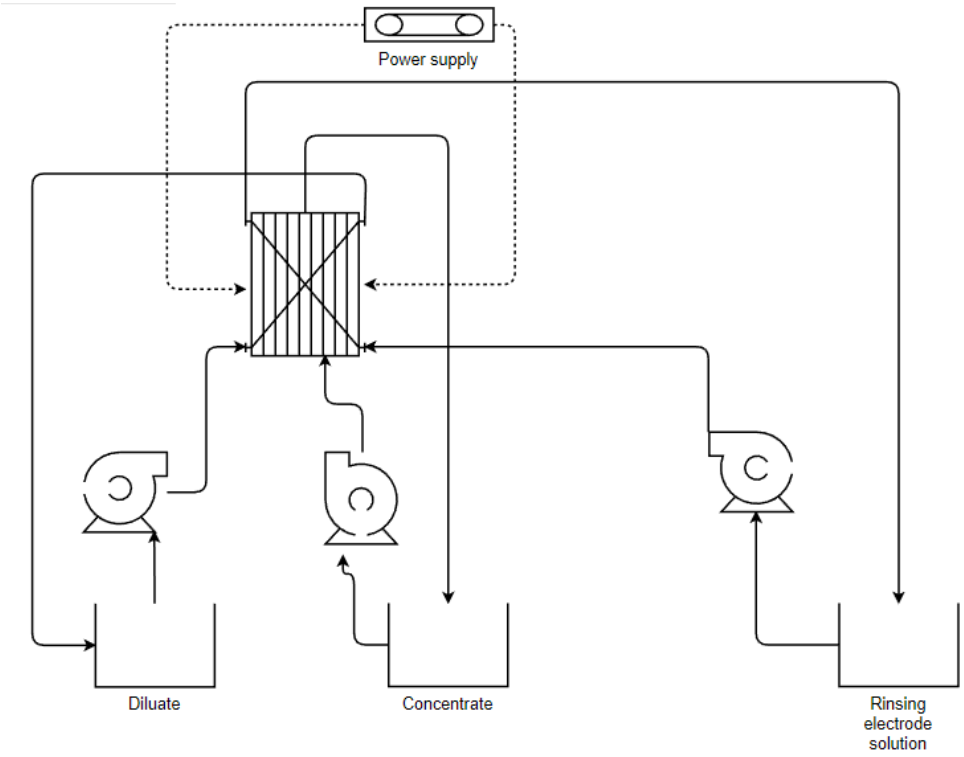

Figure 43. *Schematic of Electrodialysis (ED) module set up.*

Table 11. *ED specification and characteristics.*

Component		**Characteristics**
ED Stack	Two electrodes with the capability of reversal	
EDR-Z/2 X10-0.8_19	Dimensions:	
		Width 90 mm
		Length 128 mm
		Height 250 mm
	One hydraulic stage	10 membrane pairs
Electrodes (anode, cathode)		Ti+Pt
Ion exchange membranes	Anion exchange membranes	Ralex ® AM(H)-PES Active area: 64 cm^2
	Cation exchange membranes	Ralex ® CM(H)-PES Active area: 64 cm^2
Spacer	Thickness	0.8 mm

The membranes in the electrodialysis stack were manufactured by Mega, Czech Republic. The Ralex ® AM(H)-PES (anionic) contains quaternary ammonium as the ion exchange group and the Ralex® CM(H)-PES (cationic) contains sulphone as the ion exchange group (Figure 44). The electrodialysis stack holds 11 cation exchange membranes and 10 anion exchange membranes with a total of 10 membrane pairs and each membrane has an effective surface area of 64 cm^2 with a total installed surface of 1344 cm^2 within the stack.

Different parameters considered critical for the performance of an electrodialysis system were evaluated (Table 12).

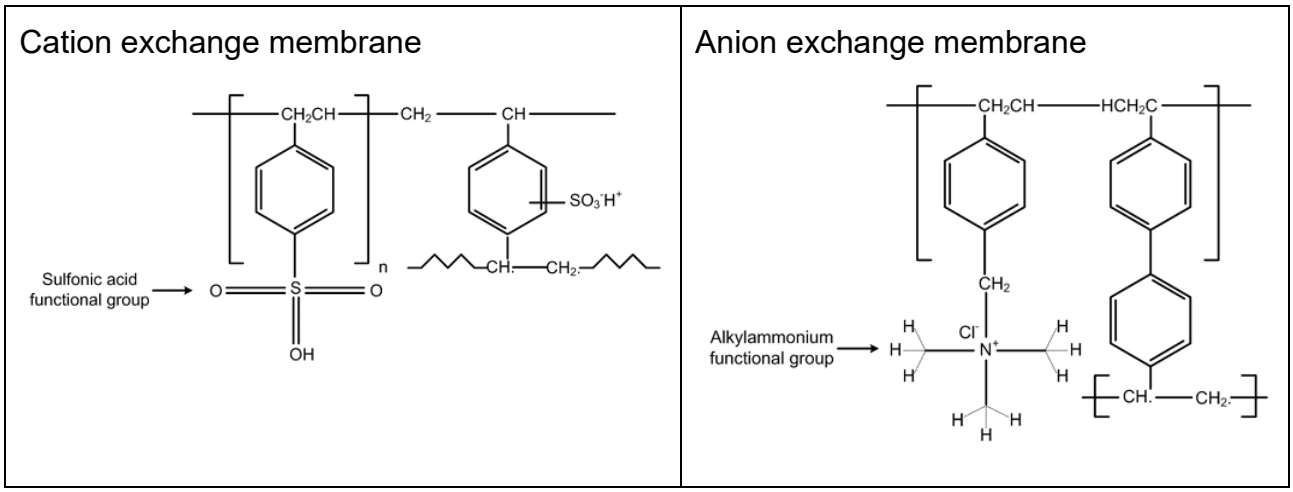

Figure 44. *Ion exchange functional group for cationic and anionic membrane.*

Table 12. *ED parameters evaluated*

Parameters	**Levels evaluated**
Applied voltage	0.4, 0.6, 1 and 2 V/membrane pair
Flow velocity	2.3, 3.3 and 4.2 cm/s
Ion concentration	Bore water and synthetic water with higher ion concentration

To maintain similar conditions and avoid concentration polarisation, before each experiment the ED stack was chemically cleaned by a sequence of recirculation of 2% NaOH for 30 minutes followed by flushing with deionised water, then circulation of 2% HNO_3 for 30 minutes followed by flushing with deionised water.

7.8 Results and Discussion

7.8.1 Nanofiltration

Nanofiltration performance and ion rejection

The performance of the two membranes (4040A and NF90 4040) in rejecting calcium, magnesium, sodium, sulphate, and chloride ions was evaluated under various conditions. The pattern of ion rejection is similar for the two membranes; as the transmembrane pressure increases, the ion rejection increases, which agrees with results reported by other researchers (Ahmad, et al., 2004). From Figure 45, it can be observed that while the recovery increases, the membrane performance decreases. This is because the concentrate returning to the feed stream increases the concentration of ions to be rejected,

increasing the ion driving force and changing membrane surface characteristics affecting the rejection of ions. Table 13 shows the ion concentration achieved under different operating conditions. Removal of problematic ions for mineral processing operations such as calcium, magnesium and sulphate can be achieved to the extent where the ionic concentrations have a negligible effect on the processes (<50 mg/L) with pressures as low as 4 bar. For processes such as flotation of monazite where the concentration of monovalent ions such as sodium and chloride are also important, pressures over 16 bar are necessary to achieve anion concentrations <500 mg/L which is required to avoid a detrimental effect on the process.

Figures 45 and 46 show the trend of ion rejection (R_{abs} (%)) by the membranes, which reveals that 4040A and NF90 4040 performed well overall. The rejection mechanism of these membranes appears to be strictly driven by the transmembrane pressure, where rejection increases with increased pressure, with a maximum rejection achieved at over 12 bar of pressure. Additionally, the NF90 4040 seems to have a high rejection of divalent ions when 8 bar of pressure was applied.

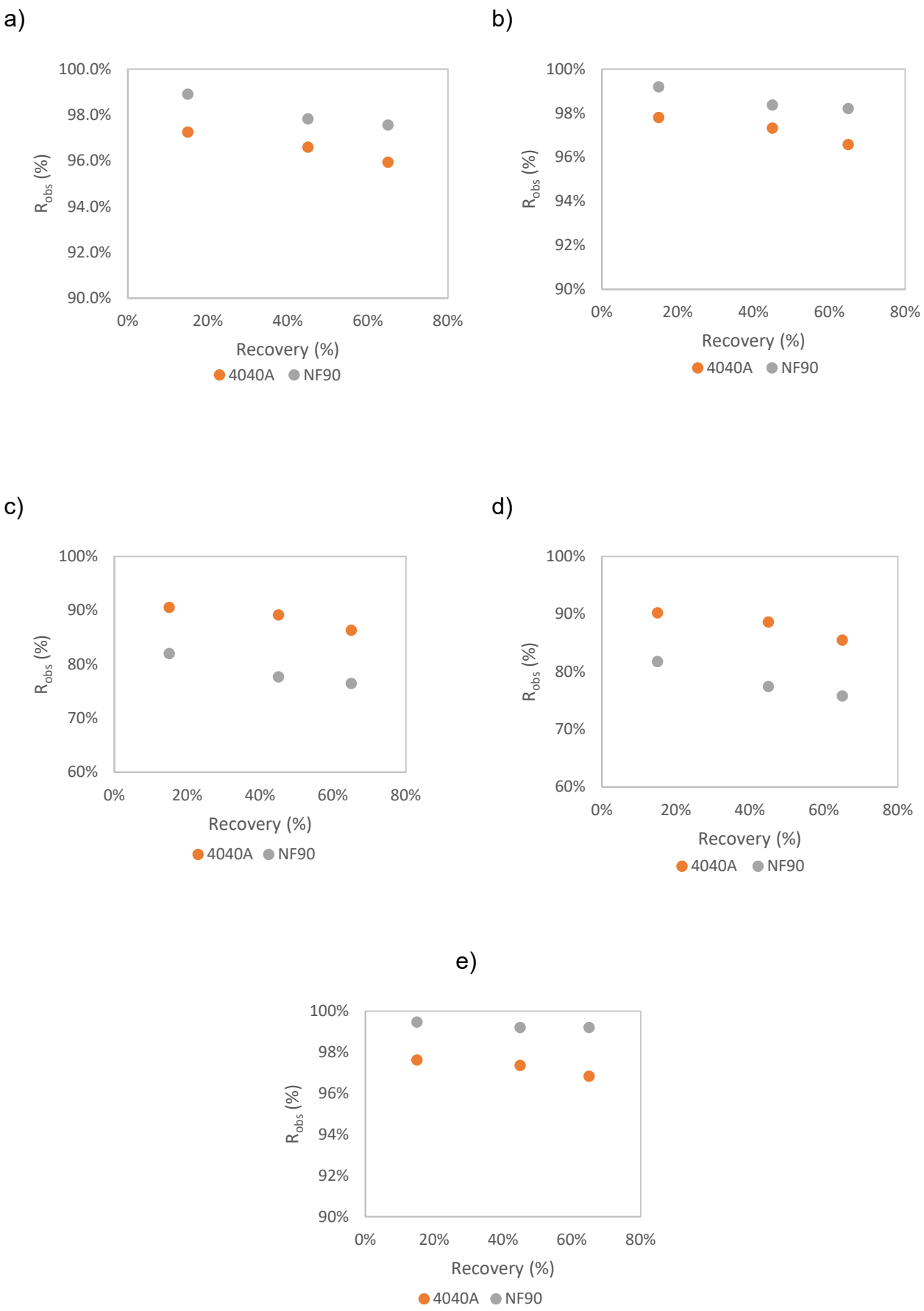

Figure 45. *Effect of water recovery on ion rejection at 12 bar. a: Ca^{2+}, b: Mg^{2+}, c: Na^{+}, d: Cl^{-} and e: SO_4^{2-}*

Table 13. *Ion concentration in the permeate as a function of pressure and recovery.*

Pressure (bar)	Recovery	Ca^{2+} (mg/L)		Mg^{2+} (mg/L)		Na^{+} (mg/L)		SO_4^{2+} (mg/L)		Cl^{-} (mg/L)	
		NF90 (±0.06)	4040A (±0.39)	NF90 (±1.03)	4040A (±0.83)	NF90 (±19.45)	4040A (±15.67)	NF90 (±1.00)	4040A (±1.41)	NF90 (±30.41)	4040A (±67.18)
8	15%	1.55	16.45	1.51	8.72	325.03	274.57	4.00	58.00	473.00	416.00
	45%	3.17	16.09	2.92	11.18	366.61	365.45	6.00	59.00	532.00	545.00
	65%	3.35	27.96	3.12	20.21	398.95	605.75	6.00	96.00	595.00	886.00
12	15%	1.54	3.88	1.35	3.68	278.22	146.15	4.00	18.00	403.00	216.00
	45%	3.07	4.80	2.74	4.49	345.56	167.46	6.00	20.00	499.00	251.00
	65%	3.44	5.72	3.00	5.75	364.08	211.43	6.00	24.00	535.00	321.00
16	15%	1.74	4.14	1.22	4.04	203.71	147.68	3.00	18.00	300.00	214.00
	45%	2.11	4.45	2.11	4.83	258.16	170.50	4.00	21.00	384.00	257.00
	65%	2.54	5.83	2.50	5.98	304.52	212.84	5.00	25.00	456.00	308.00
20	15%	1.26	3.79	1.35	4.35	195.10	150.24	4.00	20.00	288.00	231.00
	45%	3.22	4.74	2.68	5.30	257.73	180.50	5.00	23.00	377.00	270.00
	65%	2.78	5.90	2.93	6.60	309.76	222.19	6.00	28.00	458.00	335.00

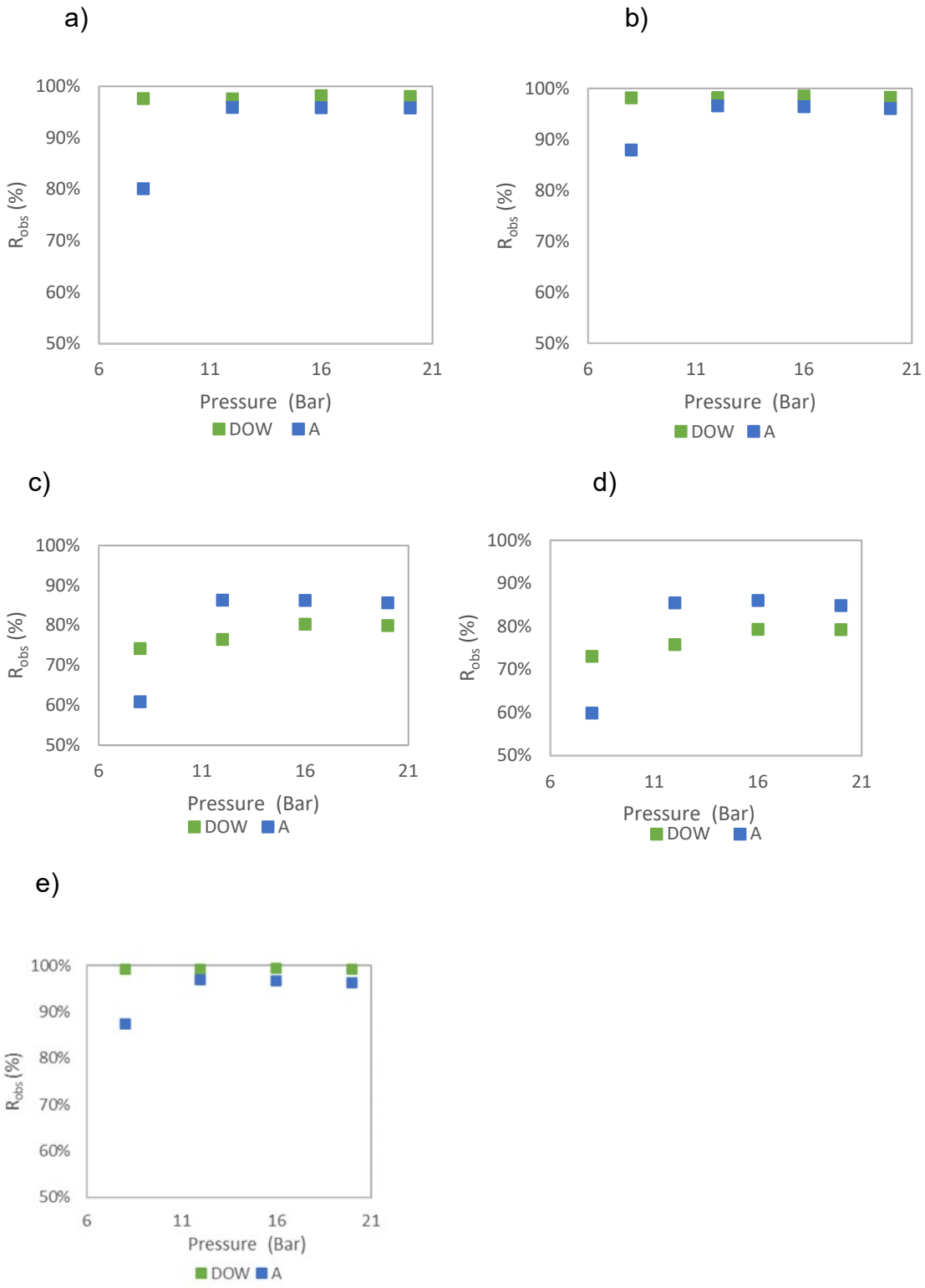

Figure 46. *Ion rejection at different pressures at 65% recovery DOW (NF90 4040), A (4040A). a: Ca^{2+}, b:Mg^{2+}, c: Na^{+}, d: Cl^{-} and e: SO_4^{2}*

It can be further seen from Figure 46 that the 4040A and the NF90 4040 membranes reject more than 95% of the divalent cations (Ca^{2+}, Mg^{2+}) and more than 74% of Na^{+} at a pressure higher than 12 bar and for all recovery ranges evaluated. In the case of the anions, membranes 4040A and NF90 4040 could reject over 87% of sulphate and over 73% of chloride.

Estimation of reflection coefficient (σ) and ion permeability (Ps) through the Spiegler-Kedem-Katchalsky (SKK) model

Detailed explanation of the SKK model and the relevant parameters has been provided by (Guerra et al, 2023).

Table 14. Reflection coefficient and ion permeability predicted using the SKK model.

		σ		Ps (m/h)	
Recovery		N90 4040	4040A	N90 4040	4040A
15%	Ca^{2+}	0.989	0.973	$6.4X10^{-5}$	$1.3\ X10^{-4}$
	Na^{+}	0.903	0.925	$3.8\ X10^{-3}$	$1.7\ X10^{-3}$
	Mg^{2+}	0.993	0.983	$9.0\ X10^{-5}$	$4.9\ X10^{-4}$
	SO_4^{2-}	0.898	0.923	$3.8\ X10^{-3}$	$1.9E\ X10^{-3}$
	Cl^{-}	0.995	0.976	$4.1\ X10^{-5}$	$9.4\ X10^{-5}$
45%	Ca^{2+}	0.981	0.968	$2.4\ X10^{-4}$	$1.5\ X10^{-4}$
	Na^{+}	0.848	0.934	$3.7\ X10^{-3}$	$2.8\ X10^{-3}$
	Mg^{2+}	0.984	0.982	$2.0\ X10^{-5}$	$6.7\ X10^{-4}$
	SO_4^{2-}	0.841	0.931	$3.7\ X10^{-3}$	$2.9\ X10^{-3}$
	Cl^{-}	0.992	0.995	$2.0X10^{-5}$	$9.0\ X10^{-4}$
65%	Ca^{2+}	0.981	0.962	$2.4\ X10^{-4}$	$1.7\ X10^{-4}$
	Na^{+}	0.839	0.881	$4.2\ X10^{-3}$	$2.3\ X10^{-3}$
	Mg^{2+}	0.983	0.965	$5.0\ X10^{-5}$	$1.6\ X10^{-4}$
	SO_4^{2-}	0.803	0.876	$3.6\ X10^{-3}$	$2.4\ X10^{-3}$
	Cl^{-}	0.992	0.967	$2.0\ X10^{-5}$	$1.6\ X10^{-4}$

Table 14 shows the ion permeability (P_s) and the reflection coefficient (σ) for different ions for the membranes evaluated. The reflection coefficient of the NF90 for calcium ions was the highest of the two membranes as the divalent ion rejection of this membrane was superior to the other membrane. In contrast, the σ value for

monovalent ions was greater for the 4040A which was the membrane that performed better on monovalent ion rejection. From Figure 47, it can be concluded that the SKK model can be used to explain the retention obtained experimentally as the experimental data fits well with the theoretical data from the model.

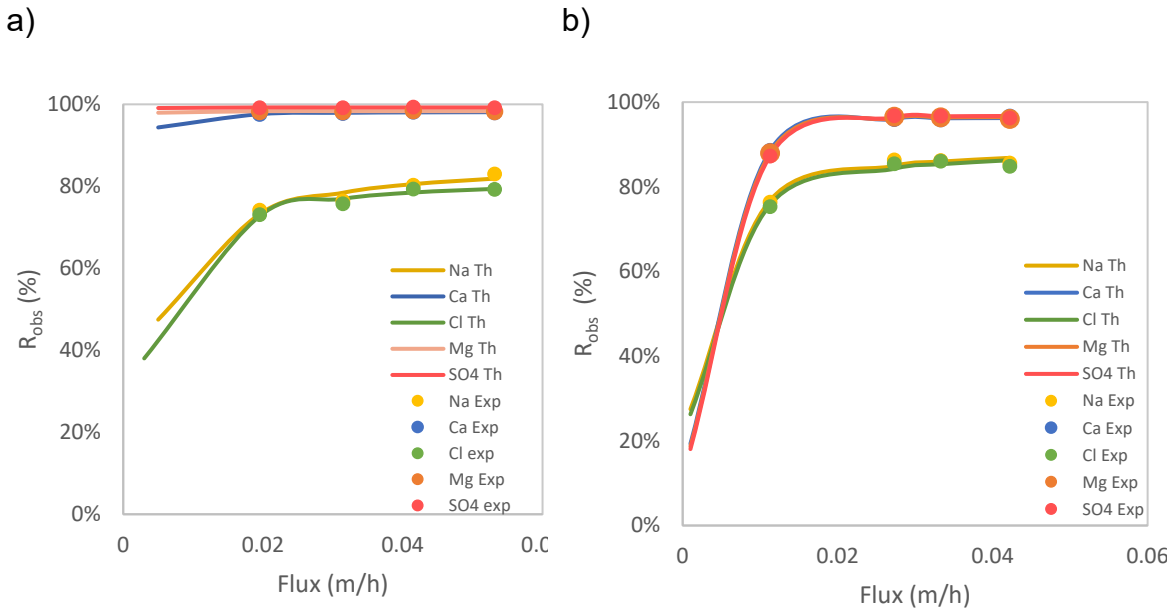

Figure 47. *SKK NF modelling results for: a) NF90 and b) 4040A.*

7.8.2 Membrane properties

Hydraulic permeability of the membranes

As has been reported in previous studies with similar membranes, the flux through the membranes (J_v) is proportional to the transmembrane pressure (Figure 48) (Yammine et al., 2019 and Aktas et al., 2017), obeying the homogenous solution diffusion through the polymeric membrane model. This describes the proportionality of the water mass transfer flux and the pressure differential across the membrane. The permeate flux with the NF90 4040 membranes starts at an applied pressure of 0.884 bar, while the flux with membrane 4040A starts at 2.45 bar. Membrane 4040A presents a surface with the tightest pores and is more dependent on osmotic pressure, requiring more force to mobilise the feed through the membrane. Additionally, because of the differences in pore size between the membranes, the permeability of the membranes differs from one to another; as the pore size decreases, the ions in the solution make the surface of the membrane more compact, reducing the permeability of the membranes.

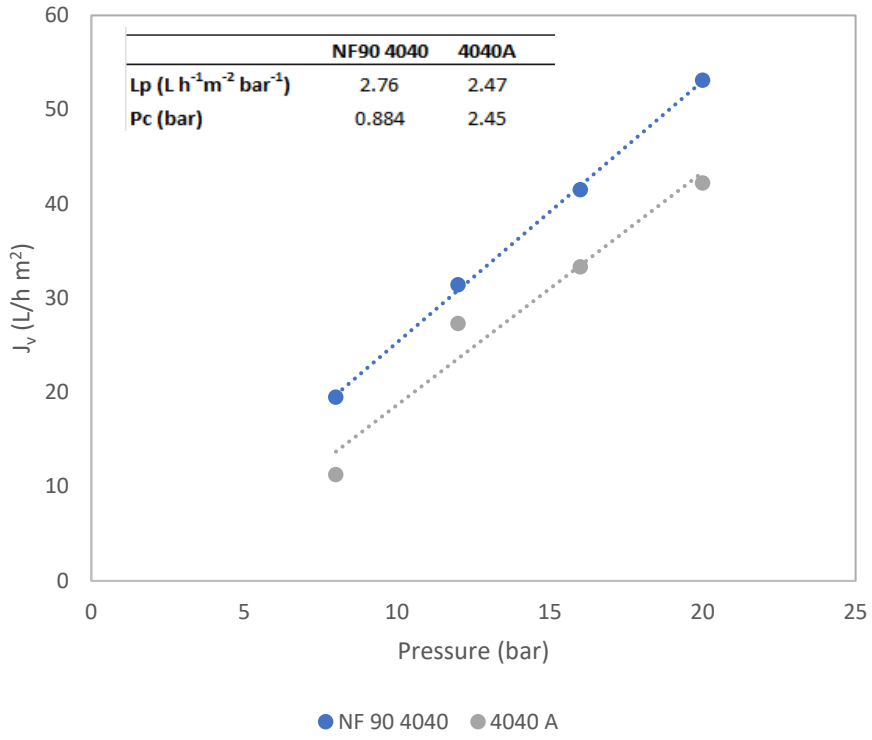

Figure 48 Bore water flux as a function of pressure.

Calculated molecular weight cut-off (MWCO) values

The molecular weight cut-off is widely used to express the ability of certain membranes to reject a solute (C_0) due to selectivity related to the pore diameter (C_{conv}) and solute characteristics such as the diameter (d_s) of the ion and the pore diameter of the membrane (d_p).

$$C_{conv} = C_0 \left[1 - \left(d_s / d_p\right)\right]^2 \quad (11)$$

As long as the ion rejection is ≥ 90%, this expression can be written in terms of the molecular weight of ionic solutes (M) and the MWCO of the membrane.

$$C_{conv} = C_0 \left[1 - \left(M / MWCO\right)^{1/3}\right]^2 \quad (12)$$

The MWCO on this occasion was established by the C_{conv} of each membrane determined for the main salt in the feed, sodium chloride. Table 15 shows the MWCO values calculated for the two membranes. The MWCO can be related to mass transport as bigger molecules will diffuse more slowly than smaller molecules; in this order of ideas, when the MWCO is small, the diffusion and the chemical interactions will increase for monovalent ions (Kelewou et al., 2011 and Van de Bruggen et al., 1999). This means that membrane 4040A is the one with the more diffusive transfer.

Table 15. *MWCO calculated from NaCl data for each membrane.*

Membrane	MWCO calculated (Da)	MWCO theoretical (Da)
NF90 4040	167	100-200 (Hidalgo et al., 2013, Luo et al., 2010, Jadhav et al., 2016, Krieg et al., 2005 and Tanne et al., 2019)
4040A	131	No Reference available

.

Estimation of membrane pore radius

An average pore radius (P_r) was determined using the data of the reflection coefficient determined by the SKK model for each ion at each recovery. Table 16 shows that the NF90 and 4040A have similar pore radius. It was expected to have a similar pattern to that obtained with the MWCO, with 4040A having a smaller pore radius than the other membrane. However, the ionic interactions, the complex separation mechanism of NF membranes, and ions present in the bore water that might not be accounted for in the analysis are obstacles for the accuracy of any model implemented.

Table 16. *Average pore radius from SHP model.*

Membrane	Recovery	Ca^{2+}	Na^{+}	Mg^{2+}	SO_4^{2-}	Cl^{-}	Average P_r	Theoretical P_r (nm)
NF90 4040	15%	0.34	0.25	0.38	0.25	0.16	0.29	0.31 (Ramdani et al., 2021)
	45%	0.35	0.27	0.39	0.25	0.18		
	65%	0.35	0.27	0.39	0.25	0.19		
4040A	15%	0.36	0.24	0.39	0.27	0.16	0.29	No reference Available
	45%	0.37	0.24	0.39	0.25	0.16		
	65%	0.37	0.26	0.42	0.27	0.17		

7.8.3 Mass transport through each membrane - hydrodynamic approach

By plotting the concentration of ions in the permeate (C_p) and the flux through each membrane (J_v), it is possible to determine the solute flux due to diffusion by the slope (j_{diff}) and the solute transport due to convection by the intercept (C_{conv}).

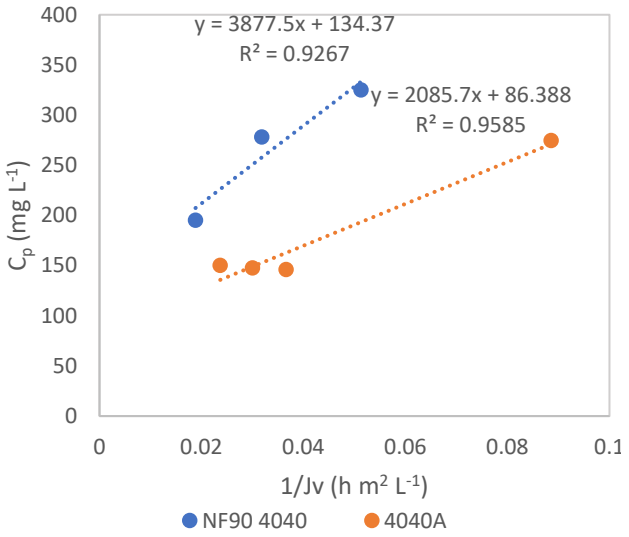

Membrane	C_{conv} (mg L^{-1})	j_{diff} (mg m^2 h^{-1})
NF90 4040	134.37	3877.50
4040A	86.39	2085.70

Figure 49. *Permeate NaCl concentration as a function of the inverse of flux at 15% recovery.*

In nanofiltration, the transport of ions is not well defined. It seems to be a complex mechanism that combines the sieving effect of ultra and microfiltration and the diffusion transport by membrane ionic strength that is characterised in reverse osmosis processes. Figure 49 displays a hydrodynamical approach, however, it is limited due the assumption of non-charged membranes.

Table 17. *Peclet (Pe) number of each membrane for Na at different pressures.*

Membrane	8 bar	12 bar	16 bar	20 bar
NF90 4040	0.68	1.09	1.44	1.84
4040A	0.47	1.13	1.38	1.75

Table 17 shows the Pe values for each membrane at different operating pressures. The mass transport through the membranes is affected by changes in pressure. At low pressures, the diffusional mass transfer is dominant for the NF90 4040 and 4040 A (Pe<1). This effect is due to convective mass transfer being governed by physical parameters such as pressure (Lhassani et al., 2001). Additionally, diffusive mass transfer is stronger than convective mass transfer, which means that the solvation energies and the effect of ion concentration are more noticeable at low operation pressures, as discussed previously (Dach, 2009).

7.8.4 The effect of a second nanofiltration stage on water recovery

The need to recover high percentages of water is one of the main limitations of water treatment processes. Figure 50 shows the implementation of two stages of nanofiltration using the membrane 4040A membrane. This experiment was evaluated at 12 bar of pressure, recovering the concentrate from the first stage and mixing it in the same proportion with bore water. This mix is fed into a second nanofiltration stage and filtration was conducted from these experiments. It was determined that the final ion removal at 90% recovery of the permeate was 91% for Ca^{2+} and Mg^{2+}, 70% for Na^{+}, 63% for Cl^{-} and 93% for SO_4^{2-}. For mineral processing operations where the presence of divalent ions (Ca^{2+}, Mg^{2+} and SO_4^{2-}) is critical such as the flotation of phosphate minerals, the operation of a two-stage system could be a promising option to maximise water utilisation. The removal of monovalent ions through the two-stage system may not be adequate for operations such as monazite flotation where a concentration of monovalent ions (Na^{+}, Cl^{-}) over 500 ppm could slightly affect the recovery and grade of the concentrate. These results indicate that nanofiltration systems could be tailored to the necessities of each operation as different minerals are susceptible to different ions in solution.

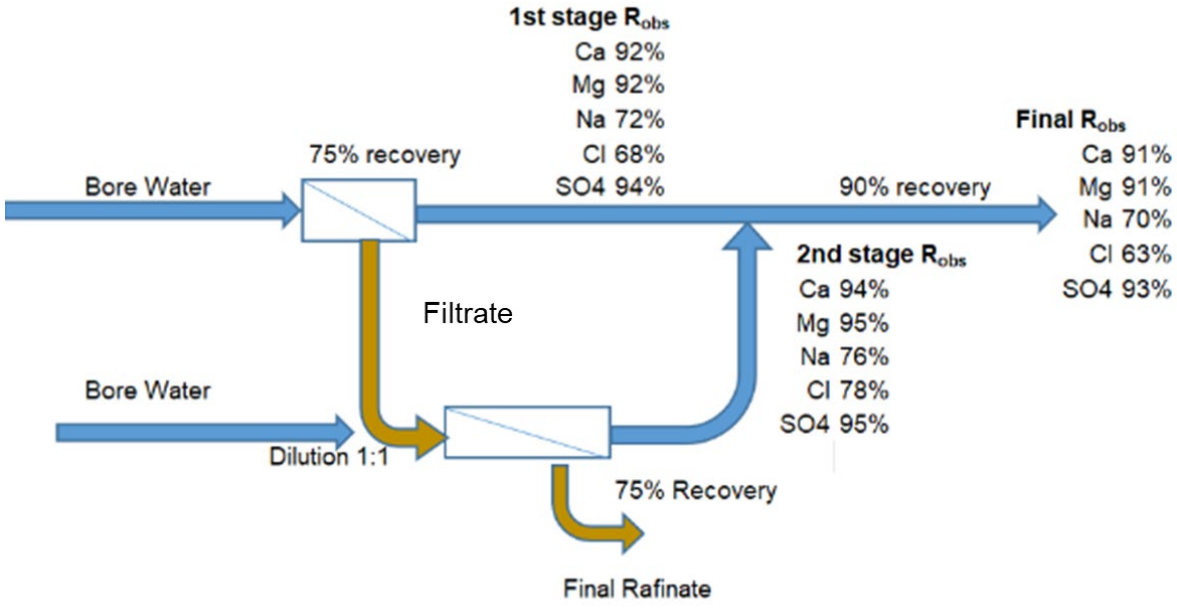

Figure 50. *Two-stage nanofiltration process with 90% recovery of permeate.*

7.8.5 Energy cost estimation for single stage and two-stage processes

In pressure-driven processes, energy cost is the main component of operating cost. The high consumption of energy in processes such as nanofiltration and reverse osmosis is principally associated with the use of high-pressure pumps which represents up to 60% of the total water treatment cost (Grano et al., 1995). The specific energy requirements for a pressure-driven process can be quantified by the correlation of pressure and the recovery of permeate, and generally, the energy requirement

increases linearly with increasing system pressure (Dach, 2009). The specific energy consumption (SEC) of membrane-based water treatment can be given by:

$$SEC = \frac{\Delta P \ 100}{\eta r \ 36} \quad (13)$$

Where ΔP is the transmembrane pressure in bar, ɳ is the global pumping efficiency (generally 85%) and r is the water recovery of the system.

Table 18. *Estimated specific energy consumption and cost as a function of pressure.*

	Single stage		**Two-stage**	
Pressure (bar)	SEC (kWh/m^3)	$/ton	SEC (kWh/m^3)	$/ton
12	0.523	0.192	0.697	0.257
16	0.697	0.257	0.930	0.343
20	0.871	0.321	1.162	0.429
25	1.089	0.401	1.452	0.536

Table 18 shows the comparison of specific energy consumption at different transmembrane pressures. In this comparison, an assumption of standard water consumption in mineral processing operations of 3 m^3 per ton of ore processed, and electricity prices of 0.123 $/kWh for industry reported by the Australian energy council in 2022 were considered (Bulut and Yenial, 2016). In this study, it was found that a single filtration stage with 4040A membrane at 12 bar of transmembrane pressure resulted in conditions to produce water with sufficient quality for mineral separation processes at an energy cost of 0.192 $/ton. Adding a second filtration stage to the process results in an incremental energy cost of 33%, but water recovery increases up to 90%. Comparing the results in Table 18 with high pressure systems such as reverse osmosis that usually require around 20 bar to treat brackish water of similar quality as the sample tested in this study suggests significant energy savings are possible, compared to producing water with ultrahigh purity that is sometimes not required in mineral processing operations (Grano et al., 1995 and Guimares and Peres 1999). Even so, a two-stage nanofiltration process consumes 25% less energy than a high transmembrane pressure process.

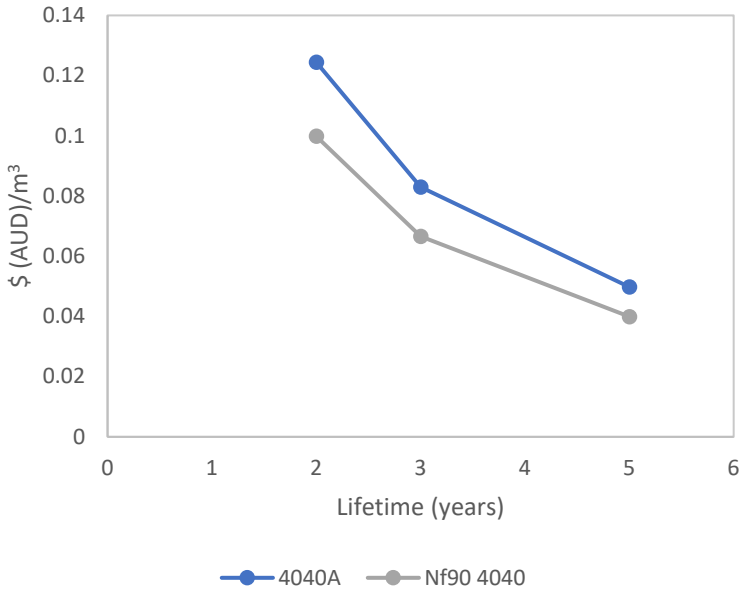

Figure 51. *Membrane replacement cost at different lifetimes (at 16 bar of transmembrane pressure and 65 % recovery).*

Membrane replacement cost is another key operating cost. This variable is associated with the permeability, production rate and lifetime of each membrane. This parameter can be expressed through the following expression (Winston and Sirkar, 1992):

$$RC = 2.74\, F_R\, M_C\, M_P^{-1} M_l^{-1} \tag{14}$$

Where RC is the unit replacement cost represented in AUD per every m^3 of water produced at different times in the membrane lifetime, M_C is the cost of the membrane (AUD/ft^2) which was obtained from a local membrane provider, F_R is the water recovery, Mp is the membrane productivity and M_l is the membrane.

Figure 51 shows how membranes with different permeabilities can have different costs of replacement for each m^3 of water produced. Therefore, a membrane with a low MWCO will have a higher replacement cost due to the low membrane production rate. The replacement cost of membranes with low ion rejection but high permeate flow rate will be lower than membranes that have similar characteristics to a reverse osmosis membrane such as the 4040A or the NF90 4040. A factor to consider in the membrane replacement cost is the lifetime of the membrane. As the ion rejection increases, the lifetime of the membrane is reduced due to multiple factors, such as fouling and concentration polarisation, resulting in an increase in the pressure required to achieve the same results (Govardan et all., 2020 and Liu et al., 2020). Nanofiltration membranes are expected to have a longer operating life and therefore lower replacement costs than RO membranes, as ion rejection is lower in nanofiltration membranes than in RO, but they are still able to produce the quality of water required.

It is important to mention that cost optimisation in pressure-driven processes will depend mainly on the operating pressure of the system and the right selection of membrane to achieve the water quality required.

7.8.6 Conclusions

The nanofiltration membranes NF90 4040 and 4040A were tested in a pilot scale rig to study their performance in producing water with concentrations under the threshold of 50 mg/L of calcium and magnesium and 500 mg/L of sodium. The influence of pressure was evaluated, and it was found that ion rejection is proportional to the transmembrane pressure. Additionally, it was determined that pressure is an important factor in the mass transfer mechanism. In this case, the rejection of ions by nanofiltration through the 4040A and the NF90 membranes at low pressures was driven by diffusional mass transfer, however, with over 12 bars of transmembrane pressure the process was driven by convection or a sieving effect through the pores. From a hydraulic point of view, it was demonstrated that high permeate flux leads to low ion rejection. Also, it was found that both membranes (NF90 4040, 4040A) rejected more than 95% of calcium and magnesium and more than 74% of sodium at pressures over 12 bar and water recovery of 65%.

The MWCO determined in this study for 4040A (Ecotechnol) was lower than for the other membrane used. The MWCO and theoretical pore size of NF90 4040 estimated in this study agrees with the range reported in other studies that used this membrane in similar conditions. The SKK model was used to predict the ion removal of the two nanofiltration membranes. The solute permeability constant and reflection coefficient were obtained, reflecting a satisfactory representation of the nanofiltration process using bore water. Furthermore, it was demonstrated that the membrane permeability was lower for divalent ions than for monovalent ions.

8. Electrodialysis

8.1 Effect of flow velocity on limiting current density

Figure 52 shows the curve to determine the limiting current density (LCD) for two flow velocities, 2.3 and 4.2 cm/s. There is no clear plateau region, however, there is a change in slope around 1.8 V and 2.1 V with corresponding LCDs of approximately 120 A/m^2 and 145 A/m^2. Possible reasons for the change from the Ohm's law relationship to the characteristic plateau of the LCD curve can include the strength of the electric field, which obscures the limiting current value, the cell's structure and the turbulence promoters inside that tend to lessen the visibility of the plateau. The experimental data for bore water at two different flow velocities shows that the LCD increases as the flow velocity increases. This is because high flow rates cause more turbulence, reducing the thickness of the diffusion layer and allowing electroactive species to move through cells more quickly, reaching the membrane surface faster

than at low flow velocities. Additionally, because current is proportional to the speed of ion movement, the latter increases at higher flow velocities (Devora-Isiordia et al., 2021).

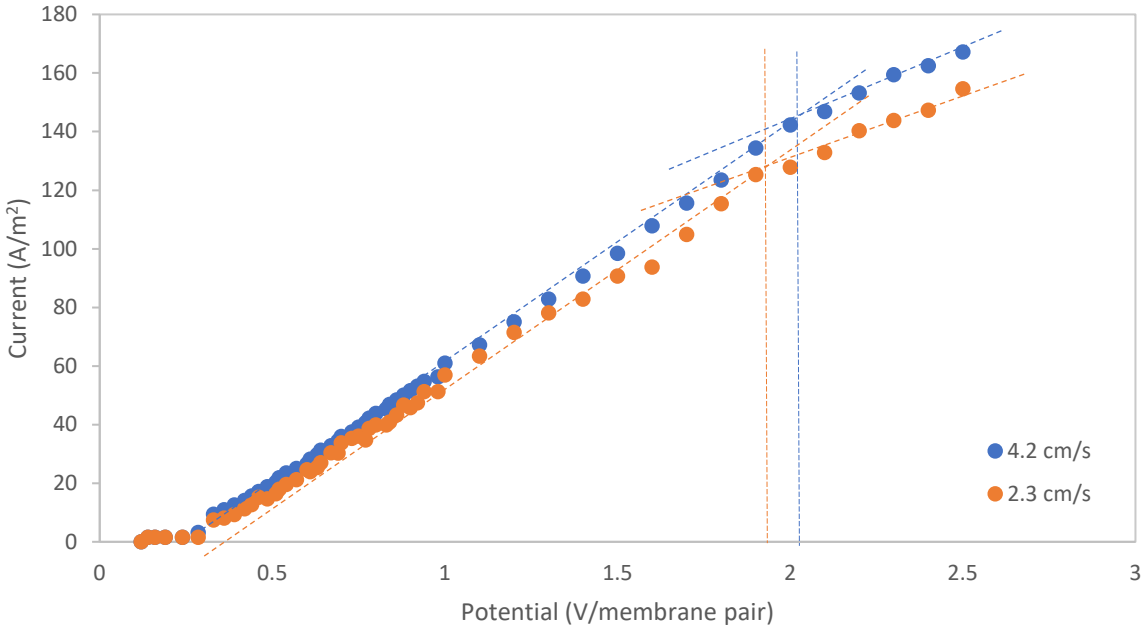

Figure 52. *Limiting current density - Bore water at different flow velocities.*

8.2 Effect of ions concentration on Limiting Current Density

The LCD is an important parameter for electrodialysis operation. This parameter defines the maximum electric current that can be used in a specific system. Figure 53 shows the voltage-current plots for bore water and for synthetic water with three times the ion concentration of the bore water. Generally speaking, the slope increases with increasing ion concentration in the feed solution. It is important to note that the slope moderately increases above 0.5 V/membrane pair due to the increase in ion mobility triggered by the Joule heat production with the increase in current (Bo et al., 2019). The bore water curve shows a slight change in slope indicating that the LCD was reached at an applied voltage of ~2.1 V/ membrane pair, which means that above this current the concentration of the electrolyte in the diluate tends to zero in the diffusion layer on the membrane surface.

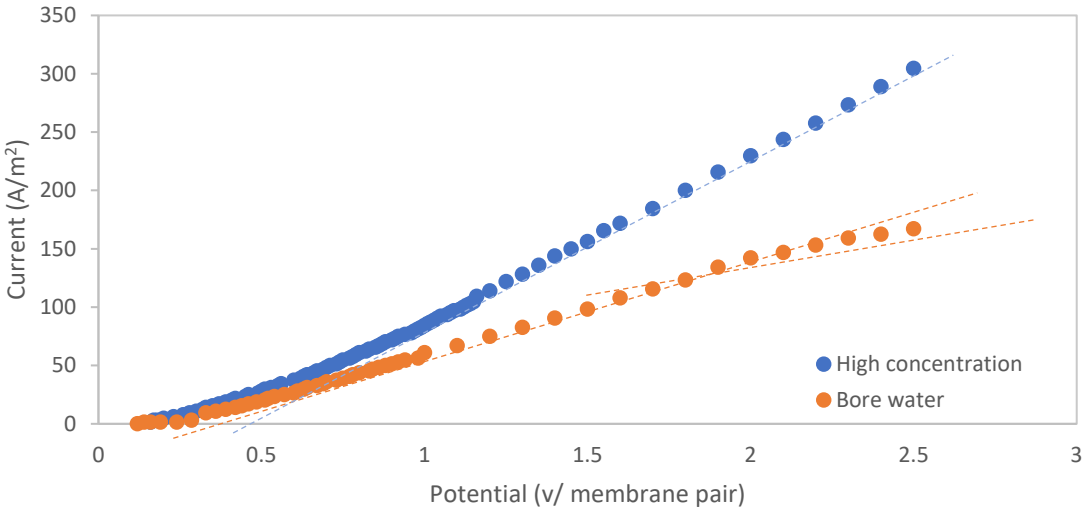

Figure 53. *Limiting current density at different ion concentrations.*

8.3 Effect of applied voltage on ion removal

The performance of the ED module was evaluated through both the concentration of ions and the change in concentration of total dissolved solids. The removal of total dissolved solids from the bore water is shown in Figure 54. In general, the total dissolved solids are removed faster at higher voltages applied to the ED stack as the current flow is also higher, which mobilises more ions from the diluate to the concentrate. It can be seen that at higher applied potentials, the required concentration is reached faster. It has been determined (Jung et al., 2022) that a TDS concentration below 1000 mg/L will provide a suitable concentration of cations and anions for mineral processing operations such as monazite flotation.

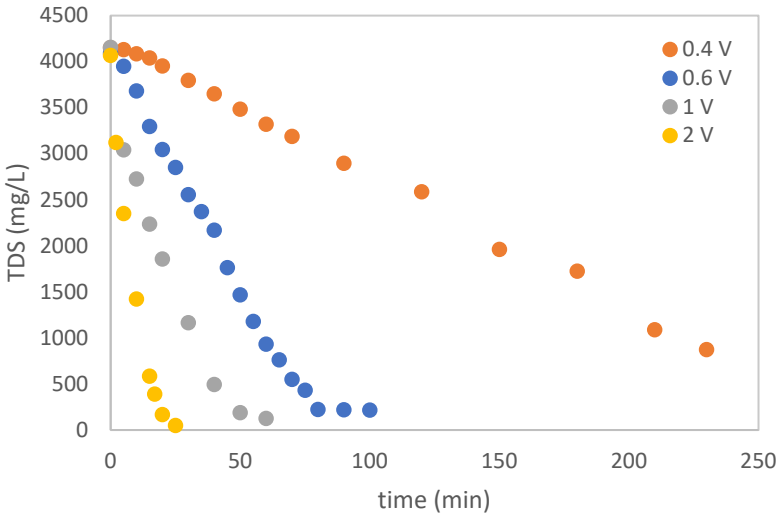

Figure 54. *TDS removal in the diluate stream at different voltages*

Ion exchange membranes enable selective permeation of ions with opposite charges, facilitating the transport of co-ions. Figure 55 shows the depletion of cations and anions from the diluate stream (Bore water). The applied voltage influences how the different ions are depleted from the diluate. As the voltage is increased, the removal of ions increases due to the increased current. At low voltages, such as 0.4 V/membrane pair, divalent and monovalent ions are depleted differently. It can be seen that divalent ions such as calcium, magnesium and sulphate are depleted at a slower rate than monovalent ions. This is due to the fact that monovalent ions are less hydrated, making them more susceptible to faster removal from the diluate. In addition, the bulkier the ion, such as monovalent ions, the more it is removed by the membrane. This agrees with the results displayed in Table 19 which shows the ion selectivity of the membranes for cations and anions at three different applied voltages. For the cations it can be seen that calcium is transported slower than sodium and magnesium and for the anions, chloride ions are transported faster than the divalent ions of sulphate. It can be seen that membrane selectivity changes at different applied voltages.

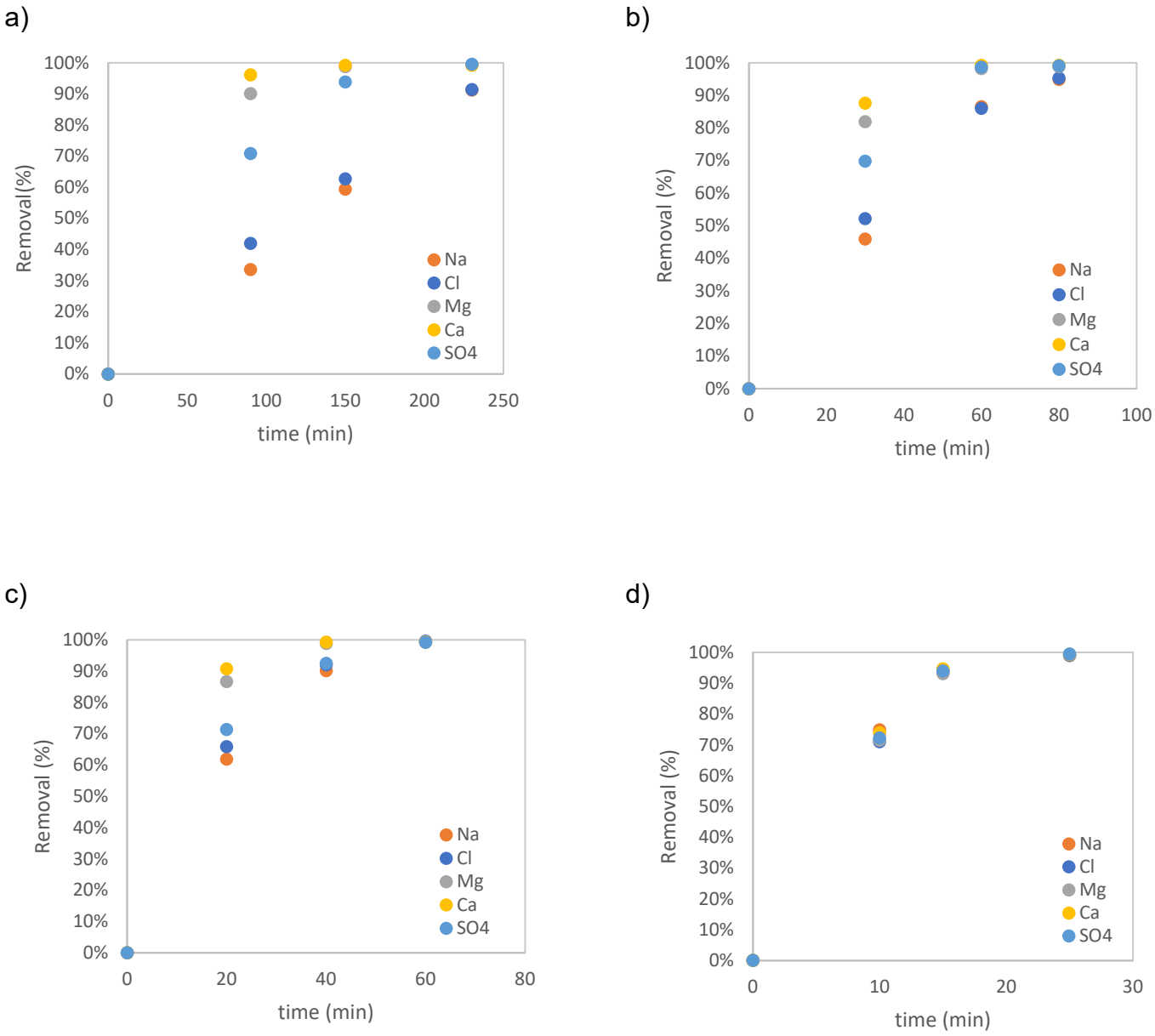

Figure 55. *Effect of voltage on ion removal. a) 0.4, b) 0.6, c) 1, and d) 2 V/ membrane pair*

8.4 Modelling of synthetic NaCl (4.5 g/L) solution by Nernst-Planck model

Figure 56 shows experimental and theoretical data for the concentration (C_d) of NaCl in the diluate over time at a current density of 14 A/m^2. Despite the fact that the model was created on a fairly idealised foundation and had a number of restrictions and assumptions, comparing the experimental results with the predicted results produces an average relative error of only 12%. This relative error is associated mainly with the assumption of maximum efficiency of the process and parameters assumed from theory and not measured experimentally. Also, problems of scaling of the membranes may have contributed to deviations from the predicted results. Additionally, it was identified from the model that migration (M = 5.18x10^{-4} m^2/h) forces are stronger than

diffusion ($2.61x10^{-9}$ m^2/h) mass transfer, however, in Figure 57 it can be seen that the diffusion coefficient increases over time, as the concentration gradient between the concentrate and the diluate increases.

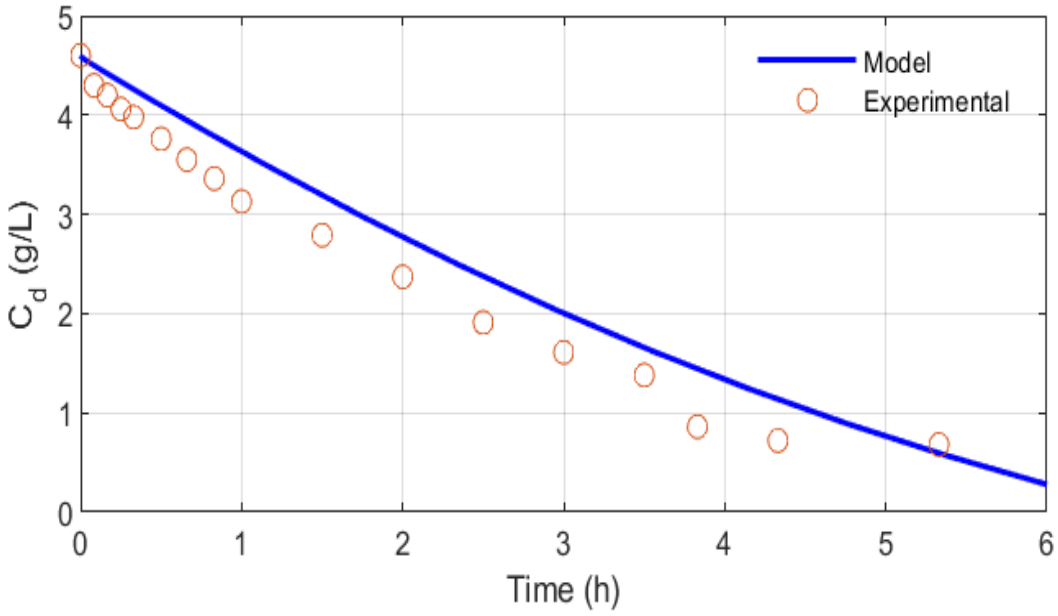

Figure 56. *Modelling of 4.5 g/L NaCl solution.*

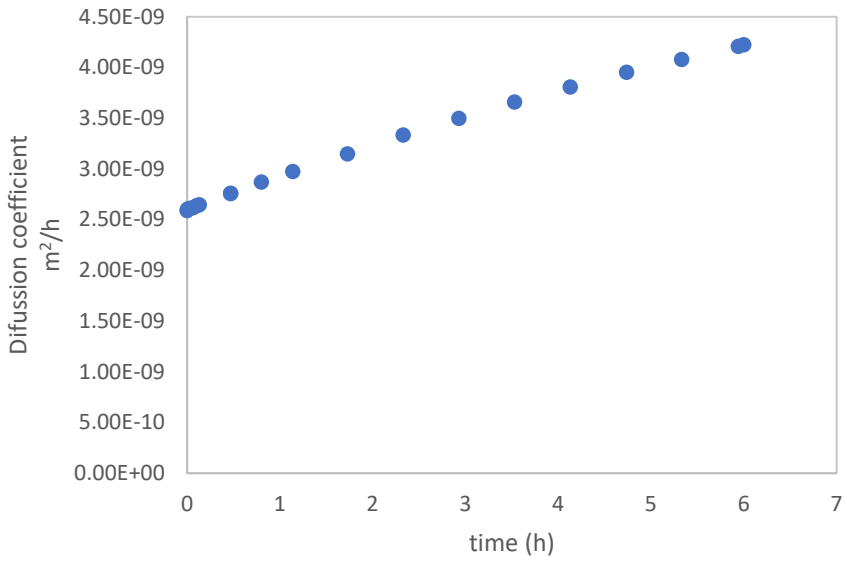

Figure 57. *Diffusion coefficient through time.*

Table 19. *Membrane selectivity*

	0.4 V/pair	**1 V/pair**	**2 V/pair**
S_{Mg}^{Ca}	-0.00494	-0.00199	-0.000849
S_{Na}^{Ca}	-0.06307	-0.04801	-0.00200
S_{SO4}^{Cl}	0.068325	0.00223	0.002299

8.5 Effect of feed velocity on TDS removal

The effect of the feed velocity on the desalination was evaluated (Figure 58). Increased feed velocity is expected to lead to shortened contact time between the streams and the membranes. At low velocities in particular, free movement of monovalent ions would allow the monovalent ions to find exchange sites available on the membrane. It is important to note that divalent ions will occupy free sites first due to the stronger electrostatic interaction with the membrane (Karimi, Ghaseemi and Zamani, 2018).

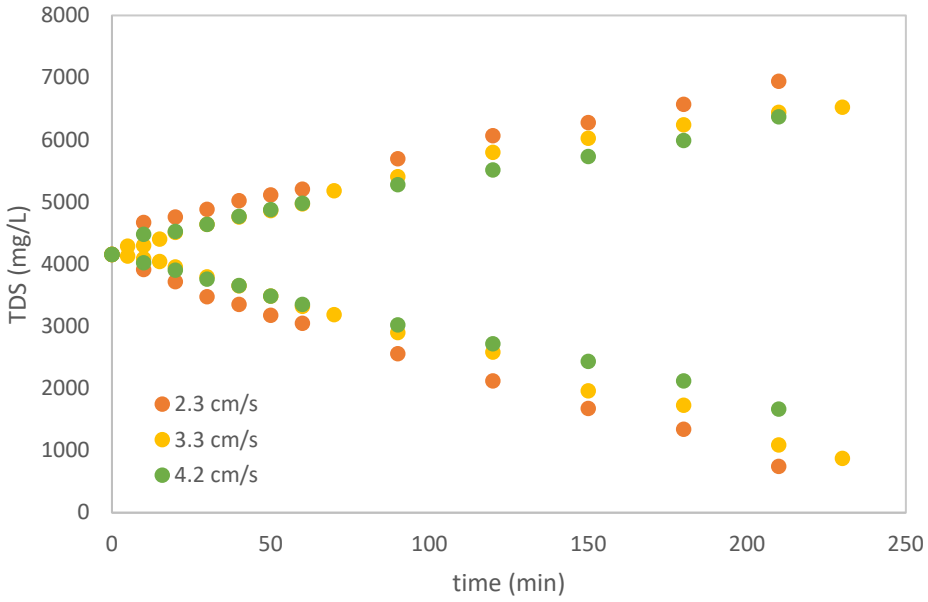

Figure 58. *Effect of linear velocity on TDS.*

8.6 Specific treatment capacity (STC)

Table 20 shows the specific treatment capacity for the bore water and the synthetic water. The results indicate that the STC highly depends on the ion concentration and the number of ions to be removed. The STC calculated for the two different samples demonstrates that the capacity is reduced when the ion concentration in the feed water increases. It has been demonstrated that systems with STC higher than 30 L/h m^2 are

difficult to operate and require high control and optimisation due to high current densities (PCCell). Considering the current characteristics of the bore water, it is not recommended to apply a voltage over 1 V/ membrane pair for ion removal.

Table 20. *Effect of voltage on STC.*

Applied voltage (V/ membrane pair)	**Water**	**STC (L/h m^2)**
0.4	Bore water	2.13
0.6	Bore water	7.44
1	Bore water	14.88
	Synthetic water	5.58
2	Bore water (4.2 g/L)	37.20
	Synthetic water (12 g/L)	16.53

8.7 Effect of ion concentration

One of the characteristics of the groundwater in Western Australia is the variability of the ion concentration. Synthetic water with three times the concentration of ions in the bore water was tested. The results in Figure 59 show that it takes 2.6 and 2.3 times more time (1 V and 2 V per cell pair, respectively) to reach a concentration of around 1000 mg/L.

8.8 Energy cost estimation

In membrane processes, energy cost is the main component in the operating cost of these systems. The high consumption of energy in processes such as nanofiltration and electrodialysis is principally due to the energy required for ion mass transfer associated with high voltage which can represent up to 60% of the total water treatment cost (Grano et al.,1995).

a) b)

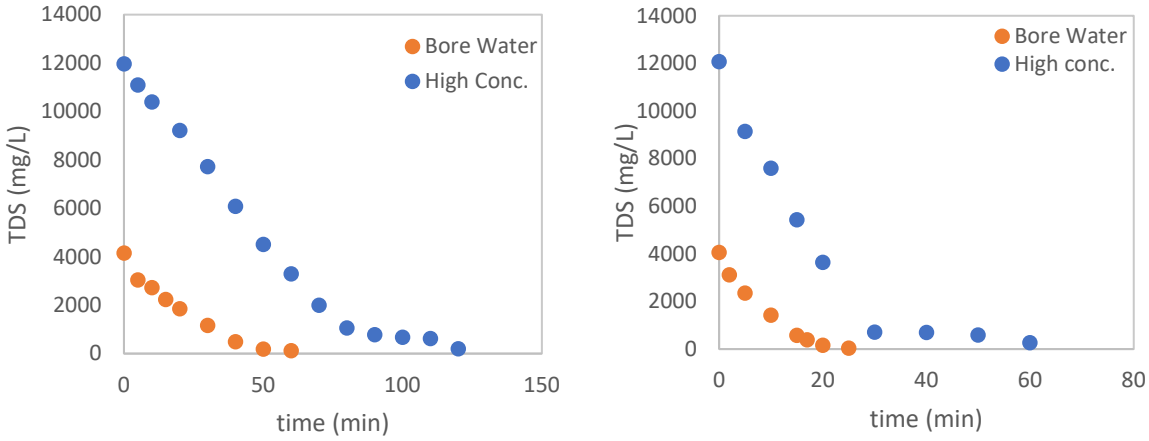

Figure 59. *Effect of feed ion concentration on processing time.*

The desalination energy for a specific flow rate is determined by:

$$SEC_{ED} = \frac{U \int_0^t I \, dt}{Q_{d*} * t} \tag{15}$$

Where U is the applied voltage, I is the current and t is the time to achieve a concentration of TDS below 1000 mg/L (Sosa et al., 2021).

Figure 60 shows the energy consumption, SEC, of ED for two different ion concentration feed water samples. Bore water and synthetic water with higher concentrations of ions were tested at a fixed productivity of 14.8 L m^{-2} h^{-1}. As expected, the SEC increases exponentially with the depletion of ions from the diluate stream and increases with the feed ion concentration.

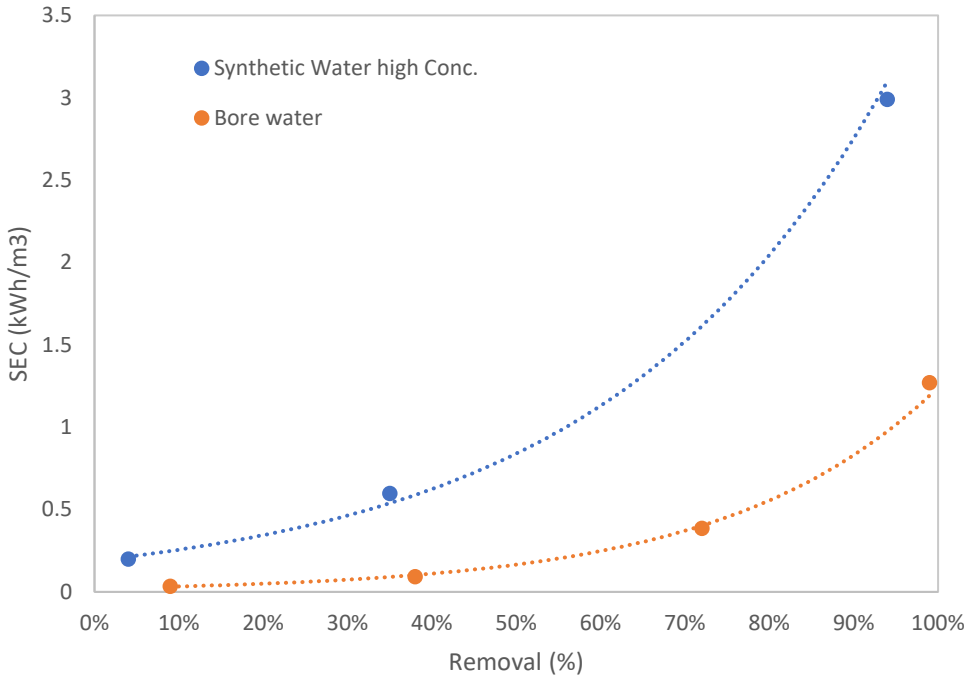

Figure 60. *Effect of feed ion concentration on energy consumption.*

Table 21. *Estimated SEC and cost for 75% TDS removal in ED.*

Electrodialysis	**Cost**
SEC (kWh/m^3)	$/ton
0.45	0.167

Table 21 shows the SEC to achieve 75% removal of TDS, which is required to reach an ion concentration below the threshold in the diluate. For this estimation, water consumption in mineral processing operations of 3 m^3 per ton of ore processed, and electricity prices of 0.123 $/kWh for industry reported by the Australian energy council in 2022 were assumed (Kitchen and Wang, 2022).

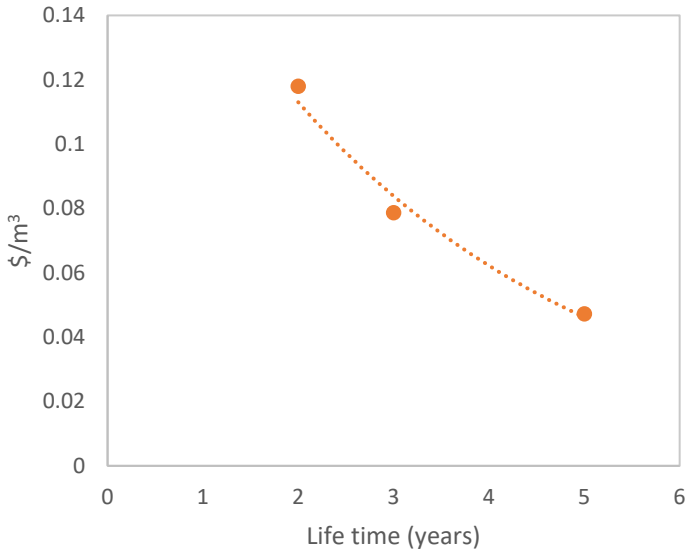

Figure 61. *Membrane replacement cost at different lifetimes.*

Membrane replacement cost shown in Figure 61 is another key operating cost. This variable is associated with the production rate of each membrane and its lifetime, and can be expressed as follows (Winston and Sirkar, 1992):

$$RC = 2.74\, F_R\, M_C\, M_P^{-1} M_l^{-1} \tag{16}$$

Where RC is the unit replacement cost in AUD per every m^3 of water produced at different points in the membrane lifetime, M_C is the cost of the membrane (AUD/ft^2) which was obtained from literature (Nayara et al., 2016), F_R is the water recovery, Mp is the membrane productivity and M_l is the membrane.

The main advantage of ED systems is that they usually provide long membrane lifetimes and depending on the critical ions for each mineral processing operation, the membranes can be perm-selective to monovalent ions, prolonging the useful life by reducing the polarisation by other ions that are not critical (Amshave et al., 2020). It is important to note that cost optimisation in membrane processes will depend mainly on the driving force of the system and the right selection of membrane to achieve the water quality required.

8.9 Conclusions

Electrodialysis results indicate that parameters such as ion concentration, linear velocity and voltage are key to considering electrodialysis for ion removal from water. The limiting current density in the ED system is affected by the concentration and the flow velocity in the cell. When the ion transport force is increased, a higher applied

voltage makes the process of ion removal faster. From the experimental results it can be concluded that ion removal is inversely proportional to the feed flow velocity, and it is associated with the reduction in contact time between the different streams and the membranes. The best performance achieved was at an applied voltage of 1 V/membrane pair, as at this voltage the treatment capacity was higher within the real processes. At these specific conditions (1V per membrane pair and 45 L/h) and 40 minutes of treatment, more than 90%, 98% and 87% of monovalent ions (Na^+ and Cl^-), divalent ions (Ca^{2+} Mg^{2+} and SO_4^{2-}), and TDS respectively were removed. The model of Nernst-Planck demonstrates that the dominant force that mobilises ions in the system is migration, however, diffusion of ions increases as the gradient of concentration increases between the concentrate and the diluate.

From the point of view of energy consumption, ED is 13% more efficient than nanofiltration. However, in terms of membrane replacement cost there does not appear to be much difference between the technologies.

9. Precipitation

9.1 Ultra-High Lime with Aluminium (UHLA)

9.1.1 Equilibrium time of ions removal

An experiment was conducted to study the kinetics of precipitation of Ca and Mg ions, and its applicability in the removal of ions. As has been reported (Abdel-Wahab and Batchelor, 2006), the main reactions expected in the system are as follows:

$$4Ca^{2+} + 2Al(OH)_4^- + 2Cl^- + 4OH^- \rightarrow Ca_4Al_2Cl_2(OH)_{12} \quad (17)$$

$$Ca^{2+} + SO_4^{2-} \rightarrow CaSO_4 \quad (18)$$

$$Ca_6Al_2(SO_4)_3(OH)_{12} \rightarrow 6Ca^{+2} + 2Al(OH)_4^- + 3SO_4^{-2} + 4OH^- \quad (19)$$

$$Mg(HCO_3) + Ca(OH)_2 \rightarrow CaCO_3 + MgCO_3 + H_2O \quad (20)$$

$$MgCO_3 + Ca(OH)_2 \rightarrow CaCO_3 + Mg(OH)_2 \quad (21)$$

Having in mind the main chemical reactions expected in the system, a kinetic study was made using a calcium hydroxide and sodium aluminate/chloride to sulphate ratio of 2:1 and 1.5:1 respectively. Figure 62 shows the removal of calcium, magnesium, chloride, and sulphate over time. These results suggest that equilibrium was reached after four hours, and the concentration of the ions was steady in almost all cases.

Since the aluminium source for the experiments was sodium aluminate, it was expected that there would be an increase in the concentration of sodium at the same rate as the precipitation. These results imply that kinetics for the precipitation of Ca^{2+}, Mg^{2+}, Cl^{-}, and SO_4^{2-} are faster, and that residence time is not an important factor when applying this precipitation method in mineral processing operations where sodium has a negligent effect on the process. Additionally, it was also demonstrated that the UHLA process could be used for calcium, magnesium, chloride, and sulphate removal with an equilibrium achievable after four or eight hours depending on the target ion concentration required.

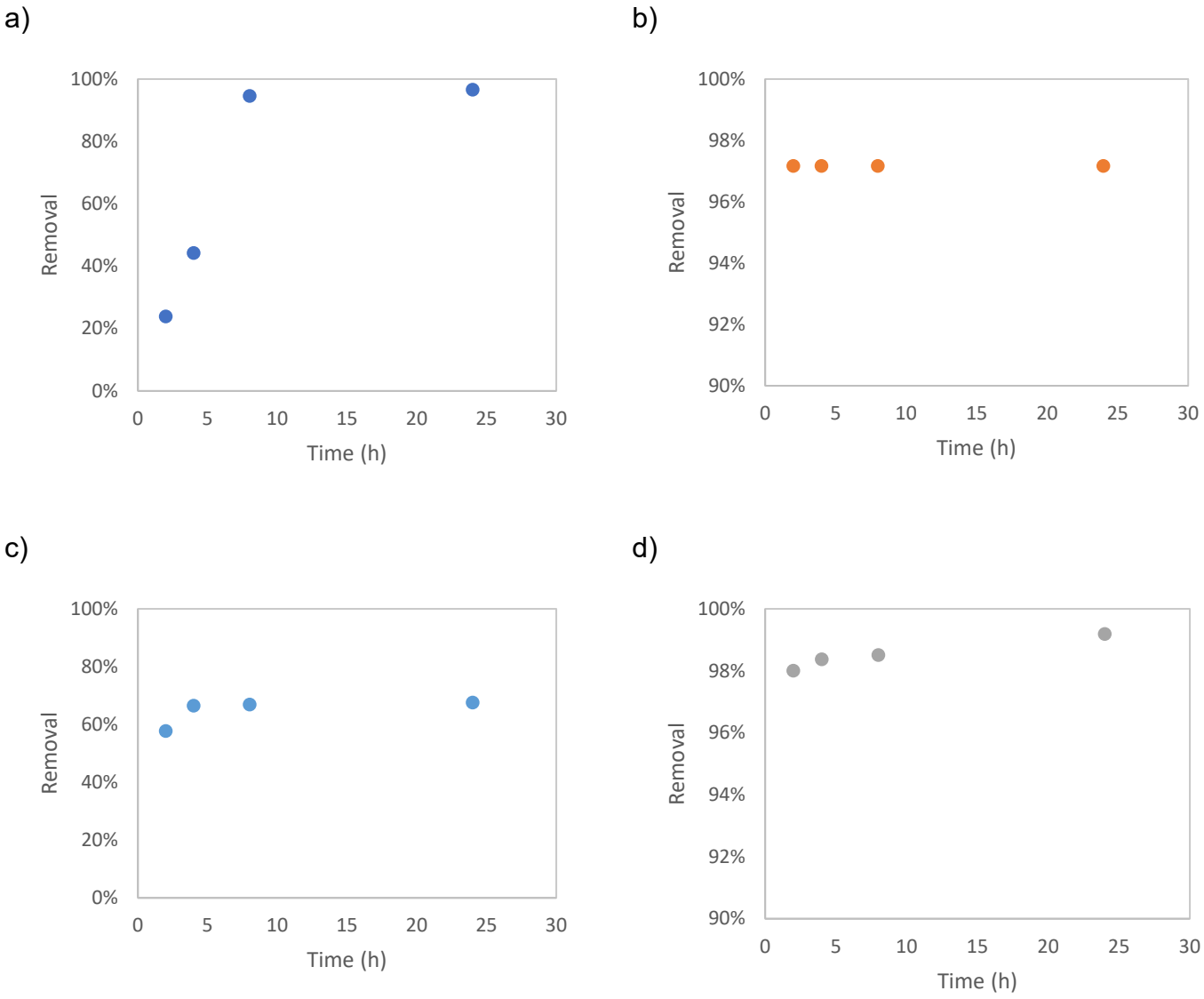

Figure 62. *Kinetics of ion removal (Ca/Cl, SO_4 ratio 2:1 and Al/Cl, SO_4 ratio 1.5:1) a) Ca^{2+}, b) Mg^{2+}, c) Cl^{-} and d) SO_4^{2-}*

9.1.2 *Effect of lime and sodium aluminate concentration*

Figure 63 displays the effect of lime and sodium aluminate on removing chloride and sulphate. Magnesium removal reaches its maximum point of 97% from the lowest concentration of lime and sodium aluminate. This was expected as the non-carbonate hardness species compounded by SO_4^{2-} and Cl^- are used to form aluminium precipitates. This allows the excess lime added to force the precipitation of magnesium as magnesium hydroxide.

The calcium removal is influenced by the amount of lime added and the aluminium available to react. When high doses of lime are used, more aluminium is required to achieve low concentrations of calcium. In addition, the calcium hydroxide used was calculated on a base of the initial concentration of anions (Cl^- and SO_4^{2-}), so at low concentrations of aluminium, the calcium added in excess to the system dissolved, increasing the dissolved calcium.

a) b)

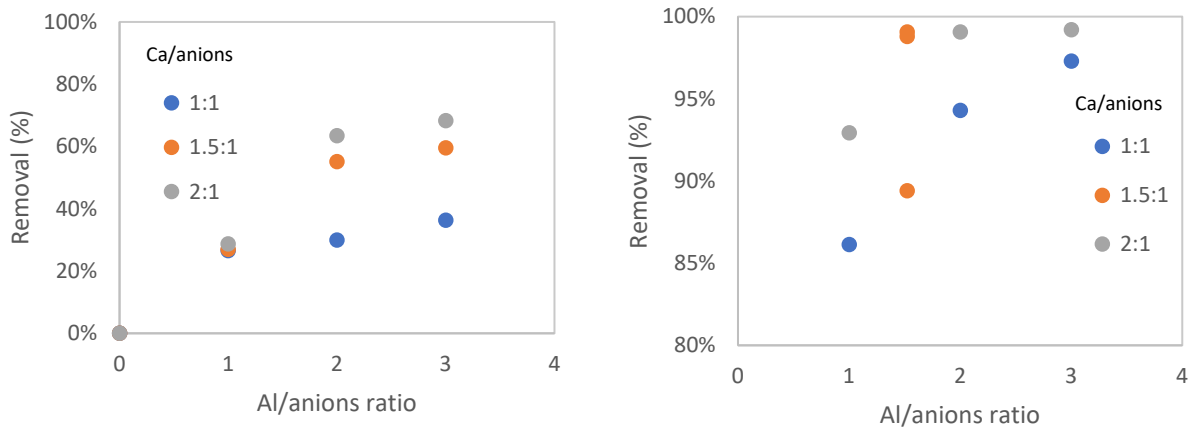

Figure 63. *Effect of lime and aluminium dose on ion removal a): Chloride, b): Sulphate*

The precipitation of chloride is highly dependent on the concentration of lime and aluminium added. Lime ratios over 1.5:1 resulted in the removal of higher amounts of chloride. However, increasing the lime ratio from 1.5:1 to 2:1 resulted in a slight increase in chloride removal. As Almasri (2003) suggests, sulphate removal is independent of the chloride concentration. Also, Abdel-Wahab and Batchelor (2006) indicate that because of the low solubility of calcium, aluminium and sulphate compounds and the high affinity between those ions, species such as calcium sulphate and calcium carbonate are the dominant species formed instead of calcium chloroaluminate. This explains why the lowest chloride removal was obtained when both ions are present (Cl^-, SO_4^{2-}) in the precipitation process. The former theory agrees

with the result obtained in Figure 62, as 99% of the sulphate was removed whilst the maximum chloride removal was 68%. One aspect that can affect the performance of chloride precipitation is the presence of bicarbonate ions that, due to their high affinity with calcium and aluminium, can compete with chloride ions for precipitate formation. The mechanism of chloride removal in a multi-ion system could be complex. However, the most reasonable path for its removal is through the formation of tetracalcium hydroxyaluminate ($Ca_4Al_2(OH)_{14}$) followed by the replacement of the hydroxyl ion by the chloride free ions in solution (Yi et al., 2020).

$$AlO_2^- + 2H_2O \rightarrow Al(OH)_4^- \quad (22)$$

$$4Ca(OH)_2 + 2\,Al(OH)_4^- \rightarrow Ca_4Al_2(OH)_{14} + 2OH^- \quad (23)$$

$$Ca_4Al_2(OH)_{14} + 2Cl^- \rightarrow Ca_4Al_2(OH)_{12}Cl_2 + 2OH^- \quad (24)$$

9.1.3 Ion removal optimisation

Two stages of experiments were conducted to optimise the precipitation of anions (chloride and sulphate), with a reduction of bicarbonate ions expected in the first stage that would negatively impact the efficiency of anion precipitation. These experiments were performed under the same conditions as in the single-stage precipitation; however, in these experiments, half of the lime dosage was fed in the first stage and the other half in the second stage with different concentrations of sodium aluminate.

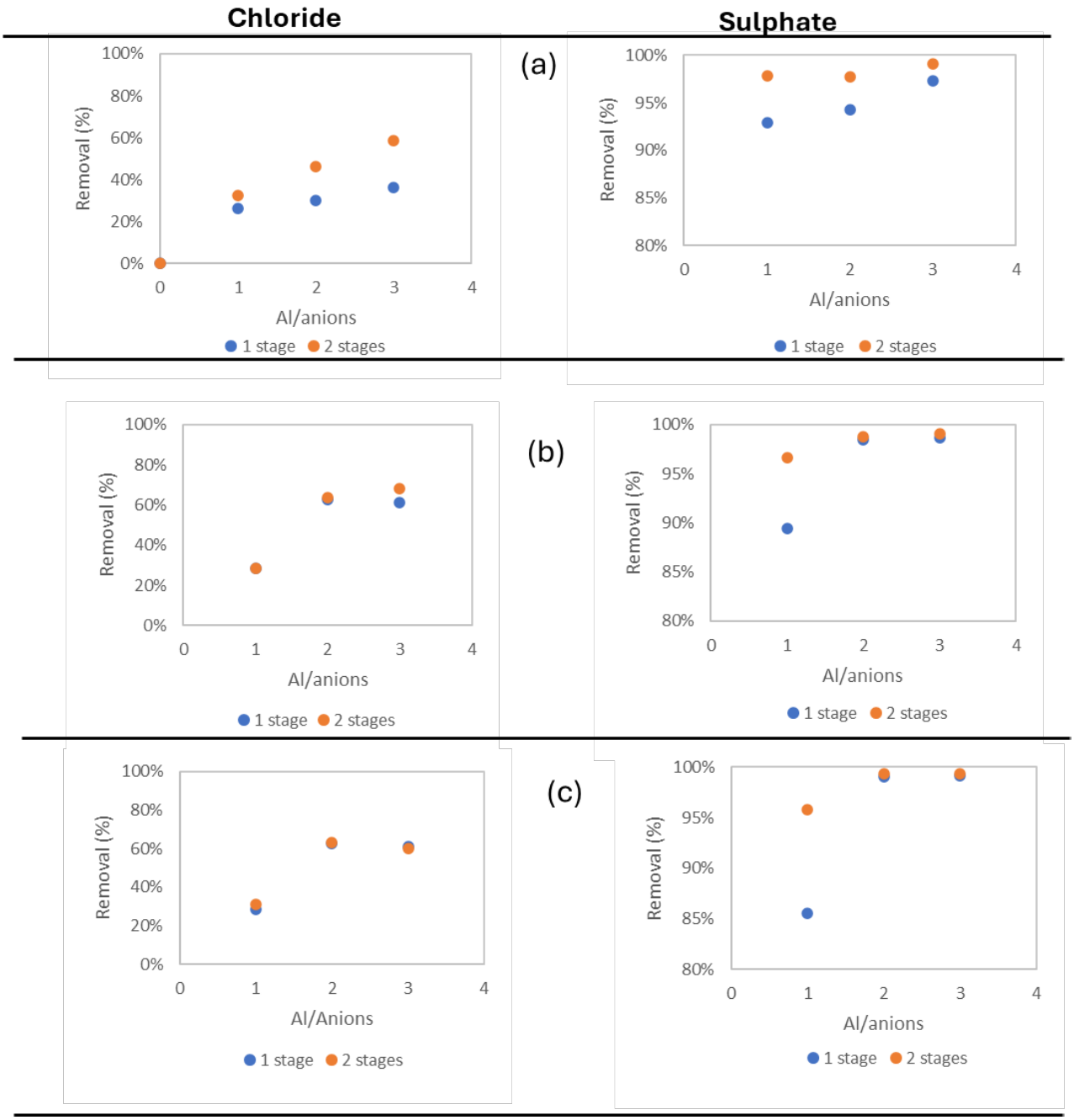

Figure 64. *Comparison of anion removal of the two-stage precipitation: ratio Ca/anions; a) 1:1, b) 1.5:1 and c) 2:1*

The precipitation process with two stages has a negligible impact on calcium and magnesium precipitation, with both reaching concentrations below 10 ppm in the filtrate. Those divalent cations are mainly used in the first stage to precipitate sulphate as calcium sulphate due to its solubility; therefore, more than 95% of calcium and magnesium removal was achieved in both the one- and two-stage processes. In addition, the excess of calcium in the first stage reacts with the carbonate ions producing calcium carbonate. A secondary effect of the calcium carbonate and calcium sulphate precipitation is an improvement of chloride removal efficiency as the

calcium and aluminium added in the second stage react mainly with chloride ions. In Figure 64, the sulphate and chloride removal performance by the two-stage process improves the precipitation, reducing the concentration of these anions by up to 5% and 22% respectively, compared with the one-stage process.

XRD was used to determine the presence of crystalline phases of the precipitates. Figure 65 shows the XRD pattern of the solids obtained at 1.5:1 lime ratio and 3:1 $NaAlO_2$ ratio, from which it could be identified that the dominant phases in the precipitate were hydrocalumite ($Ca_4Al_2(OH)_{12}(Cl)_2 \cdot 4H_2O$), bayerite ($Al(OH)_3$) and calcite ($CaCO_3$). The presence of these minerals confirms that the first stage reduces the presence of sulphate, precipitating it as calcium sulphate, allowing the aluminium on the second stage to be more selective towards chloride ions.

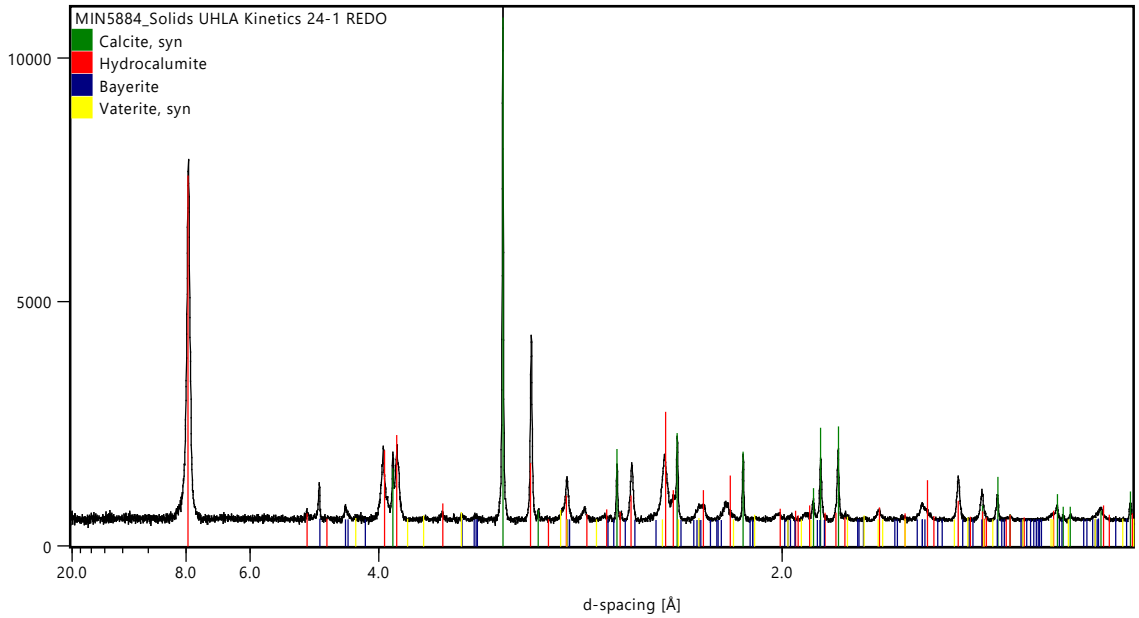

Figure 65. *X-ray diffraction results for final precipitates.*

9.1.4 Effect of Temperature

Figure 66 shows the effect of different temperatures (25, 35, 45, 55 ºC) on the final concentration of chloride and sulphate. It can be noticed that temperature has a negligible effect on the final sulphate concentration. It was also identified that the final chloride concentration decreases between the temperatures of 25 ºC and 45 ºC, improving the percentage of chloride removal by 13.8% from 60.1% at 25 ºC to 73.9% at 45 ºC. At 55 ºC, the final concentration of chloride increases again, and the efficiency of chloride removal decreases by 17.1% compared with the chloride removal achieved at 25 ºC. This decrease in chloride removal could be related to the calcium chloroaluminate temperature of stability which is 40ºC. At temperatures above 40ºC, the calcium chloroaluminate precipitate is unstable, favouring the formation of more

stable solids such as calcium aluminate ($Ca_3Al_2(OH)_{12}$). This means that for industrial applications of this process, if the temperature of the effluent to be treated is high, it will be necessary to cool the stream prior to processing to achieve high chloride removal (Xiaofang et al., 2021 and Abdel-Wahab and Batchelor, 2006).

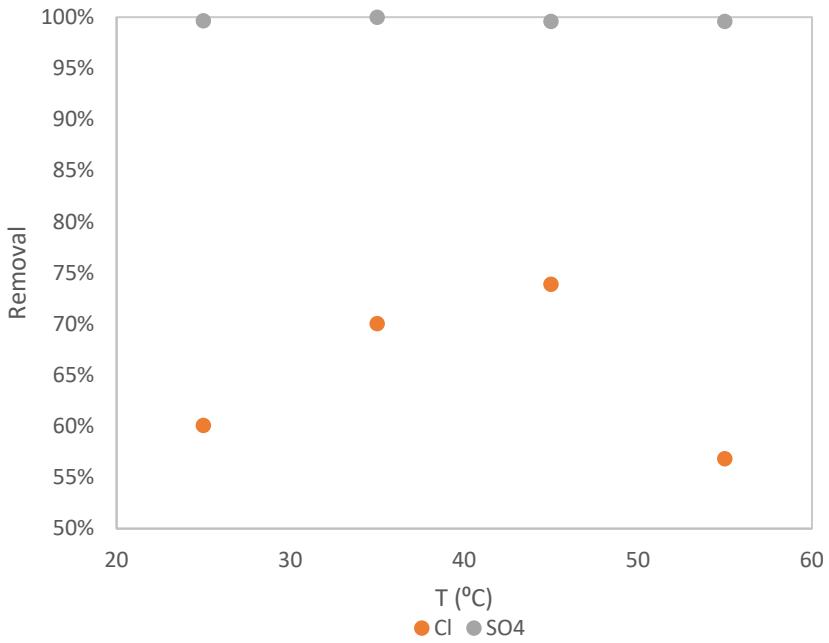

Figure 66. *Temperature effect on ion removal 1 stage process, Ca/anions ratio of 1.5:1 and Al/anions ratio of 1:1.*

9.1.5 Effect of pH on ion removal

Figure 67 shows the effect of pH on the final chloride and sulphate concentrations. Chloride and sulphate concentrations in the effluent increase with decreasing pH. In the case of chloride, the overall removal was increased by 3% from pH 4 to pH 11, reducing the final concentration by 71 mg/L. The effect of pH on the final chloride concentration can be related to the fact that the formation and stability of calcium chloroaluminate and calcium hydroxylamine solids are favoured at pH above 12. Sulphate removal is improved, increasing the pH and reaching a maximum removal of 99%. Wing and George (1978), argued that acids inhibit the growth of sulphate crystals with high negative charges, which are more likely to increase the separation of the ions by electrophoresis, avoiding crystal growth.

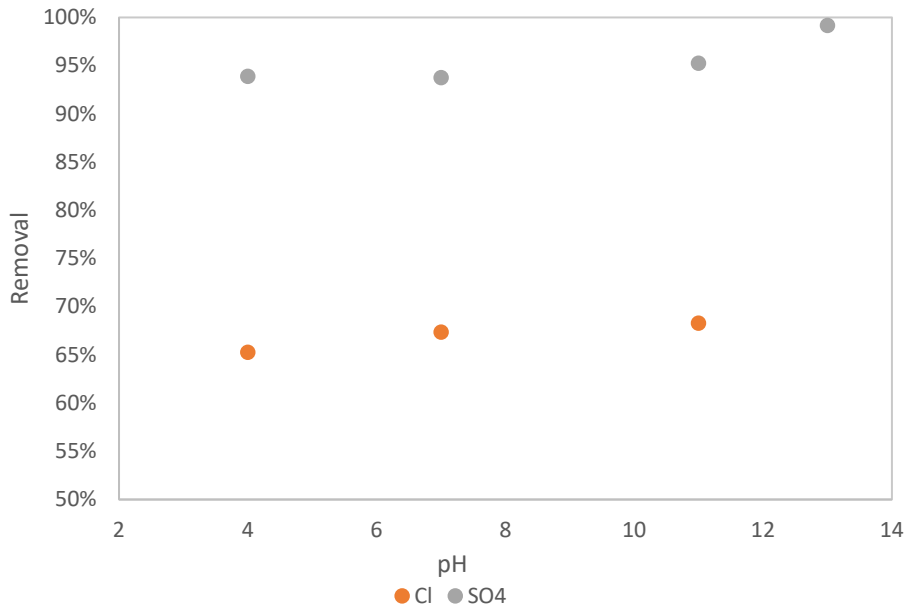

Figure 67. *pH effect on ion removal 1 stage process, Ca/anions ratio of 1.5:1 and Al/anions ratio of 1:1 at 25 ºC.*

9.1.6 Economic analysis of UHLA process

Figure 68 illustrates the change in the cost of chemical consumption for the two-stage process with 1:1 Ca/anions ratio. The precipitation of calcium, magnesium, sodium, chloride, and sulphate ions is mainly driven by chemical consumption (Xiaofang, 2021). The best performance was achieved at a Ca/anions ratio of 1:1 and an Al/anions ratio of 3:1 in a two-stage process. The chemicals CaOH and $NaAlO_2$ can be purchased at a commercial price in Australia of A$0.055/kg and A$1.305/kg, respectively. The average dose of the reagents used in this scenario is 0.0052 kg/L of CaOH in each stage for a total of 0.104 kg/L and 0.015 kg/L of $NaAlO_2$, resulting in a total cost of A$0.02017/L. Recent studies using similar processes, have published data of total operational costs related to chemical consumption of between A$0.008/L and A$0.03/L, confirming that Friedel's salt precipitation is enhanced by a two-stage process (Yi et al., 2020 and Xiaofang et al., 2021).

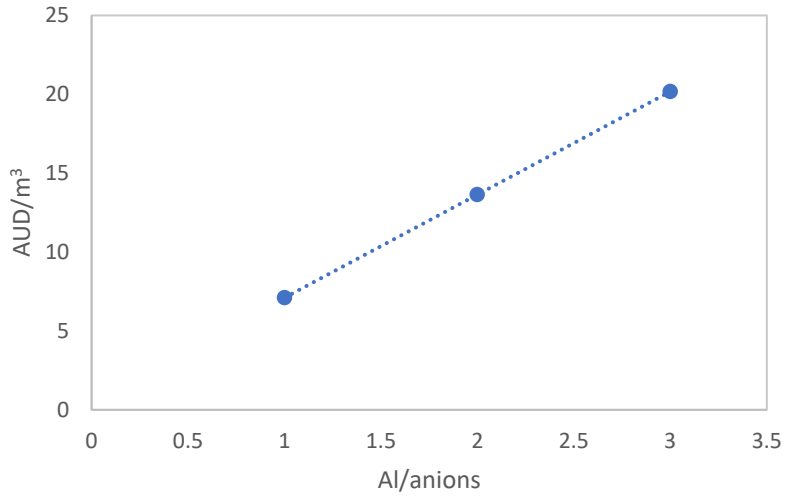

Figure 68. *Effect of Al/anions ratio on chemical precipitation cost in a two-stage UHLA process.*

9.2 Oxalic Acid

9.2.1 Equilibrium time of ion removal

Oxalic acid was used as a complexing agent (i.e., precipitation) for removal of cations from water. Precipitation experiments were performed to determine the equilibrium time for the precipitation reaction. These experiments were conducted with bore water from Mt Weld and synthetic water with a higher concentration of ions similar to sea water.

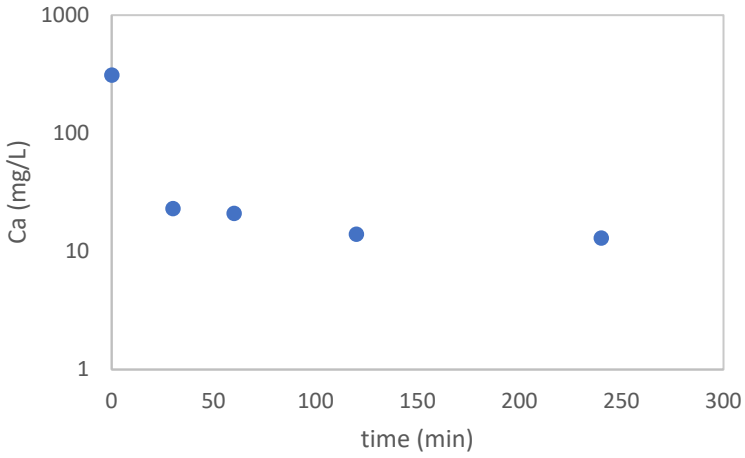

Figure 69. *Equilibrium time of precipitation, oxalic acid/cation molar ratio (2:1).*

A series of experiments to study the kinetics of the reaction and the removal of calcium and magnesium were conducted with synthetic water. Figure 69 shows the final concentration of calcium in solution at different reaction times. The results indicate that selective precipitation of calcium reached steady state within 60 min, which agrees

with Kennedy et al. (2021) who found that the kinetics of calcium oxalate formation are extremely fast.

9.2.2 Effect of oxalic dose on selective precipitation

Different doses of oxalic acid were evaluated to determine if the reaction required more than the stoichiometric concentration to precipitate the ions. As can be seen in Figure 70 there is no appreciable impact on calcium and magnesium precipitation from increasing the dose of oxalic acid. The calcium removal achieved was above 95% for all oxalic acid doses evaluated using the synthetic water (SW) and above 91.2% for the bore water (BW). Inversely, magnesium precipitation was very limited even at high oxalic acid doses, due to the pH required for the precipitation of magnesium oxalate.

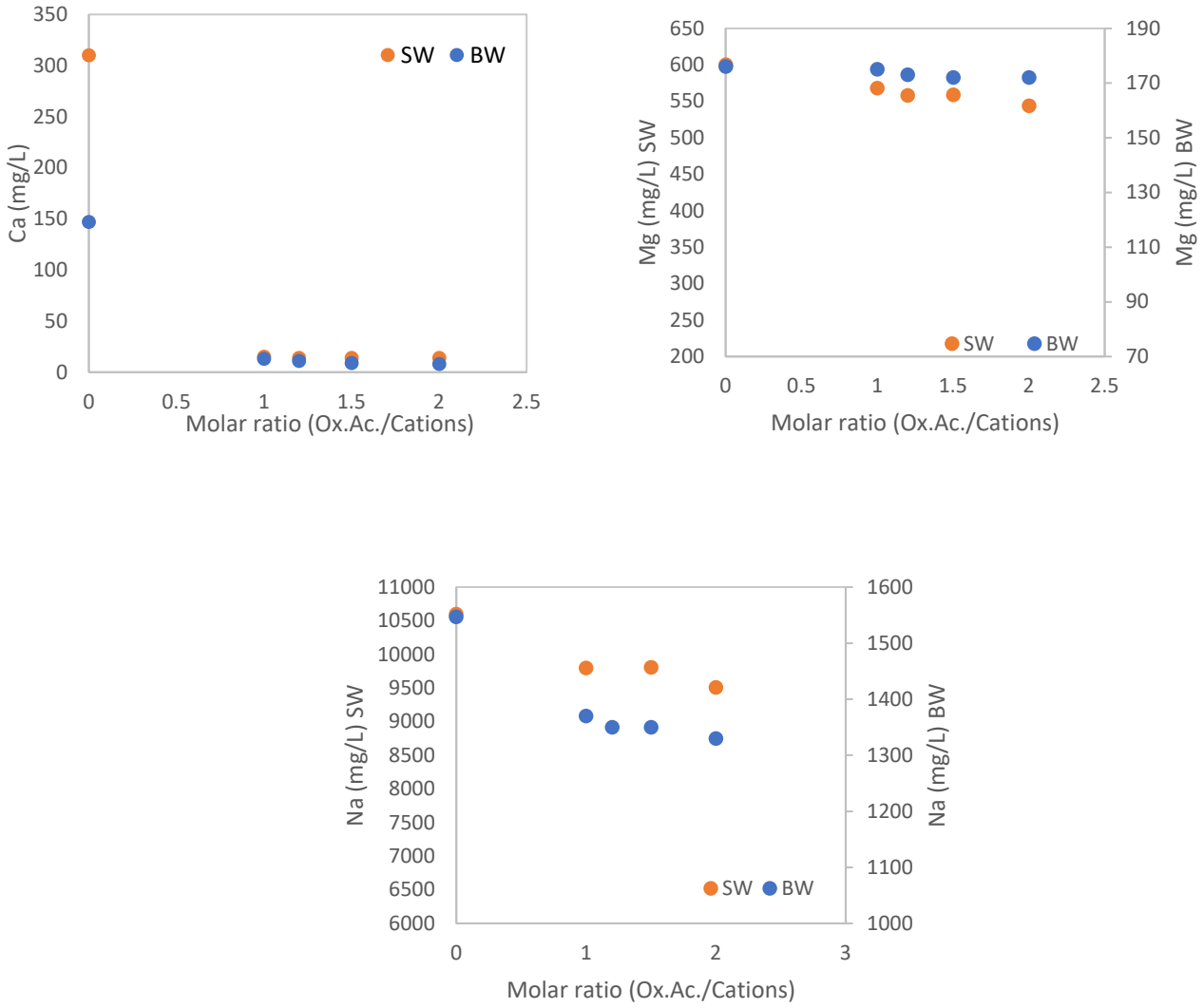

Figure 70. *Effect of oxalic acid dose on cation precipitation.*

Figure 71 shows the characterisation by XRD of the final precipitate at a molar ratio of 2:1. It can be seen that the only crystalline phase identified is Whewellite which is the

hydrate form of calcium oxalate ($CaC_2O_4 \cdot H_2O$). This agrees with the results shown in Figure 69 where the main precipitated ion is calcium.

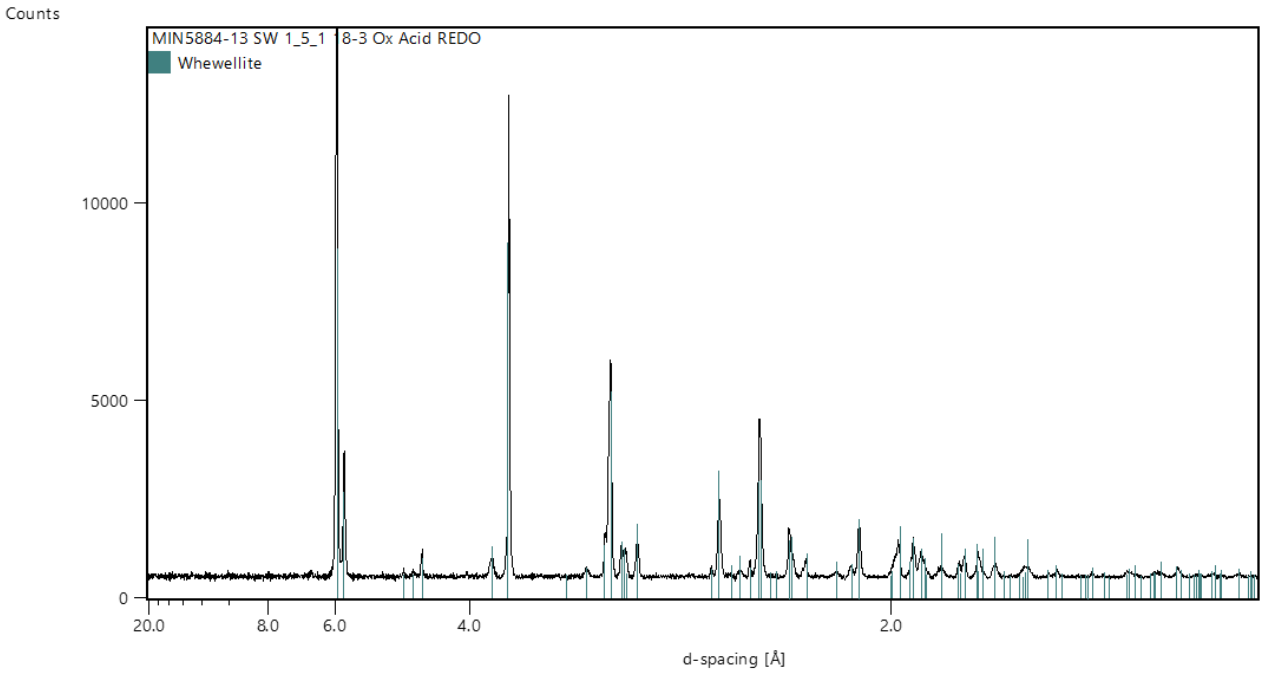

Figure 71. *X-ray diffraction analysis of precipitate. Molar ratio (oxalic:ions) of 2:1 at neutral pH.*

9.3 Conclusions

This chapter studied the precipitation of critical ions through the UHLA process and oxalic acid method and the precipitation conditions that affect these processes. Experimental results showed that the kinetics of both processes are fast, and the reaction time should not be a problem for industrial applications. From the oxalic acid results, it was evident that removal of calcium was above 95%, however, it was found that precipitation of magnesium and sodium was almost negligible. It will require certain conditions such as high concentration of ions and a pH adjustment to achieve precipitation, as demonstrated by the XRD analysis of the precipitates that shows only the presence of calcium oxalate. From the UHLA process results, it was determined that increasing the concentration of $Ca(OH)_2$ and $NaAlO_2$ improves the ion removal efficiency. Al/anion ratios over 2 did not strongly impact overall ion removal. In contrast, increasing the ratio of lime to anions improves anion removal. The maximum removal efficiency (68% of chloride and 99% of sulphate) was achieved when the Ca/anion ratio was 2:1 and the Al/anion ratio was 3:1. Removal of calcium and magnesium ions was over 97% in all the tests performed. Chloride and sulphate removal is proportional to pH with the optimum being over 12. Temperatures over 40 ºC negatively impact the removal of chloride as the stability of the calcium chloroaluminate is affected at higher temperatures. Removal of chloride and sulphate can be improved by implementing a two-stage process using half of the $Ca(OH)_2$ dose

in the first stage to avoid chloride competing with other ions such as bicarbonate and aluminium.

The method of precipitation with oxalic acid was highly efficient to produce calcium oxalate, however, it has some drawbacks such as requirements for high concentrations of magnesium for that to precipitate. The UHLA process explored in this study is highly efficient in reducing calcium, magnesium and sulphate. Furthermore, it showed high efficiencies for chloride removal which depending on the water quality required by different mineral processing operations, can be combined with other methods to refine the effluent and remove the residual concentration of chloride.

Section 4: Synthesis

10. Overall Study Conclusions

This research project aimed to investigate the impact of water quality on the flotation efficiency of RE phosphate minerals and to identify the underlying flotation mechanisms. To understand the fundamental mechanism of RE ore flotation, the flotation behaviours of both valuable and gangue single minerals were scrutinised. The study also assessed the effect of water quality using ore samples, aiming to quantify its influence and understand the associated mechanisms in a mixed mineral system.

Investigation of the monazite flotation mechanism with an oleate collector in the presence of various ions (Ca^{2+}, Mg^{2+}, Na^{+}, and K^{+}) indicated that Ca^{2+} and Mg^{2+} were highly detrimental to monazite flotation. This is attributed to the formation of insoluble oleate products with these divalent metal ions, leading to decreased adsorption of oleate ions on monazite surfaces and consequently, reduced flotation recovery. In contrast, the presence of Na^{+} or K^{+} had minimal effect on the flotation recovery of monazite because these ions do not react with oleate ions. These findings were confirmed by adsorption experiments, XPS analysis, and zeta potential measurements.

The negative effects of Ca^{2+} and Mg^{2+} on the flotation of RE minerals using ore samples were also validated through multi−stage batch flotation experiments, adsorption tests, rheological measurements, and solution chemistry analyses. Both Ca^{2+} and Mg^{2+} adversely impacted the selectivity and recovery of RE minerals due to their chemical reactions with the collector and depressant. The formation of insoluble calcium and magnesium carboxylate compounds led to a decrease in the residual collector concentration and subsequently, a reduced RE mineral recovery. Additionally, these divalent cations were found to act as bridges between the oxygen atoms of the adsorbed SiO_3^{2-} and carboxylate ions, leading to increased adsorption of the fatty acid collector ions and a higher recovery of FeO. Notably, Mg^{2+} had a more pronounced negative effect on the flotation recovery of RE minerals than Ca^{2+}, possibly because magnesium has a stronger affinity for SiO_3^{2-}, while calcium prefers oleate. The presence of $CaCl_2$ or $MgCl_2$ also increased the viscosity of flotation pulp, likely due to the compression of the electrical double layer by these divalent cations.

The presence of anions, specifically Cl^{-}, SO_4^{2-}, and HCO_3^{-}, in the flotation pulp also negatively impacted flotation efficiency. This led to a reduced recovery of RE minerals and an increased recovery of FeO minerals. Among these, Cl^{-} had the most detrimental effect on the flotation of RE minerals, likely due to a most significant increase in pulp viscosity. The reduction in zeta potential of fine particles in the presence of these ions seemed to be a key factor in increasing pulp viscosity. Stronger attractive forces between particles resulted in higher pulp viscosity, leading to increased mechanical entrainment. These observations were supported by settling experiments and DLVO theory calculations.

The effect of Ca^{2+} and Mg^{2+} on the flotation of gangue minerals was examined using sodium oleate and sodium silicate. Their presence significantly hindered goethite flotation, primarily due to the formation of insoluble compounds with the sodium oleate collector. Consequently, there was decreased adsorption of oleate ions on goethite surfaces, leading to reduced goethite recovery. Additionally, the adverse effect on goethite recovery was more significant with Ca^{2+} than with Mg^{2+}.

Lastly, it was established in this study that nanofiltration membranes and electrodialysis technologies can serve as suitable alternative methods (under the right conditions of operation) to the more expensive reverse osmosis as a potential method to treat water with high salinity. The nanofiltration and electrodialysis modules considered in this study produced water with concentrations of <50 mg/L Ca^{2+} and Mg^{2+}, and <500 mg/L Na^{+}, which were found to be under the threshold concentrations required for rare earth minerals flotation.

11. Recommendations for Future Study

- This study aims to quantify the effects of water quality on the flotation of RE phosphate minerals and to uncover the underlying mechanisms. Having understood these impacts, future research should explore methods to mitigate the adverse effects of dissolved ions.
- The detrimental effects of Ca^{2+} and Mg^{2+} were identified as stemming from the formation of insoluble precipitates with the collector, which subsequently reduced the collector concentration. Future research should consider experiments that investigate the potential of masking reagents to prevent the formation of these insoluble precipitates.
- Anions were found to influence flotation pulp rheology due to increased attraction forces between mineral particles. Exploring the effects of dispersants, which can maintain mineral particles in a dispersed state, is recommended.
- Dissolved ions might alter bubble properties within the flotation pulp. Investigating the influence of ions on bubble characteristics, such as bubble size and the probability of particle attachment to bubbles, could offer valuable insights.
- Froth stability plays a crucial role in determining flotation efficiency, as it can directly influence the degree of entrainment. Research into the effects of various dissolved ions on froth stability is recommended.
- Implementation of NF and ED systems to recover valuable metals from tailings in mineral processing operations.
- Evaluate the effect of membrane polarisation (ED and NF) and development of selective membranes (ED and NF) for recovery of specific ions.
- Test different combinations of ED membranes to reduce energy consumption.

12. References

Abaka-Wood, G.B., Addai-Mensah, J., & Skinner, W. (2018). A study of selective flotation recovery of rare earth oxides from hematite and quartz using hydroxamic acid as a collector. Advanced Powder Technology, 29 (8), 1886-1899.

Abdel-Wahab, A., & Batchelor, B. (2006). Interactions between chloride and sulfate or silica removal using advanced lime-aluminium softening process. Water Environment Research, 78, 13, 2474.

Abeidu, A.M. (1972). The separation of monazite from zircon by flotation. Journal of the Less Common Metals, 29 (2), 113-119.

Ahmad, A., Ooi, B., Mohammad, A., & Choudhury, J. (2004). Development of a highly hydrophilic nanofiltration membrane for desalination and water treatment. Desalination, 168, 215-221.

Aktas, O., Sahinkaya, E., Yutsever, A., Demir, S., Yuceyurt, M., Cakmak, A., Kulekci, C., Taahmaz, S., & Uluda, M. (2017). Treatment of a chemical industry effluent by nanofiltration and reverse osmosis. Desalination Water Treatment, 75, 274-283.

Almasri, D. (2013). Sulfate removal from reject brined in inland desalination with zero liquid discharge. MSc. Chem. Eng. Thesis. Texas A&M University.

Alonso, E., Sherman, A.M., Wallington, T.J., Everson, M.P., Field, F.R., Roth, R., & Kirchain, R.E. (2012). Evaluating rare earth element availability: A case with revolutionary demand from clean technologies. Environmental Science & Technology, 46 (6), 3406-3414.

Amshave, S., Yusri, M., Aziz, A., Geraint, D., Habib, I., & Abu, H. (2020). Electrodialysis desalination for water and wastewater: a review. Chemical Engineering, 380, 122231.

Ancey, C., & Jorrot, H. (2001). Yield stress for particle suspensions within a clay dispersion. J Rheol, 45, 297–319.

Araújo, A.C.A., & Lima, R.M.F. (2017). Influence of cations Ca^{2+}, Mg^{2+} and Zn^{2+} on the flotation and surface charge of smithsonite and dolomite with sodium oleate and sodium silicate. Int J Miner Process, 167, 35–41.

Baldassarre, F., Cacciola, M., & Ciccarella, G. (2015). A predictive model of iron oxide nanoparticles flocculation tuning Z-potential in aqueous environment for biological application. J Nanopart Res, 17, 377.

Becker, M., Yorath, G., Ndlovu, B., Harris, M., Deglon, D., & Franzidis, J.−P. (2013). A rheological investigation of the behaviour of two Southern African platinum ores. Miner Eng, 49, 92–97.

Bıcak, O., Ekmekci, Z., Can, M., & Ozturk, Y. (2012). The effect of water chemistry on froth stability and surface chemistry of the flotation of a Cu–Zn sulfide ore. International Journal of Mineral Processing, 102, 32-37.

Bo, S., Muxing, Z., Shifang, H., Wei, S., Junming, Z., & Xiaosong, Z. (2019). Performance evaluation on regeneration of high-salt solutions used in air conditioning systems by electrodialysis. Journal of Membrane Science, 582, 224-235.

Bournival, G., Du, Z., Ata, S., & Jameson, G. J. (2014). Foaming and gas dispersion properties of non-ionic surfactants in the presence of an inorganic electrolyte. Chem. Engineering Science, 116, 536-546.

Bulut, G., & Yenial, U. (2016). Effects of major ions in recycled water on sulphide minerals flotation. Minerals and Metallurgical Processing, 33 (3), 137-143.

Burns, D.B., & Zydney, A.L. (2000). Buffer effects on the zeta potential of ultrafiltration membranes. J Membrane Sci, 172, 39–48.

Cao, S., Cao, Y., Ma, Z., & Liao, Y. (2018). Metal ion release in bastnaesite flotation system and implications for flotation. Minerals, 8 (5), 203.

Castro, S., (2012). Challenges in flotation of Cu-Mo sulphide ores in sea water. In: Proc. 1st International Symposium. Water and Mineral Processing. Drelich, J. (Ed). SME, Englewood, 29-40.

Castro, S., & Laskowski, J.S. (2011). Froth flotation in saline water. KONA Powder and Particle Journal, 29 (0), 4-15.

Chen, W., Chen, F., Bu, X., Zhang, G., Zhang, C., & Song, Y. (2019). A significant improvement of fine scheelite flotation through rheological control of flotation pulp by using garnet. Miner Eng, 138, 257.

Chen, W., Honghui, H., Bai, T., & Jiang, S. (2017). Geochemistry of monazite within carbonatite related REE deposits. Resour, 6, 51.

Cheng, T.W., Holtham, P.N., & Tran, T. (1993). Froth flotation of monazite and xenotime. Minerals Engineering, 6 (4), 341-351.

Corin, K.C., Reddy, A., Miyen, L., Wiese, J.G., & Harris, P.J. (2011). The effect of ionic strength of plant water on valuable mineral and gangue recovery in a platinum bearing ore from the Merensky reef. Minerals Engineering, 24 (2), 131-137.

Dach, H. (2009). Comparing nanofiltration and reverse osmosis processes for selective desalination of brackish water feeds. PhD thesis (unpublished) Engineering science, University D Angers.

Davis, C.C., Chen, H.−W., & Edwards, M. (2002). Modeling silica sorption to iron hydroxide. Environ Sci Technol, 36, 582–7.

Devora-Isiorida, G., Espinoza, A., Rangel, L., Guzman, M., Sanchez, R., Sanchez, J., & Martinezm, M. (2021), Effect of temperature on diluate water in batch electrodialysis reversal. Separations, 8, 229.

Dietzel, M. (2002). Water−rock interaction. Water Trans, 207–235.

Dixon, D.R. (1985). Interaction of alkaline−earth−metal ions with magnetite. Colloid Surface, 13, 273.

Espiritu, E.R.L., Naseri, S., & Waters, K.E., (2018a). Surface chemistry and flotation behavior of dolomite, monazite and bastnäsite in the presence of benzohydroxamate, sodium oleate and phosphoric acid ester collectors. Colloids Surfaces Physicochem Eng Aspects, 546, 254–265.

Espiritu, E.R.L., & Waters, K.E. (2018b). Flotation studies of monazite and dolomite. Min. Eng,. 116, 101.

Farrokhpay, S., & Zanin, M. (2012). An investigation into the effect of water quality on froth stability. Adv Powder Technol, 23, 493–497.

Ferri, D., Grenthe, I., Hietanen, S., Salvatore, F., Powell, D.L., & Suchi, R. (1983). Studies on metal carbonate equilibria. 5. The cerium(III) carbonate complexes in aqueous perchlorate media. Acta Chem Scand, 37a, 359–365.

Firsching, F.H., & Mohammadzadei, J. (1986). Solubility products of the rare−earth carbonates. J Chem Eng Data, 31, 40–42.

Fu, Y., Yin, W., Yang, B., Li, C., Zhu, Z., & Li, D. (2018). Effect of sodium alginate on reverse flotation of hematite and its mechanism. Int J Minerals Metallurgy Mater, 25, 1113–1122.

Golev, A., Scott, M., Erskine, P.D., Ali, S.H., & Ballantyne, G.R. (2014). Rare earths supply chains: Current status, constraints and opportunities. Resources Policy, 41, 52-59.

Govardhan, B., Fatima, S., Madhumala, M., & Sridhar, S. (2020). Modification of used commercial reverse osmosis membranes to nanofiltration modules for the production of mineral-rich packaged drinking water. Applied Water Science, 10, 230.

Grano, S., Wong, P., Skinner, W., Johnson, N., & Ralston, J. (1995). Detection and control of calcium sulfate precipitation in the lead circuit of the hilton concentrator of Mount Isa Mines Limited. Proceedings of the XIX IMPC. Australia.

Gregory, G.R.E.C. (1966). The determination of residual anionic surface-active reagents in mineral flotation liquors. Analyst, 91, 251–257.

Guerra, H., Tadesse, B., Albijanic, B., & Dyer, L. (2023) Nanofiltration for treatment of Western Australian bore water for mineral processing operations: A pilot scale study, Journal of Water Process Engineering,52, 103484.

Guimares, R., & Peres, A. (1999). Interfering ions in the flotation of a phosphate ore in a batch column. Minerals Engineering. 12, 7, 757-768.

Gupta, C.K. & Krishnamurthy, N. (2005). Extractive Metallurgy of Rare Earths. CRC Press, Boca Raton, Florida.

Hansen, H.C.B., Wetche, T.P., Raulund−Rasmussen, K., & Borggaard, O.K. (1994). Stability constants for silicate adsorbed to ferrihydrite. Clay Miner, 29, 341–350.

Hancer, M., Celik, M.S., & Miller, J.D. (2001). The significance of interfacial water structure in soluble salt flotation systems. Journal of Colloid and Interface Science, 235 (1), 150-161.

Hao, H., Cao, Y., Li, L., Fan, G., & Liu, J. (2021). Dispersion and depression mechanism of sodium silicate on quartz: Combined molecular dynamics simulations and density functional theory calculations. Appl Surf Sci, 537, 147926.

Hidalgo, A., Leon, G., Gomez, M., Murcia, M., Gomez, E., & Gomez, J. (2013) Application of the Spiegler–Kedem–Kachalsky model to the removal of 4-chlorophenol by different nanofiltration membranes. Desalination, 315, 70-75.

Humphries, M. (2010). Rare Earth Elements: The Global Supply Chain, CRS Report for Congress. R41347 (www.crs.gov).

Ito, S., Yotsumoto, H., & Sakamoto, H. (1991). Magnetic separation of monazite and xenotime. Materials Science Forum, 70-72, 279-300.

Jadhav, S., Marathe, K., & Rathod, V. (2016) A pilot scale concurrent removal of fluoride, arsenic, sulfate and nitrate by using nanofiltration: Competing ion interaction and modelling approach. Journal of Water and Process Engineering, 13, 153–167.

Jeldres, R.I., Forbes, L., & Cisternas, L.A. (2016). Effect of seawater on sulfide ore flotation: A review. Mineral Processing and Extractive Metallurgy Review, 37 (6), 369-384.

Jordan, N., Marmier, N., Lomenech, C., Giffaut, E., & Ehrhardt, J.−J. (2007). Sorption of silicates on goethite, hematite, and magnetite: experiments and modelling. J Colloid Interf Sci, 312, 224–9.

Jordens, A., Cheng, Y.P., & Waters, K.E. (2013). A review of the beneficiation of rare earth element bearing minerals. Minerals Engineering, 41, 97-114.

Jordens, A., Marion, C., Grammatikopoulos, T., Hart, B., & Waters, K.E. (2016). Beneficiation of the Nechalacho rare earth deposit: Flotation response using benzohydroxamic acid. Min Eng, 99, 158-169.

Jordens, A., Marion, C., Kuzmina, O., & Waters, K.E. (2014). Surface chemistry considerations in the flotation of bastnäsite. Minerals Engineering, 66-68, 119-129.

Jung, M., Tadesse, B., Dick, C., Logan, A., Dyer, L., & Albijanic, B. (2022). Influence of monovalent and divalent cations on monazite flotation. Colloids Surfaces Physicochem Eng Aspects, 653, 129975.

Karimi L., Ghaseemi, L., & Zamani, H. (2018). Quantitative studies of electrodialysis performance. Desalination, 445, 159-169.

Kelewou, H., Lhassani, A., Merzouki, H., Drogui, P., & Sellamuthu, B. (2011). Salts retention by nanofiltration membranes: Physicochemical and hydrodynamic approaches and modelling. Desalination, 227(1-3) 106-112.

Kennedy, S., Zijil, L., Rooyen, C., Bertossi, L., Shekede, B., Joos-Vandewalle, J., Smith, S., & Turton, A. (2021). Coordination and precipitation of calcium oxalate: Computation to kinetics. Crystal Growth and Design, 21, 1249-1258.

Kirjavainen, V.M. (1992). Mathematical model for the entrainment of hydrophilic particles in froth flotation. Int J Miner Process, 35, 1–11.

Krieg. M., Modise, J., Keizer, K., & Neomagus, H. (2005) Salt rejection in nanofiltration for single and binary salt mixtures in view of sulfates removal. Desalination, 171, 205-215.

Laskowski, J. (1970). Role of capillary effects in bubble−particle collision in flotation. Transactions Institution of Mining and Metallurgy, 79, C6–C10.

Laskowski, J., & Castro, S. (2015). Flotation in concentrated electrolyte solutions. Int J Miner Process, 144, 50–55.

Laskowski, J., Xu, Z., & Yoon, R.H. (1991). Energy barrier in particle−bubble attachment and its effect on flotation kinetics, in: Proc. 17th Int. Mineral Processing Congress. Dresden, pp. 237–249.

Levay, G., Smart, R.S.C., & Skinner, W.M. (2001). The impact of water quality on flotation performance. Journal of South African Institute of Mining and Metallurgy, 101, 69–75.

Lhassani, A., Rumeau, M., Benjelloun, D., & Pontie, M. (2001). Selective demineralization of water by nanofiltration Application to the defluorination of brackish water. Water Research, 35, 3260-3264.

Li, D., Yin, W., Xue, J., Yao, J., Fu, Y., & Liu, Q. (2017). Solution chemistry of carbonate minerals and its effects on the flotation of hematite with sodium oleate. Int J Minerals Metallurgy Mater, 24, 736–744.

Li, G., Deng, L., Cao, Y., Wang, B., Ran, J., & Zhang, H. (2017). Effect of sodium chloride on fine coal flotation and discussion based on froth stability and particle coagulation. Int J Miner Process, 169, 47–52.

Li, L.Z., & Yang, X. (2006). China's rare earth ore deposits and beneficiation techniques. Proc. of 1st Eur. Rare Earth Resour. Conf., Milos, Greece, p.26-36.

Li, Z., Rao, F., Guo, B., Zuo, W., Song, S., & Lopez-valdiviseo, A. (2019). Effects of calcium ions on malachite flotation with octyl hydroxamate. Minerals Engineering, 105854.

Liu, W., Wang, X., Wang, Z., & Miller, J.D. (2016). Flotation chemistry features in bastnaesite flotation with potassium lauryl phosphate. Minerals Engineering, 85, 17-22.

Long, K.R., Van Gosen, B.S., Foley, N.K., & Cordier, D. (2010). The principal rare earth elements deposits of the United States — A summary of domestic deposits and a global perspective Gd Pr Sm Nd La Ce. US Geological Survey Scientific Investigations, 89 (5220), 96.

Luo, J., & Chen, X. (1987). Research into the recovery of high-grade rare-earth concentrate from baotou complex iron ore, China. ISTIC-Technical Report. The Institute of Scientific and Technical Information of China.

Luo, J., Ding, L., Su, Z., Wei, S., & Wan, Y. (2010). Concentration polarization in concentrated saline solution during desalination of iron dextran by nanofiltration. J Membrane Science, 363 (1-2), 170-179.

Marrucci, G., & Nicodemo, L. (1967). Coalescence of gas bubbles in aqueous solutions of inorganic electrolytes. Chemical Engineering Science, 22 (9), 1257-1265.

Miettunen, H., Kaukonen, R., Corin, K., Ojala, S., & Keiski, R.L. (2012). Effect of reducing grinding conditions on the flotation behaviour of low-S content PGE ores. Min Eng, 36-38, 195-203.

Moreno, P.A., Aral, H., Cuevas, J., Monardes, A., Adaro, M., Norgate, T., & Bruckard, W. (2011). The use of seawater as process water at Las Luces copper–molybdenum beneficiation plant in Taltal (Chile). Minerals Engineering, 24 (8), 852-858.

Nayara, G., Sundararamana, P., O'Connorb, C., Schacherla, J., Heath, M., Orozco, M., Shaha, S., Wrighta, N., & Winter, A. (2016). Feasibility study of an electrodialysis system for in-home water desalination in urban India. Development Engineering, 2, 38-46.

Nied, D., Enemark−Rasmussen, K., L'Hopital, E., Skibsted, J., & Lothenbach, B. (2016). Properties of magnesium silicate hydrates (M−S−H). Cement Concrete Res, 79, 323–332.

Niriella, D., & Carnahan, R.P. (2006). Comparison study of zeta potential values of bentonite in salt solutions. J Disper Sci Technol, 27, 123–131.

Ong, B.C., Leong, Y.K., & Chen, S.B. (2008). Yield stress−zeta potential relationship of oxide dispersions with adsorbed polyacrylate — Steric effect and zeta potential at the flocculated−dispersed transition state. Powder Technol, 186, 176–183.

Özcan, Ö., Çelik, M.S., Nickolov, Z.S., & Miller, J.D. (2003). Effect of thermal stability on the flotation response of sodium carbonate salts. Miner Eng, 16, 353–358.

Ozdemir, O., Çelik, M.S., Nickolov, Z.S., & Miller, J.D. (2007). Water structure and its influence on the flotation of carbonate and bicarbonate salts. J Colloid Interf Sci, 314, 545–551.

Partridge, A.C., & Smith, G.W. (1971). Small-sample flotation testing: a new cell. Trans. Inst. Min. Metall., Sect. C, 80, 118.

Pavez, O., Brandao, P.R.G., & Peres, A.E.C. (1996). Technical note adsorption of oleate and octyl-hydroxamate on to rare-earths minerals. Minerals Engineering, 9 (3), 357–366.

Peng, Y., & Bradshaw, D. (2012). Mechanisms for the improved flotation of ultrafine pentlandite and its separation from lizardite in saline water. Minerals Engineering, 36-38, 284-290.

Pereira, C. A., & Peres, A. E. C. (1997). Flotation concentration of a xenotime pre-concentrate. Minerals Engineering, 10 (11), 1291-1295.

Potapova, E., Grahn, M., Holmgren, A., & Hedlund, J. (2010). The effect of calcium ions and sodium silicate on the adsorption of a model anionic flotation collector on magnetite studied by ATR−FTIR spectroscopy. J Colloid Interf Sci, 345, 96–102.

Pradip, & Fuerstenau, D.W. (1983). The adsorption of hydroxamate on semi-soluble minerals. Part I: Adsorption on barite, calcite and bastnaesite. Colloids and Surfaces, 8 (2), 103-119.

Pradip, & Fuerstenau, D.W. (2013). Design and development of novel flotation reagents for the beneficiation of Mountain Pass rare-earth ore. Mining, Metallurgy & Exploration, 30 (1), 1-9.

Qi, G.W., Klauber, C., & Warren, L.J. (1993). Mechanism of action of sodium silicate in the flotation of apatite from hematite. Int J Miner Process, 39, 251–273.

Ralston, J., Fornasiero, D., Grano, S., Duan, J., & Akroyd, T. (2007). Reducing uncertainty in mineral flotation—flotation rate constant prediction for particles in an operating plant ore. Int J Miner Process, 84, 89–98.

Ramdani, A., Deratanni, A., Taleb, S., Drouiche, N., & Lounici, H. (2021). Performance of NF90 and NF270 532 commercial nanofiltration membranes in the defluoridation of Algerian brackish water. Desalination, 212, 286-296.

Rao, S.R., Espinosa-Gomez, R., Finch, J.A., & Biss, R. (1988). Effects of water chemistry on the flotation of pyrochlore and silicate minerals. Minerals Engineering, 1 (3), 189-202.

Ren, J. (1993). Flotation behavior and mechanism of bastnaesite with N-hydroxyl phthalicimide, Proc. of ACTA Metallurgica Sinica (English Edition), 6 (6), pp. B432-B438.

Ren, J., Lu, S., Song, S., & Niu, J. (1997). A new collector for rare earth mineral flotation. Minerals Engineering, 10 (12), 1395-1404.

Ren, J., Song, S., Lopez-Valdivieso, A., & Lu, S. (2000). Selective flotation of bastnaesite from monazite in rare earth concentrates using potassium alum as depressant. International Journal of Mineral Processing, 59 (3), 237-245.

Rijsberman, F.R. (2006). Water scarcity: Fact or fiction? Agricultural Water Management, 80, 5-22.

Roonasi, P., & Holmgren, A. (2010). An ATR–FTIR study of carbonate sorption onto magnetite. Surf. Interface Anal., 42, 1118–1121. https://doi.org/10.1002/sia.3382

Sajjad, M., & Otsuki, A. (2022). Coupling flotation rate constant and viscosity models. Metals−basel, 12, 409.

Salgin, S., Salgin, U., & Soyer, N. (2013). Streaming potential measurements of polyethersulfone ultrafiltration membranes to determine salt effects on membrane zeta potential. Int. J. Electrochem. Sci., 8, 4073–4084.

Schott, H. (1988). Effect of electrolytes on foaming of nonionic surfactant solutions. Journal of the American Oil Chemists' Society, 65 (10), 1658-1663.

Shackleton, N.J., Malysiak, V., & O'Connor, C.T. (2007). Surface characteristics and flotation behaviour of platinum and palladium tellurides. Minerals Engineering, 20 (13), 1232-1245.

Schulz (1970). Separation efficiency, Society of Mining Engineer. In AMIE, 247, 81–87.

Sorensen, E., & Lundgaard, T. (1966). Selective flotation of steenstrupine and monazite from Kvanefjeld Lujavrite - Report for the Danish Atomic Energy Commission. (133).

Subrahmanyam, T.V., & Forssberg, E. (1988). Froth stability, particle entrainment and drainage in flotation — A review. International Journal of Mineral Processing, 23 (1-2), 33-53.

Swedlund, P.J., & Webster, J.G. (1999). Adsorption and polymerisation of silicic acid on ferrihydrite, and its effect on arsenic adsorption. Water Res, 33, 3413–3422.

Tang, M., & Wen, S. (2019). Effects of cations/anions in recycled tailing water on cationic reverse flotation of iron oxides. Mineral−basel, 9, 161.

Tanne, N., Xu, R., Zhou, M., Zhang, P., Wang, X., & Wen, X. (2019). Influence of pore size and membrane surface properties on arsenic removal by nanofiltration membranes. Frontiers Environ Sci Eng, 13,19.

Van der Bruggen, B., Schaep, J., Wilms D., & Vandecasteele C. (1999). Influence of molecular size, polarity and charge on the retention of organic molecules by nanofiltration. Journal of Membrane Science, 156 (1), 29-41.

Wang, B., & Peng, Y. (2014). The effect of saline water on mineral flotation – A critical review. Minerals Engineering, 66-68, 13-24.

Wiese, J., Harris, P., & Bradshaw, D. (2007). The response of sulphide and gangue minerals in selected Merensky ores to increased depressant dosages. Minerals Engineering, 20 (10), 986-995.

Wing, H., & George, N. (1978). A kinetic study of the seeded growth of barium sulfate in the presence of additives. Journal of Inorganic and Nuclear Chemistry, 40(11), 1871-1875.

Winston, W., & Sirkar, K. (1992). Membrane Handbook. Springer Science+Business Media New York.

Xia, L., Hart, B., & Loshusan, B. (2015). A Tof-SIMS analysis of the effect of lead nitrate on rare earth flotation. Minerals Engineering, 70, 119-129.

Xiaofang, Y., Xiaodan, Z., Qiang, M., Jun, Z., Jiaming, G., Dongqi, S., Sheng, Z., Jie, X., & Zhen, Z. (2021). Process optimization to enhance utilization efficiency of precipitants for chloride removal from flue gas desulfurization wastewater via Friedel's salt precipitation. Journal of Environmental Management, 299, 113682.

Xiong, W., Deng, J., Chen, B., Deng, S., & Wei, D. (2018). Flotation-magnetic separation for the beneficiation of rare earth ores. Minerals Engineering, 119, 49-56.

Yammine, S., Rabagliato, R., & Vitrac, X. (2019). The use of nanofiltration membranes for the fractionation of polyphenols from grape pomace extracts. Oeno one, 53, 11-23.

Yang, X., Roonasi, P., & Holmgren, A. (2008). A study of sodium silicate in aqueous solution and sorbed by synthetic magnetite using in situ ATR−FTIR spectroscopy. J Colloid Interf Sci, 328, 41–47.

Yi, X., Zhen, Z., Qian, M., Dongqi, S., Jun, H., Xiaofang, Y., Shifend, D., Lu, J., Xiaodan, Z., & Ying, Z. (2020). A two-stage desalination process for zero liquid discharge of flue gas desulfurization wastewater by chloride precipitation. Journal of Hazardous Materials, 397, 122744.

Yuehua, H., Chi, R., & Xu, Z. (2003). Solution chemistry study of salt−type mineral flotation systems: Role of inorganic dispersants. Ind Eng Chem Res, 42, 1641–1647.

Zhang, W., & Honaker, R.Q. (2018). Flotation of monazite in the presence of calcite part II: Enhanced separation performance using sodium silicate and EDTA. Minerals Engineering, 127, 318-328.

Zhang, W., Honaker, R.Q., & Groppo, J.G. (2016). Fundamental study of the monazite-calcite flotation separation. Proc. of 28th International Mineral Processing Congress., IMPC 2016, Quebec, Canada, pp.4704-4713.

Zhang, Y., & Anderson (2017). A comparison of sodium silicate and ammonium lignosulfonate effects on xenotime and selected gangue mineral microflotation. Minerals Engineering, 100, 1-8.

Zhao, Y., Xing, W., Xu, N., & Wong, F.−S. (2005). Effects of inorganic electrolytes on zeta potentials of ceramic microfiltration membranes. Sep Purif Technol 42, 117–121.